

**STUDIES ON PLASMA MEMBRANE PROTEINS INVOLVED IN  
MEMBRANE TRAFFIC: SYNTAXINS AND E-SYTS**

APPROVED BY SUPERVISORY COMMITTEE

**Thomas C. Südhof, M.D.**

---

**Gang Yu, Ph.D.**

---

**Helmut Krämer, Ph.D.**

---

**Jay R. Gibson, Ph.D.**

---

**To**  
**My Family**

**To**  
**My Wife, Jiyeon Oh**

## **ACKNOWLEDGEMENTS**

I am extremely grateful to my mentor, Dr. Thomas Südhof, who gave me this wonderful opportunity to work in this great environment. His encouragements and guidance really made my thesis work an exciting and enjoyable experience. I always have been impressed by his insightful view and endless enthusiasm on science.

I would like to thank my thesis committee members, Drs. Gang Yu, Helmut Krämer and Jay Gibson for their advice and support.

I would like to thank Dr. Tomohiro Yamaguchi, a former post-doc, who gave me a lot of help when I first joined the lab. I would also like to thank all the other members of the Südhof lab for their helpful suggestions and technical advice. Especially, I am grateful to Iza Kornblum, Andrea Roth, Ewa Borowicz, Lin Fan and Jason Mitchell for their excellent technical supports.

My deep gratitude also goes to my collaborators, Dr. Jianyuan Sun and his group for their excellent expertise in electrophysiology, to Xinran Liu for his support in morphological analyses.

I am deeply grateful to my sweet and beloved wife, Jiyeon Oh, who always has been and will be together with me as a lifetime partner.

Most of all, I owe everything to my beloved family. Their unconditional love and supports have been giving me strength throughout all the courses of my life.

**STUDIES ON PLASMA MEMBRANE PROTEINS INVOLVED IN  
MEMBRANE TRAFFIC: SYNTAXINS AND E-SYTS**

by

**SANG-WON MIN**

**DISSERTATION**

Presented to the Faculty of the Graduate School of Biomedical Sciences

The University of Texas Southwestern Medical Center at Dallas

In Partial Fulfillment of the Requirements

For the Degree of

**DOCTOR OF PHILOSOPHY**

The University of Texas Southwestern Medical Center at Dallas

Dallas, Texas

December, 2006

Copyright

by

**Sang-Won Min**

All Rights Reserved

# **STUDIES ON PLASMA MEMBRANE PROTEINS INVOLVED IN MEMBRANE TRAFFIC: SYNTAXINS AND E-SYTS**

**Sang-Won Min, Ph.D.**

The University of Texas Southwestern Medical Center at Dallas, 2006

Supervising Professor: **Thomas C. Südhof, M.D.**

Fusion of synaptic vesicles is catalyzed by SNARE complex assembly which requires that the SNARE proteins syntaxin-1A and -1B, two isoforms of syntaxin-1, switch from a ‘closed’ to an ‘open’ conformation. To test the physiological significance of this switch, I analyzed mutant mice with a point mutation in syntaxin-1B which renders it predominantly ‘open’ in the syntaxin-1A null background. Whereas deletion of syntaxin-1A caused no detectable phenotype, opening of syntaxin-1B produced lethal epilepsy, independent of the presence of syntaxin-1A. Morphological and electrophysiological analyses revealed that opening of syntaxin-1B impaired steps in exocytosis upstream of vesicle priming, but enhanced  $\text{Ca}^{2+}$ -triggering of fusion-pore opening downstream of priming, indicating that the

conformational switch from closed to open syntaxin-1 controls the entry of vesicles into, and their exit from the exocytosis reaction, leading to a model whereby vesicle priming is initiated by the closed conformation of syntaxin-1, but executed by opening of syntaxin-1.

To understand the differential roles of syntaxin-1A and -1B, GFP-KI mice were generated, which unexpectedly phenocopied KO mice, suggesting functional inactivation by GFP-fusion. Interestingly, GFP-syntaxin-1A and -1B fusion proteins showed differential binding properties to its major binding partners, Munc18-1 and other SNARE proteins. While loss of syntaxin-1A resulted in no detectable phenotype, syntaxin-1B GFP-KI mice died at P14 and showed major phenotype, such as unbalanced coordination of their body with shortening of cerebellar purkinje cell layer and specific innervations on neuromuscular junction synapse, suggesting possible mechanisms for lethality caused by loss of syntain-1B.

C<sub>2</sub>-domains are autonomously folded protein modules that generally function as Ca<sup>2+</sup>- and phospholipid-binding domains, usually involved in membrane trafficking. A family of evolutionarily conserved mammalian proteins, referred to as E-Syts (Extended Synaptotagmin-like proteins), contains an N-terminal transmembrane region, and five (E-Syt1) or three (E-Syt2 and E-Syt3) C-terminal C<sub>2</sub>-domains. In vitro phospholipid binding assay showed the first C<sub>2</sub>-domain of E-Syt2 was capable of Ca<sup>2+</sup>-dependent phospholipid binding, suggesting that E-Syts bind Ca<sup>2+</sup> via their first C<sub>2</sub>-domain in a phospholipid complex. Expression of myc-tagged E-Syt proteins demonstrated localization to intracellular membranes for E-Syt1 and to plasma membranes for E-Syt2 and E-Syt3 in a C<sub>2</sub>C-domain-dependent manner, revealing an unexpected mechanism by C<sub>2</sub>C-domain functions as a targeting motif, independent of transmembrane region.

# TABLE OF CONTENTS

<i>Title</i>	<i>i</i>
<i>Dedication</i>	<i>ii</i>
<i>Acknowledgements</i>	<i>iii</i>
<i>Abstract</i>	<i>vi</i>
<i>Table of Contents</i>	<i>viii</i>
<i>List of Publications</i>	<i>xi</i>
<i>List of Figures</i>	<i>xii</i>
<i>List of Tables</i>	<i>xiv</i>
<i>List of Abbreviations</i>	<i>xv</i>

## Chapter I

<b>Conformational Change of Syntaxin-1 Controls Synaptic Exocytosis</b>	<b>18</b>
<b>Introduction</b>	<b>19</b>
<b>Material and Methods</b>	<b>24</b>
<b>Results</b>	<b>35</b>
Generation of syntaxin-1A <sup>KO</sup> and syntaxin-1B <sup>Open</sup> mutant mice	35
Molecular analysis of syntaxin-1 mutant mice	39
Effect of syntaxin-1B <sup>Open</sup> mutation on vesicle docking	47
Spontaneous neurotransmitter release in syntaxin mutant synapses	51
Increased sensitivity to hypertonic sucrose of primed vesicles in syntaxin 1B <sup>Open</sup> synapses	52
Evoked synaptic responses	58
Ca <sup>2+</sup> -dependence of neurotransmitter release	62
Potentiation of synaptic responses by phorbol esters	63
<b>Discussion</b>	<b>65</b>
Properties of the syntaxin-1B <sup>Open</sup> mutation	66
Role of closed syntaxin-1 in vesicle docking	66
Munc18/syntaxin complex in vesicle priming	68
The closed conformation of syntaxin-1B controls fusion pore opening	68
Lowered phorbol ester response in syntaxin-1B <sup>Open</sup> synapses	72
<b>References</b>	<b>74</b>



## Chapter II

<b>Genetic approach to analyze the differential function of syntaxin-1A and 1B</b>	<b>80</b>
<b>Introduction</b>	<b>81</b>
<b>Material and Methods</b>	<b>84</b>
<b>Results</b>	<b>86</b>
Generation of syntaxin-1A- and 1B GFP-KI mice and expression level of syntaxin-1A and 1B proteins	86
Postnatal lethality of Syntaxin-1B <sup>GFP</sup> mice	89
Functional redundancy between syntaxin-1A and 1B protein and failure of GFP-syntaxin-1A fusion protein to rescue perinatal lethality of syntaxin-1A <sup>KO</sup> /1B <sup>GFP</sup>	91
Protein quantitation of syntaxin-1A <sup>KO</sup> /1B <sup>GFP</sup> mice	93
Differential binding of GFP-syntaxin-1A and -1B fusion proteins to other SNAREs and Munc18-1	96
GFP-fusion syntaxin-1 proteins show normal synaptic staining	98
Decrease in cerebellar purkinje cell layer in syntaxin-1B <sup>GFP</sup> mice	101
Morphology of neuromuscular junction (NMJ) of syntaxin-1A <sup>GFP</sup> and syntaxin-1B <sup>GFP</sup> mice	102
<b>Discussion</b>	<b>103</b>
Lethality of syntaxin-1B <sup>GFP</sup>	103
Non-functionality of GFP-syntaxin-1 fusion protein	103
Impaired morphology of cerebellar purkinje cell	104
Lack of innervation of GFP-syntaxin-1A fusion protein into NMJ	105
<b>References</b>	<b>106</b>

## Chapter III

<b>E-Syts: A Family of Plasma Membrane C<sub>2</sub>-domain Proteins with an Unusual Targeting Mechanism</b>	<b>109</b>
<b>Introduction</b>	<b>110</b>
<b>Material and Methods</b>	<b>113</b>
<b>Results</b>	<b>117</b>
Structure and expression of E-Syts	117
Phospholipid binding by E-Syt2	123
Subcellular localization of E-Syts	128
Plasma membrane targeting of E-Syt2 and E-Syt3 is mediated by its C-terminal C <sub>2</sub> -domain	132
Effects of disrupting the actin or microtubule cytoskeleton	

on the plasma membrane localization of E-Syt2	136
<b>Discussion</b>	<b>140</b>
<b>References</b>	<b>144</b>
 <b>VITAE</b>	 <b>147</b>

## LIST OF PUBLICATIONS

1. Park KC, Choi EJ, **Min SW**, Chung SS, Kim H, Suzuki T, Tanaka K, Chung CH (2000). Tissue-specificity, functional characterization and subcellular localization of a rat ubiquitin-specific processing protease, UBP 109, whose mRNA expression is developmentally regulated. *Biochem J.* 349:443-53
2. Park KC, Kim JH, Choi EJ, **Min SW**, Rhee S, Baek SH, Chung SS, Bang O, Park D, Chiba T, Tanaka K, Chung CH (2002). Antagonistic regulation of myogenesis by two deubiquitinating enzymes, UBP45 and UBP69. *Proc Natl Acad Sci U S A* 99:9733-8
3. Yamaguchi T, Dulubova I, **Min SW**, Chen X, Rizo J, Südhof TC (2002). Sly1 binds to Golgi and ER syntaxins via a conserved N-terminal peptide motif. *Dev Cell* 2:295-305
4. Dulubova I, Yamaguchi T, Gao Y, **Min SW**, Huryeva I, Südhof TC, Rizo J (2002). How Tlg2p/syntaxin16 'snares' VPS45. *EMBO J.* 21:3620-31
5. Dulubova I, Yamaguchi T, Arac D, Li H, Huryeva I, **Min SW**, Rizo J, Südhof TC (2003). Convergence and divergence in the mechanism of SNARE binding by Sec1/Munc18-like proteins. *Proc Natl Acad Sci U S A* 100:32-7
6. **Min SW**, Chang WP, Südhof TC (submitted to *JBC*). E-Syt2 and E-Syt3: Plasma membrane C<sub>2</sub>-domain proteins with an unusual targeting mechanism.

## LIST OF FIGURES

<b>Fig. 1.1.</b>	<b>Generation of syntaxin-1A knockout (1A<sup>KO</sup>) and syntaxin-1B open-conformation mutant mice (1B<sup>Open</sup>): Effect on survival and synaptic protein levels.</b>	<b>37</b>
<b>Fig. 1.2.</b>	<b>Analysis of recombinant syntaxin/Munc18 complexes.</b>	<b>42</b>
<b>Fig. 1.3.</b>	<b>Analysis of syntaxin/Munc18-1 binding by Isothermal Titration Calorimetry (ITC).</b>	<b>44</b>
<b>Fig. 1.4.</b>	<b>Interaction of the open form of syntaxin-1B (1B<sup>Open</sup>) with Munc18-1.</b>	<b>46</b>
<b>Fig. 1.5.</b>	<b>Increased vesicle docking in syntaxin-1B<sup>Open</sup> synapses.</b>	<b>49</b>
<b>Fig. 1.6.</b>	<b>Spontaneous neurotransmitter release and hypertonic sucrose-evoked release in syntaxin-1-mutant synapses.</b>	<b>52</b>
<b>Fig. 1.7.</b>	<b>Release evoked by hypertonic sucrose in syntaxin-1B<sup>Open</sup> synapses.</b>	<b>56</b>
<b>Fig. 1.8.</b>	<b>Effect of syntaxin-1B<sup>Open</sup> mutation on Ca<sup>2+</sup>-triggered release.</b>	<b>59</b>
<b>Fig. 1.9.</b>	<b>Comparative analysis of the synaptic release probability Pr in syntaxin 1B<sup>WT</sup> and 1B<sup>Open</sup> synapses using the irreversible NMDA-receptor blocker MK-801.</b>	<b>61</b>
<b>Fig. 1.10.</b>	<b>Syntaxin-1B<sup>Open</sup> mutation reduces potentiation of synaptic responses by phorbol esters.</b>	<b>64</b>
<b>Fig. 2.1.</b>	<b>Schematic diagram of targeting strategy to generate syntaxin-1A and syntaxin-1B GFP-KI (syntaxin-1A<sup>GFP</sup> and syntaxin-1B<sup>GFP</sup>) mice.</b>	<b>87</b>
<b>Fig. 2.2.</b>	<b>Expression of syntaxin-1 and GFP-syntaxin fusion protein in syntaxin-1A<sup>GFP</sup> and syntaxin-1B<sup>GFP</sup> mice.</b>	<b>88</b>
<b>Fig. 2.3.</b>	<b>Survival and weight studies of syntaxin-1A<sup>KO</sup> / syntaxin-1B<sup>GFP</sup> mice.</b>	<b>90</b>
<b>Fig. 2.4.</b>	<b>Protein quantitation of syntaxin-1A<sup>KO</sup> / syntaxin-1B<sup>GFP</sup> mice.</b>	<b>94</b>
<b>Fig. 2.5.</b>	<b>Binding experiment using GFP-syntaxin-1 fusion protein.</b>	<b>97</b>
<b>Fig. 2.6.</b>	<b>Brain structure analysis and morphological analysis of GFP-fusion protein expression of syntaxin-1A<sup>KO</sup> / syntaxin-1B<sup>GFP</sup> mice.</b>	<b>99</b>

<b>Fig. 2.7.</b>	<b>Abnormal morphology of purkinje cell of syntaxin-1B<sup>GFP</sup> mice.</b>	<b>101</b>
<b>Fig. 2.8.</b>	<b>Exclusive expression of GFP-syntaxin-1B fusion protein in synapse of neuromuscular junction.</b>	<b>102</b>
<b>Fig. 3.1.</b>	<b>Structures of E-Syts.</b>	<b>119</b>
<b>Fig. 3.2.</b>	<b>Alignment of E-Syts.</b>	<b>120</b>
<b>Fig. 3.3.</b>	<b>Expression patterns of E-Syts determined by RT-PCR of RNA from human adult tissues.</b>	<b>122</b>
<b>Fig. 3.4.</b>	<b>Ca<sup>2+</sup>-dependent phospholipid binding by various fragments from E-Syt2.</b>	<b>124</b>
<b>Fig. 3.5.</b>	<b>Ca<sup>2+</sup>- and phospholipid-dependence of membrane-binding of E-Syt2.</b>	<b>126</b>
<b>Fig. 3.6.</b>	<b>Subcellular localization of E-Syts in HEK293 cells.</b>	<b>130</b>
<b>Fig. 3.7.</b>	<b>Subcellular localization of E-Syt2 deletion mutants in transfected HEK293 cells.</b>	<b>133</b>
<b>Fig. 3.8.</b>	<b>The C-terminal C<sub>2</sub>-domain of E-Syt2 and E-Syt3 but not E-Syt1 is sufficient for plasma membrane localization.</b>	<b>135</b>
<b>Fig. 3.9.</b>	<b>Disruption of the actin or microtubule cytoskeleton does not alter plasma membrane localization of an E-Syt2 C<sub>2</sub>B-/C<sub>2</sub>C-domain fragment.</b>	<b>138</b>

## LIST OF TABLES

<b>Table 1.1</b>	<b>Protein quantitation of syntaxin-1A<sup>KO</sup> and syntaxin-1B<sup>Open</sup> mice: total forebrain homogenates at P30.</b>	<b>40</b>
<b>Table 2.1</b>	<b>Survival tables of mice of syntaxin-1A<sup>KO</sup> / 1B<sup>GFP</sup> and syntaxin-1A<sup>GFP</sup> / 1B<sup>GFP</sup> lines.</b>	<b>92</b>
<b>Table 2.2</b>	<b>Protein quantitation table of syntaxin-1A<sup>KO</sup> / 1B<sup>GFP</sup> mice line.</b>	<b>95</b>

## LIST OF ABBREVIATIONS

AP	action potential
cDNA	complementary DNA
CMV	cytomegalovirus
DMSO	dimethyl sulfoxide
DNA	deoxyribonucleic acid
ECFP	enhanced cyan fluorescent protein
EGTA	ethyleneglycobistetraacetic acid
EPSC	excitatory postsynaptic current
EST	expressed sequence tag
E-Syt	extended synaptotagmin
EYFP	enhanced yellow fluorescent protein
FITC	fluorescein isothiocyanate
GAPDH	glyceraldehyde-3-phosphate dehydrogenase
GDP	guanidine diphosphate
GFP	green fluorescent protein
GST	glutathione S-transferase
IP	immunoprecipitation
ITC	isothermal titration calorimetry
kDa	kilodalton
KI	knockin
KO	knockout

K-S test	Kolmogorov-Smirnov test
mEPSC	miniature excitatory postsynaptic current
NMDA	N-methyl D-aspartate
NP-40	nonidet P-40
PAP	peroxidase-antiperoxidase
PBS	phosphate-buffer saline
PC	phosphatidyl choline
PCR	polymerase chain reaction
PDBu	phorbol ester dibutyrate
PE	phosphatidyl ethanolamine
PI	phosphatidyl inositol
PIP	phosphatidyl inositol phosphate
PMSF	phenylmethylsulfonyl fluoride
$P_r$	synaptic release probability
PS	phosphatidyl serine
PSD	postsynaptic density
$P_{vr}$	vesicular release probability
RNA	ribonucleic acid
RRP	readily releasable pool
RT-PCR	reverse transcriptase-polymerase chain reaction
SDS-PAGE	sodium dodecyl sulfate-polyacrylamide gel electrophoresis
SEM	standard error of measurement



SNAP25	synaptosomal associated protein of 25 kDa
SNARE	soluble N-ethylmaleimide-sensitive fusion protein attachment protein receptor
tk	thymidine kinase
TMR	transmembrane region
TTX	tetrodotoxin
VCP	vasolin-containing protein
WT	wild-type

## **Chapter I**

### **Conformational Change of Syntaxin-1**

#### **Controls Synaptic Exocytosis**

## Introduction

At the synapse, neurotransmitters are released from presynaptic terminals by synaptic vesicle exocytosis (Katz, 1969). Synaptic vesicle exocytosis involves multiple steps: Vesicles first dock at the active zone of the presynaptic terminal, are then primed to become  $\text{Ca}^{2+}$ -responsive, and finally are stimulated by  $\text{Ca}^{2+}$  to release their neurotransmitter content. Because  $\text{Ca}^{2+}$ -triggering of release is very rapid ( $<0.4$  msec), fusion of synaptic vesicles is probably executed, at least in part, during the priming reaction. Thus priming is thought to create a metastable state, allowing  $\text{Ca}^{2+}$  to trigger release rapidly by inducing the final step in fusion, fusion pore opening. Fusion of synaptic vesicles – like other intracellular fusion reactions – is catalyzed by assembly of SNARE complexes, which at the synapse are composed of the synaptic vesicle SNARE protein synaptobrevin/ VAMP, and the plasma membrane SNARE proteins syntaxin-1 and SNAP-25 (reviewed in Brunger, 2005; Sorensen, 2005). SNARE complex assembly is mediated by a characteristic sequence, the SNARE motif, which associates into a four-helical bundle (Sutton et al., 1998). Assembly of SNARE motifs into SNARE complexes forces the participating membranes into close proximity, thereby catalyzing fusion.

Synaptobrevin and SNAP-25 are relatively simple SNARE proteins largely composed of SNARE motifs and a membrane attachment sequence (a transmembrane region for synaptobrevin, and a palmitoylated sequence for SNAP-25; Jahn et al., 2003). Different from synaptobrevin and SNAP-25, syntaxin-1 contains an additional N-terminal three-helical domain (the  $\text{H}_{\text{abc}}$ -domain) that accounts for half of the protein (Fernandez et al., 1998). When syntaxin-1 is not in the SNARE complex, it assumes a default ‘closed’ conformation in

which the H<sub>abc</sub>-domain folds back onto the C-terminal SNARE motif (Dulubova et al., 1999; Misura et al., 2000). The closed conformation of syntaxin-1 binds to Munc18-1, an SM-protein that is critical for membrane fusion (Hata et al., 1993; Garcia et al., 1994; Pevsner et al., 1994; Verhage et al., 2000). When syntaxin-1 assembles into SNARE complexes, it has to 'open' and can no longer bind Munc18-1. Since both Munc18-1 and SNARE proteins are essential for synaptic vesicle fusion, both the closed and open conformation of syntaxin-1 are presumably important for fusion.

At a synapse, application of hypertonic sucrose is thought to induce exocytosis of all vesicles in the readily-releasable pool (RRP) of primed vesicles by a Ca<sup>2+</sup>-independent mechanism (Rosenmund and Stevens, 1996). Hypertonic sucrose-induced exocytosis requires SNARE proteins, Munc18-1, and the active zone proteins RIM and Munc13 (Augustin et al., 1999; Schoch et al., 2001; Schulze et al., 1995; Verhage et al., 2000; Richmond et al., 2001; Koushika et al., 2001; Calakos et al., 2004). Extensive genetic studies of syntaxin-1 were performed in *C. elegans* and *D. melanogaster* (reviewed in Richmond and Broadie, 2002), but no such analysis is available in vertebrates. In *C. elegans*, mutant syntaxin-1 with a two-amino acid substitution that renders syntaxin-1 predominantly open and impairs Munc18-1 binding (the so-called LE-mutation; Dulubova et al., 1999) still allows syntaxin-1 to function in synaptic vesicle priming and fusion, suggesting that the closed conformation of syntaxin-1 is not essential for fusion (Richmond et al., 2001). Interestingly, in these experiments the mutant 'open' syntaxin-1 rescued the paralytic phenotype induced by deletion of RIM or Munc13, indicating that the closed conformation of syntaxin-1 with bound Munc18 is

inhibitory, and has to be opened by Munc13 and RIM in order to allow SNARE complex assembly and fusion to proceed (Richmond et al., 2001; Koushika et al., 2001).

Vertebrates express two closely related isoforms, syntaxin-1A and -1B (Bennett et al., 1992; Inoue et al., 1992), that have similar structures and are thought to function similarly in synaptic vesicle exocytosis. In addition, syntaxin-1A was linked to a large number of other functions, ranging from regulating neurotransmitter uptake over modulating  $\text{Ca}^{2+}$ -channels to controlling CFTR function (see for example, Bezprozvanny et al., 1995; Sheng et al., 1996; Naren et al., 1997; Sutton et al., 1999; Deken et al., 2000; Arien et al., 2003; Leung et al., 2003; Sung et al., 2003; Condliffe et al., 2004; Hurley et al., 2004). However, no direct test of these functions is available.

The precise role of Munc18 and the significance of its syntaxin-1 binding also remain uncertain. In knockout (KO) mice and mutant *Drosophila* and *C. elegans*, Munc18-1 is essential for all synaptic exocytosis (Verhage et al., 2000; Harrison et al., 1994; Weimer et al., 2003). Moreover, in mouse chromaffin cells and in *C. elegans* synapses, deletion of Munc18-1 impairs vesicle docking, whereas deletion of SNAREs did not alter vesicle docking (Voets et al., 2001; Weimer et al., 2003). In contrast, synaptic vesicle docking was not decreased in Munc18-1 deficient synapses in mice, although the synapses were unstable and few synapses could be analyzed (Verhage et al., 2000). Viewed together, these experiments suggest that Munc18 may act upstream of SNARE proteins in docking of vesicles, although the discrepancy between the morphology of Munc18-deficient chromaffin cells and synapses remains unresolved. Moreover, these experiments demonstrate that Munc18 does not serve as an inhibitor of SNARE complex formation *in vivo* because fusion

is inactivated instead of enhanced, although Munc18 binding to syntaxin-1 precludes SNARE complex formation and the experiments with open syntaxin-1 in *C. elegans* suggested that it is inhibitory.

In the present study, I have examined the functions of synaptic syntaxin-1A and -1B and their Munc18-binding using a genetic approach. I produced KO mice that lack syntaxin-1A (syntaxin-1A<sup>KO</sup>), and knockin mice that contain a point mutation in syntaxin-1B which renders it predominantly open (syntaxin-1B<sup>Open</sup>). I show that syntaxin-1A is not required for exocytosis or survival, whereas syntaxin-1B represents an essential component of the exocytotic machinery. I demonstrate that in syntaxin-1B<sup>Open</sup> synapses, docking of vesicles is not impaired, whereas in syntaxin-1B<sup>Open</sup> chromaffin cells, it is severely decreased, demonstrating that docking of these two types of vesicles follows distinct mechanisms. In contrast, vesicle docking is unimpaired in either cell by SNARE deletions, confirming that Munc18-binding to syntaxin operates upstream of SNARE complex assembly. In syntaxin-1B<sup>Open</sup> synapses, the size of the RRP is decreased, presumably because the levels of SNARE proteins and Munc18-1 are depressed, but primed vesicles in the RRP more easily undergo both spontaneous and evoked exocytosis. My studies thus reveal that the switch of syntaxin-1 between closed and open conformations sets a precise energetic barrier to fusion, thereby playing a critical role in regulating neurotransmitter release. My results suggest a model whereby Munc18-binding to syntaxin-1 functions in setting up vesicle priming which produces a metastable vesicle state that involves SNARE complex assembly and partial fusion of primed vesicles. According to this model, individual vesicles contain both assembled and free SNARE proteins, with the relative preponderance of the assembled

SNARE complexes determining the ease with which these vesicles will fuse. This model provides an explanation for the role of Munc18 in fusion, suggests a mechanism by which an upstream mutation in syntaxin-1 causes a downstream effect on  $\text{Ca}^{2+}$ -triggering of fusion, and accounts for the heterogeneous  $\text{Ca}^{2+}$ -responsiveness of vesicles.

## Materials and Methods

### Generation of syntaxin-1A- and 1B-mutant mice

**1. Construction of a syntaxin-1A knockout vector** Two overlapping  $\lambda$  clones containing exons 2-9 of mouse syntaxin-1A were subcloned into p-Bluescript II SK by NotI (plmStxA3 and plmStxA5). Furthermore a deletion clone of plmStxA3 was generated by KpnI digest and religation containing Exons 2 and 3 (plmStxA3KpnIdel). For vector construction, first a BsiWI restriction site was introduced into Exon 2 at residue 10 by site-directed mutagenesis with primers A+B (A: CAACCCTGTCCAGGCCCGTACGGCCAAG GACAGCG, B: CGCTGTCCTTGGCCGTACGGGCCTGGACAGGGTTG). Approximately 400 bp 5' of exon 2, a BstBI site was introduced by site-directed mutagenesis, destroying a PmlI restriction site with primers C+D (C: GTGCACCCACACTTCGAAAAATATGCGTA C; D: GTACGCATATTTTTCGAAGTGTGGGTGCAC). A single loxP site flanked by an AatII and a PmlI restriction site was subcloned into a unique BglII restriction site ~65 bp 3' of exon 3 using oligonucleotides E and F (E: GAAGATCTGACGTCATAACTTCGTATAGCA TACATTATACGAAGTTATCACGTGAGATCTTC; F: GAAGATCTCACGTGATAACTT CGTATAATG TATGCTATACGAAGTTATGACGTCAGATCTTC). As a next step, a 2 kb KpnI fragment from plmStxA3 was subcloned into the KpnI site of plmStxA3KpnIdel containing a unique MfeI site in the middle. A Neomycin resistance gene cassette flanked by flp sites and a loxP site at the 3' end of the Neomycin cassette was subcloned into the new BstBI site of plmStxA3KpnIdel. Next a XhoI deletion clone of plmStxA3 was generated using a unique XhoI restriction site about 3kb from the 3' end of plmStxA3 clone. An oligonucleotide containing a unique SpeI and AscI site was subcloned into the XhoI site to be



able to linearize the vector after completion using oligonucleotides G+H (G: CCGCTCGAG CGGACTAGTCTTGGCGCGCCCCGCTCGAGCGG; H: CCGCTCGAGCGGGGCGCGC CAAGACTAGTCCGCTCGAGCGG).

An ECFP construct flanked by BsiWI sites with removed stop-codon and an artificial 6 residue ASG-linker and an artificial Exon 1 at the 3'end was constructed by PCR and oligonucleotides I+J (I: GCCCGTACGGTGAGCAAGGGCGAGGAGCTGTTC; J: GGCCG TACGGAGCTCCTGGGTTCGGTCCTTGGCGGATCCGGCGGATCCCTTGTACAGCTC GCTCGTCCATGCCGAGAGTG).

For final assembly of the vector an NotI-MfeI fragment from plmStxA3KpnI del with the above mentioned modifications was subcloned into the plmStxA3 XhoI deletion clone. The ECFP-construct was put into the BsiWI site of Exon 2. Finally a diphteria toxin was subcloned into the NotI site of the vector. The vector was verified by sequence analysis. The vector was linearized by AscI and electroporated into R-1 mouse embryonic stem cells. Colonies were selected with G418. Resistant colonies were analysed for homologous recombination by Southern blotting with an outside probe. Clones containing homologously recombined genes were expanded, confirmed by southern blotting and used to generate mice by blastocyst injection. To obtain Syntaxin-1A knockout mice were crossed against a transgene mouse expressing Cre under control of a protamine promoter.

**2. Construction of a syntaxin-1B knockin vector** A single lambda clone containing exons 2 to 10 was subcloned in overlapping fragments into pluescript II SK resulting in the following clones plmStx1B5BglII-94 using NotI and BglII, plmStx1B1-2BamHI using BamHI, plmStx1B3-169EcoRI using EcoRI and plmStx1BBglII14 using BglII. As a first

step, a cassette containing a single loxP site flanked by a 5' BstBI site and a 3' NheI site, an artificial Exon 7 preceded by about 20 bp of the 5' intron sequence and about 200 bp of the 3' intron sequence was constructed by PCR and oligonucleotides A+B (A: CCGTTCGAAAT AACTTCGTATAGCATACATTATACGAAGTTATCGGCTAGCTCCTCTCTGGAGCGG ACTCTG; B: CCATCGATGGACCCCGTGTGTCGTACTAG) introducing a 5' BstBI and a 3' ClaI restriction site and subcloned into a TA-cloning vector (Invitrogen). A SspI restriction site was introduced into the Exon 7 PCR fragment by site-directed mutagenesis using Site directed mutagenesis kit from Qiagen and oligonucleotides C+D (C: GAAAGCGGGAAGCT GGCAATATTCACTGATGATGTGAGC, D: GCTCACATCATCAGTGAATATTGCCAG CTTCCCGCTTTC). From the rat c-DNA the 3' end of Syntaxin-1B (residues 178-290) was amplified by PCR removing the stop-codon and adding a 10 aminoacid GS-linker by oligonucleotides E+F (E: GCAATATTACGGACGACATCAAAATGGAC; F: CGAGCC AGACCCACTACCTGAGCCGCTTCCCAAGCCCAGTGTCCCCCAAT). EYFP was modified by PCR to introduce a 3' SspI restriction site by oligonucleotides G+H (G: GGAAGCGGCTCAGGTAGTGGGTCTGGCTCGGTGAGCAAGGGCGAGGAGCTG; H: CCGAATATTCTACTTGTACAGCTCGTCCATGCC) and subsequently subcloned into the rat c-DNA fragment and later on into the artificial Exon7. Finally the cassette was completed by subcloning of a Neomycin cassette flanked by to flp-sites and a 3' loxP site into the ClaI site of the cassette.

In clone plmStx1B3-169EcoRI Exon 7 L165/E166 was mutated into alanins by site directed mutagenesis also introducing a SacII restriction site by oligonucleotides I+J (I: CTACTACCAATGAAGAAGCCGCGGACATGTTGGAAAGC; J: GCTTTCCAACATGT

CCGCGGCTTCTTCATTGGTAGTAG). In a second round of mutagenesis a BstBI restriction site was introduced into the intron proceeding Exon 7 (K: CACCCCCGCCAGGGGTTCGAATCCTCTCTGGAGCGG; L: CCGCTCCAGAGAGGATTCGAA CCCCTGGCGGGGGTG. Finally a BglII site at the 3' end of plmStx1B3-169EcoRI was mutated into a ClaI site by oligonucleotides M+N (M: GTGTGTGTGTGTGTATCGATTG ATCTGTGCCCATAC; N: GTATGGGCACAGATCAATCGATACACACACACACAC). Clone plmStx1bBglII-14 was amplified by PCR introducing ClaI restriction sites at both ends by oligonucleotides O+P (O: CCATCGATTGATCTGTGCCCATACAGTGTA; P: CCATC GATGCTGTCAGAGCTGGCTCAGAG). As a next step the BamHI fragment from plmStx1B1-2 was subcloned in the plmStx1B3-169EcoRI clone modified as described above. Then the ClaI fragment from the modified plmStx-1BglII-14 clone was subcloned into the new ClaI site of the construct described above. For final assembly the cassette containing the duplicated Exon 7 was subcloned into the BstBI site of the construct. Finally a diphtheria-toxin was subcloned into the 5' NotI site of the construct. The construct was verified by sequence analysis. For electroporation in R-1 mouse embryonic stem cells the vector was linearized by KpnI. Colonies were selected with G418. Resistant colonies were analysed for homologous recombination by Southern blotting with an outside probe. Clones containing homologously recombined genes were expanded, confirmed by southern blotting and used to generate mice by blastocyst injection. To obtain the open conformation of the Syntaxin-1B gene mice were crossed against a transgene mouse expressing Cre under control of a protamine promoter.

## Biochemical procedures

**1. Syntaxin immunoprecipitations** Total brain homogenates from mice at P30 were prepared in buffer A (50 mM HEPES-NaOH pH7.2, 100 mM NaCl, 1 mM EDTA, proteinase inhibitor cocktail [Roche]), mixed with an equal volume of extraction buffer (50 mM HEPES-NaOH pH 7.2, 100 mM NaCl, 1 mM EDTA, 1% Triton X-100, proteinase inhibitor cocktail [Roche]), and rotated at 4 °C for 1 hr. The homogenate was centrifuged at 100,000 g and 4 °C for 1 hr. Protein-A and protein-G agarose beads (Stratagene) were washed with 50 mM HEPES-NaOH pH 7.2, 100 mM NaCl, 1 mM EDTA, 0.5% Triton X-100 several times, and 20 µl of beads were added to the solubilized proteins obtained in the supernatant from the centrifuged brain extracts. The samples were rotated at 4 °C for 1 hr, and centrifuged at 2,000 g at 4 °C for 3 min. The protein concentration of the supernatant was measured, and ~3 mg of protein were added to a tube containing washed protein A- and G-agarose (20 µl) containing 15 µl of the syntaxin-1 antibody U6250. Samples were rotated at 4 °C for at least 2 hr to overnight, washed 6 times in buffer A containing 1% Triton X-100, and beads were recovered by centrifugation. Proteins on beads were solubilized in sample buffer and analysed by SDS-PAGE and quantitative immunoblotting.

**2. Subcellular fractionations** Tissues of forebrain and cerebellum were collected from 4 animals (P30) per genotype and homogenized in buffer A. The homogenate was centrifuged at 100,000 g for 1 hr at 4 °C, and the levels of Munc18-1 and of syntaxin-1 in the pellet and supernatant were measured by quantitative immunoblotting using vasolincontaining protein as an internal control.

**3. Quantitative immunoblotting** Total brain homogenates were prepared from mice at P30 in buffer A and boiled 10 minutes after addition of SDS sample buffer. 40 µg proteins were analyzed by SDS-PAGE and quantitative immunoblotting by using  $^{125}\text{I}$ -conjugated secondary antibodies and PhosphorImager detection with vasolin-containing protein (VCP) or GDP dissociation inhibitor as internal controls as described (Rosahl et al., 1995; Schoch et al. 2001; Chandra et al., 2005).

## **Electron microscopy**

**1. Adrenal cells** Adrenal glands were removed from control and Syntaxin-1B Open littermates at embryonic day 18 and fixed for 2.5 h at room temperature with 2% paraformaldehyde, 2.5 % glutaraldehyde in 0.1 M cacodylate buffer (pH 7.2). Adrenals were then washed two times for 15 min with 0.1 M cacodylate buffer (pH 7.2), postfixed for 2 h at room temperature with 1% OsO<sub>4</sub> in 0.1 M cacodylate buffer (pH 7.2), dehydrated through a series of increasing ethanol concentrations and embedded in Epon. Ultrathin sections were collected on formvar-coated copper grids and stained with uranyl acetate and lead citrate. Analysis of secretory vesicle distribution was done blinded for the genotype of the animal. For each genotype the distribution of secretory vesicles was analyzed in serial ultrathin sections (~ 90 nm) of 60 randomly selected chromaffin cells from three different animals (and three different grids per animal). Chromaffin cells were selected at low magnification in the JEOL 1010 electron microscope and subsequently examined at 20.000x magnification. Only cells with a visible nucleus and clear-cut plasma membrane were taken into account. Secretory vesicles were recognized by their round, dense core and had a diameter of

approximately 90 nm. Distances histograms were created for each genotype and the relative frequency of vesicles was calculated according to the number of vesicles counted in this area. In addition, the total number of vesicles was counted and the diameter of secretory vesicles was analyzed.

**2. Synapses** Cortical neurons were cultured from littermate syntaxin-1A<sup>KO</sup>/1B<sup>WT</sup> and syntaxin-1A<sup>KO</sup>/1B<sup>Open</sup> mice for 14 days in vitro, and fixed for 45 min with 2% glutaraldehyde in 0.1 M sodium cacodylate buffer pH 7.4 at 37 °C (Deak et al., 2004). Neurons were rinsed twice in buffer and postfixed in 0.5% OsO<sub>4</sub>, 0.8% potassium ferricyanide (K<sub>3</sub>FeCN<sub>6</sub>) in the same buffer for 30 min at room temperature. After rinsing with distilled water, specimens were stained en bloc with 2% aqueous uranyl acetate for 15 min, dehydrated in a graded series of ethanol to 100%, and embedded in Poly/bed 812 (Polysciences Inc., Warrington, PA) for 24 hr. Thin sections (65 nm) were post-stained with uranyl acetate and lead citrate, and viewed with a JEOL 1200 EX transmission electron microscope at 80 kv accelerating voltage. Ultrastructural analyses were conducted on randomly selected synapses on anonymized digitized electron micrographs at 300 dpi using MetaMorph software (Universal Imaging, West Chester, PA). Only tangentially cut asymmetric synapses on postsynaptic spines (50%) or dendritic shafts (50%) were included (n=3 independent cultures with 136 synapses (syntaxin-1B<sup>WT</sup>) or 108 synapses (syntaxin-1B<sup>Open</sup>) for all parameters except for the synaptic vesicle distance from the active zone (Fig. 3J) where we selected 25 synapses from each genotype (n=1189 vesicles for syntaxin-1B<sup>WT</sup> or =1359 vesicles for syntaxin-1B<sup>Open</sup> from a single culture). Statistical significance among various groups was evaluated with Student's t-test and the data

distribution of cumulative frequency was evaluated with the Kolmogorov-Smirnov test (K-S test).

## **Electrophysiology**

Microisland cultures of mouse hippocampal neurons were prepared and maintained as described previously (Bekkers and Stevens 1991, Pyott and Rosenmund, 2002). Briefly, hippocampi were dissected from neonatal P0 or P1 mouse brains in ice cold Hanks balanced salt solution and incubated with papain solution for 1 hr at 37 °C with gentle shaking. Tissues were mechanically dissociated by gentle trituration and were plated on prepared confluent microisland astrocyte culture in serum-free B-27/Neurobasal A medium. Cultures were incubated at 37 °C, with 5% carbon dioxide and 95% humidity for 9 days or longer before being used for electrophysiological recordings. Approximately the same numbers of neurons from respective genotypes were recorded after same number of days in vitro. The experimenter was blind to the genotype. The standard extracellular medium contained (mM): NaCl, 140; KCl, 2.4; HEPES, 10; glucose, 10; CaCl<sub>2</sub>, 4; MgCl<sub>2</sub>, 4, indicated otherwise. Patch pipettes were pulled from thick-walled borosilicate glass capillaries and filled with the internal solution containing (mM): phosphocreatin, 12; GTP-Na, 0.3; ATP-Mg, 4; MgCl<sub>2</sub>, 0.6; potassium-EGTA, 1; KCl 136; HEPES, 17.8 and 50 units/ml creatin-phosphokinase was added. Osmolarity and pH were adjusted to ~300 mOsm and 7.4 respectively to maintain physiological conditions during recording.

Neurons were somatically voltage-clamped in the whole-cell patch-clamp configuration at a holding membrane potential of -70 mV. EPSCs were recorded every 5 s to

monitor the quality of voltage clamping and evaluate non-specific changes in EPSC amplitude. Currents were filtered at 5 kHz and recorded using a patch-clamp amplifier (Axopatch 200A; Axon Instruments, Union city, CA), and were digitalized at 10 kHz using Digidata 1321A and Clampex 8.03 software and subsequently analyzed using Axograph 4.5 software (Axon Instruments).

Detection of mEPSCs was performed from data sets of 50 s or longer. Data were analyzed with a template-based detection program (Axograph 4.5, Molecular Devices, CA). Threshold for detection was set to 3.5 times the baseline standard deviation. Captured mEPSCs of individual cells were averaged to determine mean amplitude and charge. These values were also used to normalize evoked release and pool size to the number of quanta released. By comparing the frequency of events to the number of vesicles in RRP, spontaneous release activity was normalized for variation in size of RRP, which defined the spontaneous release rate of individual vesicles and were expressed as (pool unit/s).

To determine the readily releasable pool (RRP), the charge induced by application of hypertonic sucrose solution was measured as described in (Rosenmund and Stevens, 1996). 0.5 M sucrose added to the standard extracellular solution was extracellularly applied for more than 3 s, using a application system with solution exchange times of less than 30 ms. The integral of the fast, transient inward current component -after subtraction of steady state component- was defined as total charge of the RRP. To determine vesicular release probability, evoked responses and responses to hypertonic sucrose solutions were always recorded successively from the same cell. The sustained component of the hypertonic response was measured to estimate the vesicular pool turnover rate.



## Electron microscopy

**1. Adrenal cells** Adrenal glands were removed from control and Syntaxin-1B<sup>Open</sup> littermates at embryonic day 18 and fixed for 2.5 h at room temperature with 2% paraformaldehyde, 2.5 % glutaraldehyde in 0.1 M cacodylate buffer (pH 7.2). Adrenals were then washed two times for 15 min with 0.1 M cacodylate buffer (pH 7.2), postfixed for 2 h at room temperature with 1% OsO<sub>4</sub> in 0.1 M cacodylate buffer (pH 7.2), dehydrated through a series of increasing ethanol concentrations and embedded in Epon. Ultrathin sections were collected on formvar-coated copper grids and stained with uranyl acetate and lead citrate. Analysis of secretory vesicle distribution was done blinded for the genotype of the animal. For each genotype the distribution of secretory vesicles was analyzed in serial ultrathin sections (~ 90 nm) of 60 randomly selected chromaffin cells from three different animals (and three different grids per animal). Chromaffin cells were selected at low magnification in the JEOL 1010 electron microscope and subsequently examined at 20.000x magnification. Only cells with a visible nucleus and clear-cut plasma membrane were taken into account. Secretory vesicles were recognized by their round, dense core and had a diameter of approximately 90 nm. Distances histograms were created for each genotype and the relative frequency of vesicles was calculated according to the number of vesicles counted in this area. In addition, the total number of vesicles was counted and the diameter of secretory vesicles was analyzed.

**2. Synapses** The cultured cells were fixed for 45 min with 2% glutaraldehyde in 0.1 M sodium cacodylate buffer, pH7.4 at 37 °C. They were rinsed twice in buffer and then postfixed in 0.5% OsO<sub>4</sub>, 0.8% potassium ferricyanide (K<sub>3</sub>FeCN<sub>6</sub>) in the same buffer for 30

min at room temperature. After rinsing with distilled water, specimens were stained en bloc with 2% aqueous uranyl acetate for 15 min, dehydrated in a graded series of ethanol to 100% and embedded in Poly/bed 812 (Polysciences Inc., Warrington, PA) for 24 hr. Thin sections (65nm) were post-stained with uranyl acetate and lead citrate, and viewed with a JEOL 1200 EX transmission electron microscope at 80kv of accelerating voltage kV with a final magnification of 50,000 $\times$ . All quantitative analysis were conducted on the digitized EM negatives at 300dpi, using the MetaMorph software (Universal Imaging, West Chester, PA). The sampled synapses were randomly selected from three independent cultures (14 d.i.v.) with control (1A<sup>KO</sup>&1B<sup>WT</sup>) and mutant (1A<sup>KO</sup>&1B<sup>Open</sup>) in pair. The measurement was carried out blindly without knowledge of genotyping. The all parameters are derived from the asymmetric synapses on either postsynaptic spines (50%) or dendritic shaft (50%). Only those synapses cut tangentially were included. I analyzed total 136 synapses from control, and 108 synapses from mutant for the following measurement: number of docked vesicles, length of PSD profile, number of total vesicles within boutons, areas of boutons and postsynaptic spines. For the measurement of synaptic vesicle distance from the active zone, I selected 25 synapses from each genotype total vesicles of 1189 (control), 1359 (mutant) from a single culture. The statistical significance among various groups was evaluated with the student *t*-test and the data distribution of cumulative frequency was evaluated with the Kolmogorov-Smirnov test (K-S test).

## Results

### Generation of syntaxin-1A<sup>KO</sup> and syntaxin-1B<sup>Open</sup> mutant mice

To investigate the functional significance of the conformational switch in synaptic syntaxins, I needed to overcome possible redundancy between syntaxin-1A and -1B. To achieve this, gene targeting was used to inactivate expression of syntaxin-1A (which is less abundant than syntaxin-1B; Foletti et al., 2000), resulting in syntaxin-1A<sup>KO</sup> mice (Fig. 1.1.A). The 'LE' point mutation that renders it predominantly open was also introduced into syntaxin-1B (Dulubova et al., 1999; Fig. 1.1.A), resulting in syntaxin-1B<sup>Open</sup> mice. I then crossed double-heterozygous syntaxin-1A<sup>KO</sup> and 1B<sup>Open</sup> mice, and systematically studied the survival of littermate offspring that are hetero- and/or homozygous for the syntaxin-1A<sup>KO</sup> and/or the syntaxin-1B<sup>Open</sup> alleles (Fig. 1.1.B), with the eventual goal of analysing syntaxin-1B<sup>Open</sup> mice on the background of the syntaxin-1A<sup>KO</sup>.

Homozygous syntaxin-1A<sup>KO</sup> mice exhibit no decrease in survival (Fig. 1.1.B), and display no apparent behavioral abnormalities (data not shown). The expendability of syntaxin-1A was unexpected in view of its high concentrations in brain, its proposed central role in vesicle fusion (Jahn et al., 2003), and its many other proposed functions (see for example, Bezprozvanny et al., 1995; Sheng et al., 1996; Naren et al., 1997; Sutton et al., 1999; Deken et al., 2000; Arien et al., 2003; Leung et al., 2003; Sung et al., 2003; Condliffe et al., 2004; Hurley et al., 2004). In contrast to syntaxin-1A<sup>KO</sup> mice, syntaxin-1B<sup>Open</sup> mice exhibited a lethal epileptic phenotype that killed the mice within 3 months (Fig. 1.1.B). The presence or absence of the syntaxin-1A<sup>KO</sup> had no major effect on the phenotype of the syntaxin-1B<sup>Open</sup> mutation; thus syntaxin-1A could not compensate for the syntaxin-1B<sup>Open</sup>

mutation. Heterozygous syntaxin-1B<sup>Open</sup> mutant mice displayed no apparent phenotype, demonstrating that the syntaxin-1B<sup>Open</sup> mutation does not act as a dominant negative (Fig. 1.1.B). In spite of the distinct phenotypes of the syntaxin-1A and -1B mutant mice, it seems likely that the two syntaxins are functionally similar, but that their mutations have differential effects because syntaxin-1B is much more widely expressed than syntaxin-1A (Folletti et al., 2000). As a result, loss of syntaxin-1A function would be tolerated, whereas loss of syntaxin-1B function would not.

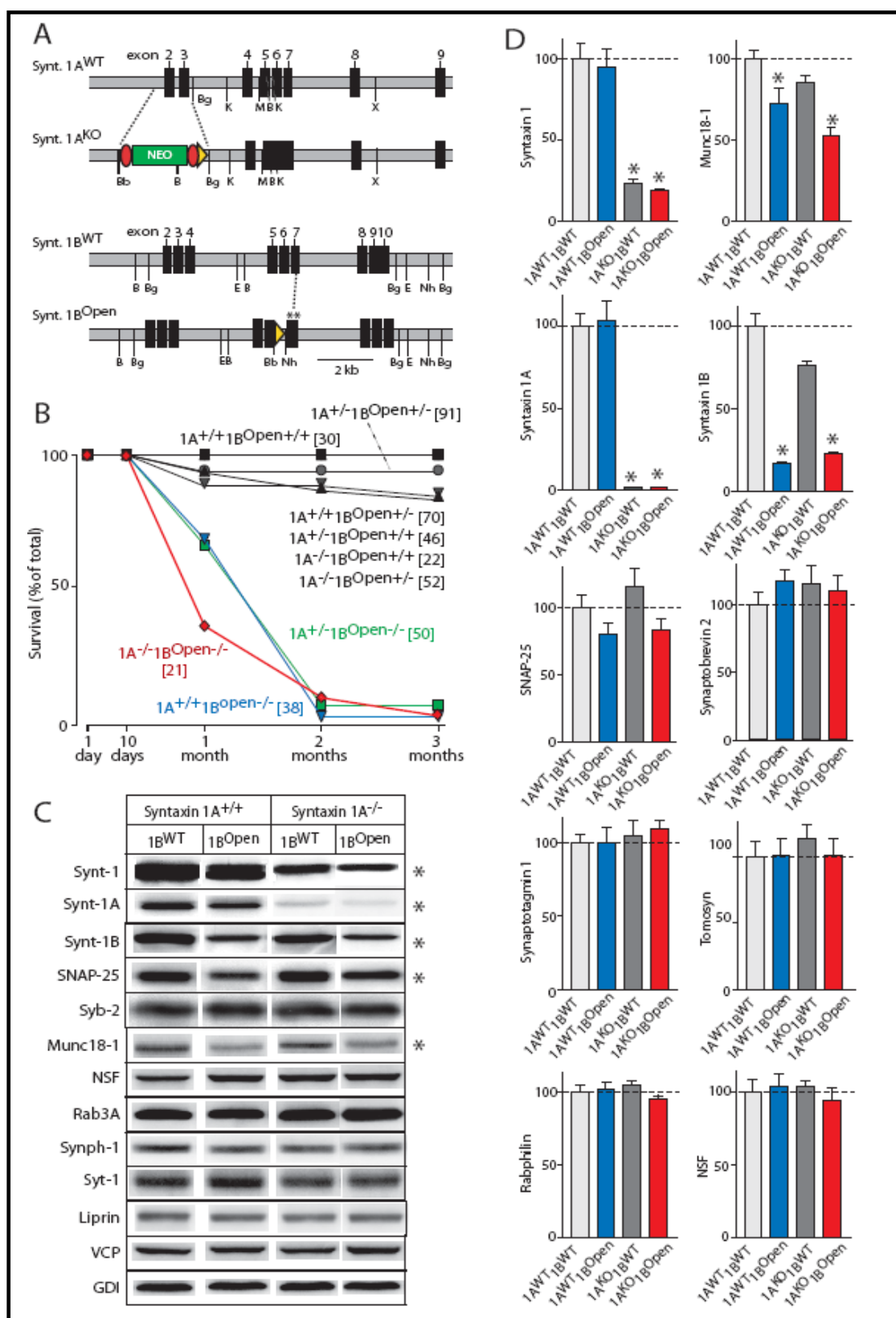


**Figure 1.1. Generation of syntaxin-1A knockout (1A<sup>KO</sup>) and syntaxin-1B open-conformation mutant mice (1B<sup>Open</sup>): Effect on survival and synaptic protein levels.** (A) Schematic diagram of the mutagenesis strategy to generate mice carrying the syntaxin-1A<sup>KO</sup> and 1B<sup>Open</sup> mutant alleles. Numbered black rectangles illustrate coding exons; yellow and red triangles denote loxP and flp recombination sites, respectively (NEO = neomycin resistance gene cassette); asterisks mark sites of point mutations, and letters identify selected restriction enzyme cleavage sites (B=BamHI; Bg=BglII; E=EcoRI; K=KpnI; M=MluI; Nh=NheI; X=XhoI). Scale bar applies to all diagrams. (B) Survival of mice with various combinations of syntaxin-1A<sup>WT</sup>, 1A<sup>KO</sup>, 1B<sup>WT</sup>, and 1B<sup>Open</sup> alleles. (C) and (D) Representative immunoblots of synaptic proteins (C) and mean levels of synaptic proteins (D) from syntaxin-1A<sup>WT</sup>/1B<sup>WT</sup>, 1A<sup>WT</sup>/1B<sup>Open</sup>, 1A<sup>KO</sup>/1B<sup>WT</sup>, and 1A<sup>KO</sup>/1B<sup>Open</sup> mutant mice. Data of panel D and of all subsequent figures containing averages are means  $\pm$  SEMs; asterisks indicate statistically significant changes compared to the wildtype control.

**Molecular analysis of syntaxin-1 mutant mice**

I next performed quantitative immunoblotting analyses of brain proteins from littermate mice that were homozygous mutant for the syntaxin-1A<sup>KO</sup> and/or 1B<sup>Open</sup> alleles or for their corresponding wild type alleles (Fig. 1.1.C). The syntaxin-1B<sup>Open</sup> mutation decreased syntaxin-1B levels ~75%, presumably because it destabilizes syntaxin-1B (Fig. 1.1.D). Both the syntaxin-1A<sup>KO</sup> and the syntaxin-1B<sup>Open</sup> mutation decreased Munc18-1 levels, inducing a ~45% decline of Munc18-1 in the double syntaxin-1A<sup>KO</sup>/1B<sup>Open</sup> mutant. In addition, a small decrease in SNAP-25 levels was observed. No other major changes in protein levels were detected (Table 1.1).

**Table 1.1. Protein quantitation of syntaxin-1A<sup>KO</sup> and syntaxin-1B<sup>Open</sup> mice: total forebrain homogenates at P30.**

	1A <sup>WT</sup> 1B <sup>WT</sup>	1A <sup>KO</sup> 1B <sup>WT</sup>	1A <sup>WT</sup> 1B <sup>Open</sup>	1A <sup>KO</sup> 1B <sup>Open</sup>	p-value: A <sup>WT</sup> B <sup>WT</sup> vs. A <sup>KO</sup> B <sup>WT</sup>	p-value: A <sup>WT</sup> B <sup>WT</sup> vs. A <sup>WT</sup> B <sup>Open</sup>	p-value: A <sup>WT</sup> B <sup>Open</sup> vs. A <sup>KO</sup> B <sup>Open</sup>	p-value: A <sup>KO</sup> B <sup>WT</sup> vs. A <sup>KO</sup> B <sup>Open</sup>
Syntaxin-1A T3748	100 ± 7.3	1.8 ± 0.2	103 ± 12.7	1.5 ± 0.2	<b>0.004</b>	0.676	<b>0.009</b>	<b>0.018</b>
Syntaxin-1B 4191	100 ± 8.0	56.4 ± 2.5	16.8 ± 0.7	23.4 ± 0.3	0.065	<b>0.004</b>	<b>0.003</b>	<b>0.002</b>
Syntaxin-1 HPC-1	100 ± 5.9	50.1 ± 5.6	60.9 ± 4.9	17.6 ± 2.2	<b>0.002</b>	<b>0.000</b>	<b>0.004</b>	<b>0.013</b>
Syntaxin-1 I-379	100 ± 9.5	50.3 ± 6.8	94.8 ± 11.0	38.0 ± 3.6	0.063	0.678	<b>0.032</b>	0.213
Syntaxin-1 U6250	100 ± 9.8	23.1 ± 2.3	62.4 ± 7.6	18.9 ± 0.7	<b>0.014</b>	<b>0.003</b>	<b>0.018</b>	0.197
SNAP-25 Monocl.	100 ± 4.7	128.0 ± 6.8	61.2 ± 3.8	69.5 ± 5.3	0.059	<b>0.001</b>	0.350	<b>0.006</b>
SNAP-25 P913	100 ± 9.6	138.1 ± 12	80.2 ± 8.0	83.4 ± 8.1	<b>0.014</b>	<b>0.011</b>	0.822	0.079
Synaptobrevin-2	100 ± 9.1	116.0 ± 12	118.0 ± 7.9	111.0 ± 11.2	0.441	0.157	0.133	0.761
Munc18-1 Monocl.	100 ± 8.0	67.9 ± 4.6	62.5 ± 3.7	60.3 ± 1.3	0.104	<b>0.007</b>	0.544	0.166
Munc18-1 J370	100 ± 9.3	84.3 ± 3.1	77.7 ± 5.0	65.8 ± 1.2	0.194	0.063	0.132	<b>0.008</b>
Munc18-1 J371	100 ± 9.7	65.9 ± 2.3	62.5 ± 4.6	62.1 ± 2.4	<b>0.039</b>	<b>0.010</b>	0.947	0.277
Munc18-1 K329	100 ± 8.8	78.5 ± 7.3	81.1 ± 4.3	59.9 ± 1.0	0.175	0.067	0.004	0.108
Munc18-1 P592	100 ± 5.9	86.1 ± 3.8	72.5 ± 9.9	53.3 ± 4.9	<b>0.022</b>	<b>0.033</b>	0.053	<b>0.011</b>
Complexin-A	100 ± 6.0	83.3 ± 5.6	91.0 ± 6.2	79.1 ± 4.0	0.193	0.247	0.099	0.553
Synaptotagmin 1	100 ± 5.5	105 ± 9.9	99.7 ± 10.8	109 ± 6.3	0.449	0.975	0.383	0.709
Rab3A	100 ± 13.5	116 ± 8.4	106.6 ± 5.5	100.2 ± 5.7	0.178	0.575	0.373	0.155
Rabphilin	100 ± 4.8	105 ± 2.4	102 ± 4.6	94.8 ± 2.4	0.195	0.728	0.148	<b>0.019</b>
Synapsin	100 ± 3.0	83.8 ± 3.2	108.7 ± 2.6	82.2 ± 7.1	<b>0.027</b>	<b>0.047</b>	<b>0.013</b>	0.705
Synaptophysin 1	100 ± 11.6	98.1 ± 11.9	84.7 ± 3.7	105.9 ± 12.3	0.912	0.173	0.112	0.716
NSF	100 ± 9.2	104 ± 4.2	104 ± 8.5	94.6 ± 8.1	0.733	0.696	0.352	0.324
Synaptojanin 1	100 ± 11.2	106 ± 3.6	108 ± 6.1	104 ± 3.6	0.622	0.492	0.518	0.726
RIM1α	100 ± 14.4	91.4 ± 5.7	103 ± 7.3	93.2 ± 7.0	0.519	0.787	0.253	0.871
ELKS	100 ± 12.8	120 ± 10.0	107 ± 17.1	119 ± 12.2	0.367	0.702	0.508	0.958
Liprin	100 ± 8.2	105 ± 8.8	103 ± 2.1	99 ± 9.7	0.679	0.664	0.627	0.662
Tomosyn	100 ± 11.3	114 ± 10.0	101 ± 12.4	101 ± 12.1	0.398	0.944	1.000	0.466
Vglut 1	100 ± 11.9	113 ± 7.3	101 ± 9.4	110 ± 8.4	0.467	0.936	0.419	0.360
Mint 1	100 ± 7.0	109 ± 20.2	108 ± 17.1	103 ± 16.3	0.695	0.613	0.797	0.592



Previous studies showed that the syntaxin-1<sup>Open</sup> 'LE' mutation decreases the interaction of syntaxin-1 with Munc18-1 (Dulubova et al., 1999; Yamaguchi et al., 2002), but the magnitude of the change in binding affinity was unknown. Using solution binding assays (gel filtration, isothermal titration calorimetry, and analytical ultracentrifugation; see Figs. 1.2 and 1.3), I found that the 'LE' mutation still allows syntaxin-1 to form a stable complex with Munc18-1, but with a ~100-fold decreased affinity. Analytical ultracentrifugation showed that Munc18-1 forms a weak homodimer in the absence of syntaxin-1 ( $K_d \approx 25 \pm 2 \mu\text{M}$ ). In the presence of syntaxin-1, Munc18-1 and syntaxin-1 associate into a heterodimer that exhibits a high-affinity for wildtype syntaxin-1 ( $K_d \approx 20 \pm 5 \text{ nM}$ ), but a low-affinity for mutant syntaxin-1<sup>Open</sup> ( $K_d \approx 2.2 \pm 0.3 \mu\text{M}$ ; Fig. 1.2.C).

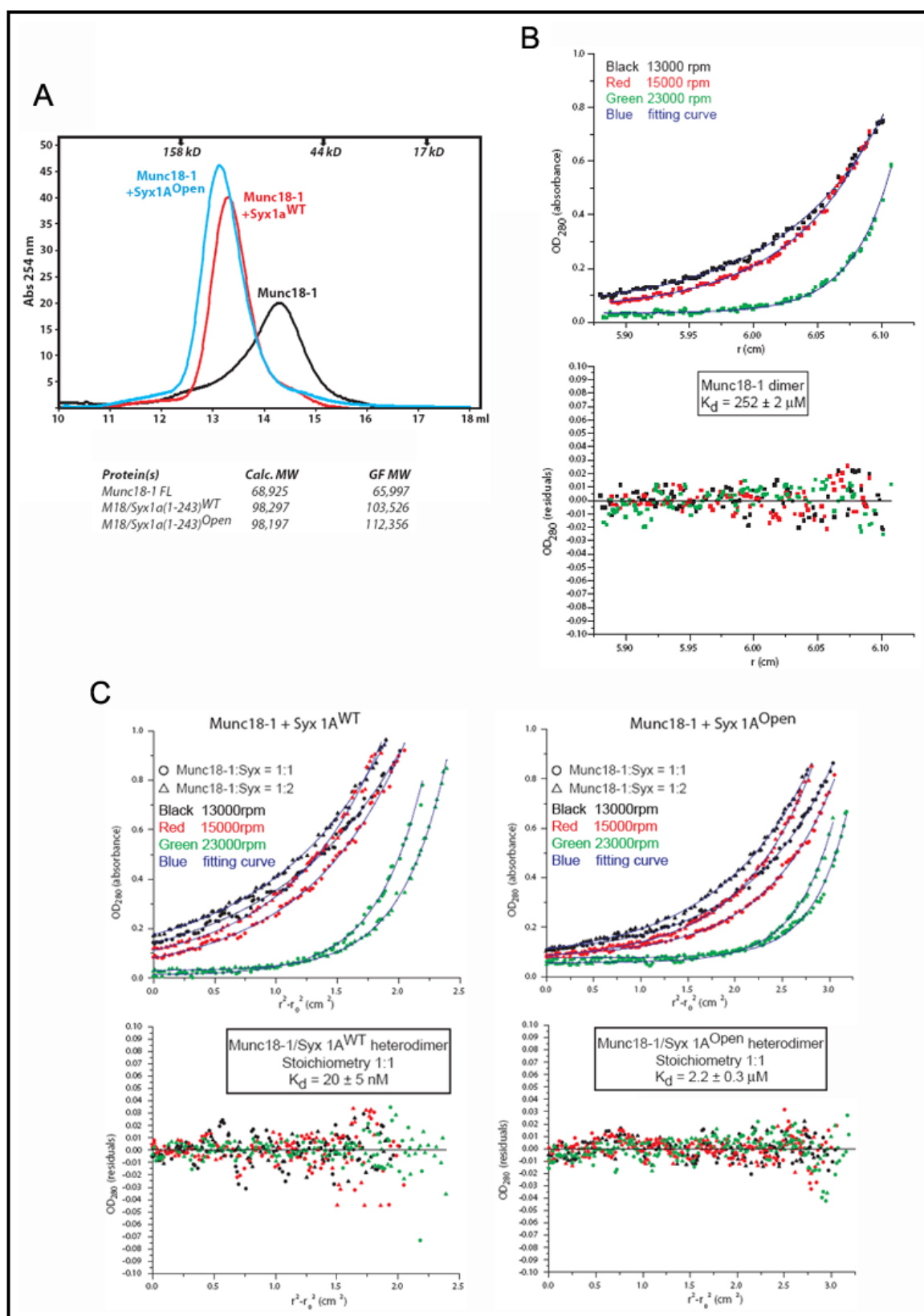


**Figure 1.2. Analysis of recombinant syntaxin/Munc18 complexes.** (A) Gel filtration analysis of recombinant syntaxin/Munc18 complexes. Elution profiles of recombinant Munc18-1, or Munc18-1/ syntaxin 1A<sub>2-243</sub><sup>WT</sup> and Munc18-1/syntaxin 1A<sub>2-243</sub><sup>Open</sup> complexes analysed by gel filtration on a Superdex S200 column. Positions of molecular mass markers are shown on top. Both syntaxin 1A<sup>WT</sup> and syntaxin 1A<sup>Open</sup> co-eluted as ~1:1 heterodimeric complexes with Munc18-1. (B) Analysis of Munc18-1 homodimerization by sedimentation equilibrium analytical ultracentrifugation. Munc18-1 (6  $\mu$ M) was centrifuged at 13,000 rpm (black), 15,000 rpm (red), and 23,000 rpm (green) at 4 °C until equilibrium had been reached. Data in the top panel are fitted to the monomer-dimer equilibrium model. Data in the bottom panel display the differences between raw and fitted data. The fitted curves are colored in blue. Calculated  $K_d$  value for the Munc18-1 dimer is  $25.2 \pm 2$   $\mu$ M. (C) Analysis of syntaxin-1/Munc18-1 heterodimerization by sedimentation equilibrium analytical ultracentrifugation. Munc18-1 was mixed in a 1:1 ( $\circ$ ) or 1:2 ( $\Delta$ ) molar ratio with either syntaxin 1A<sub>2-243</sub><sup>WT</sup> or syntaxin 1A<sub>2-243</sub><sup>Open</sup> mutant. Samples were centrifuged at 13,000 rpm (black), 15,000 rpm (red), or 23,000 rpm (green) at 4 °C until equilibrium had been reached. Data in the top panels show the original data fitted to a 2-component hetero-associating equilibrium model, while the bottom panels display the residuals between observed data and fitted curves for the syntaxin 1A<sup>WT</sup> and 1A<sup>Open</sup> complexes, respectively. The fitted curves are colored in blue. Calculated  $K_d$  value for the Munc18-1/syntaxin complex is  $0.020 \pm 0.005$   $\mu$ M, and for the Munc-18/syntaxin Open 'LE' mutant complex is  $2.20 \pm 0.3$   $\mu$ M.

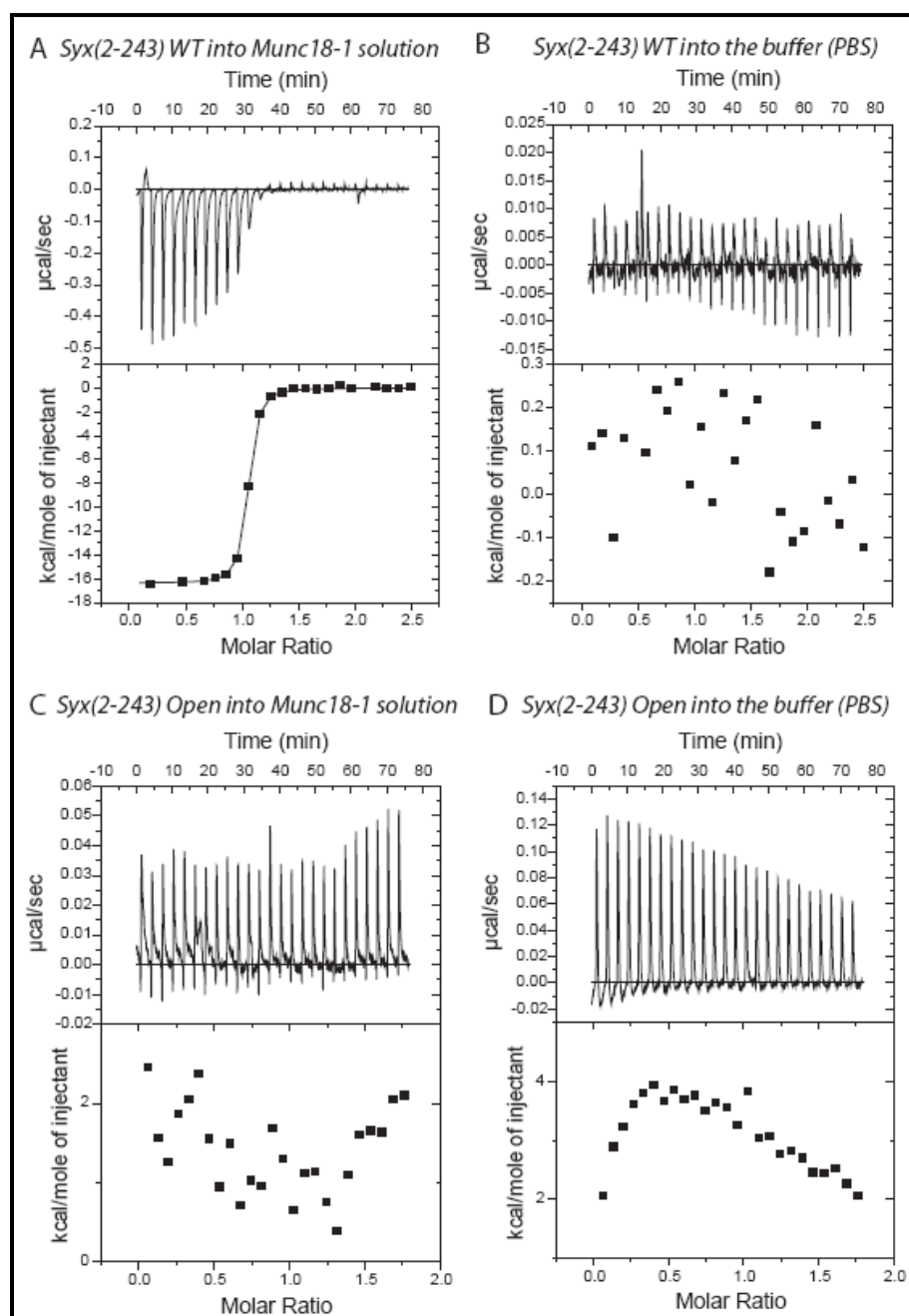


**Figure 1.3. Analysis of syntaxin/Munc18-1 binding by Isothermal Titration Calorimetry (ITC).** ITC binding isotherm for titration of Munc18-1 with syntaxin 1A<sub>2-243</sub> fragment. Data were analyzed with Origin for ITC v.7.0 (Microcal) using single-site binding model. In agreement with the analytical ultracentrifugation data (Fig. 1.2.C), the calculated  $K_d$  for the wild-type syntaxin 1A / Munc18-1 interaction is 11.77 $\pm$ 2.04 nM (average of 3 independent experiments).

I next examined whether the syntaxin-1B<sup>Open</sup> mutation alters Munc18-1 binding to syntaxin-1 in brain. Using subcellular fractionation of forebrain and cerebellum extracts from wildtype syntaxin-1B (1B<sup>WT</sup>) or syntaxin-1B<sup>Open</sup> mice (both on a syntaxin-1A<sup>KO</sup> background), I found that pelletable Munc18-1 was decreased ~2-fold in syntaxin-1B<sup>Open</sup> mutant brains, whereas soluble Munc18-1 was not significantly altered (Figs. 1.4.A and 1.4.B). Thus the decrease in total Munc18-1 levels (Fig. 1.1.D) is due to a decrease in membrane-bound Munc18-1 (Fig. 1.4.B). I also tested whether the syntaxin-1B<sup>Open</sup> mutation alters the abundance of Munc18/syntaxin-1B complexes in brain homogenates by immunoprecipitation (Fig. 1.4.C). I solubilized brain proteins in Triton X-100, and measured the amount of Munc18-1, SNAP-25, synaptobrevin-2, and synaptotagmin-1 that could be co-immunoprecipitated with syntaxin-1B<sup>WT</sup> or -1B<sup>Open</sup> on the syntaxin-1A<sup>KO</sup> background. The relative abundance of Munc18-1/syntaxin-1B<sup>Open</sup> complexes was <25% of wildtype, whereas the relative abundance of SNARE complexes was unchanged (Fig. 1.4.D). Since I normalized the bound Munc18-1 in these experiments for the amount of immunoprecipitated syntaxin-1B, and since syntaxin-1B accounts only for roughly half of the total syntaxin and is additionally decreased to ~25% in the syntaxin-1B<sup>Open</sup> mice, the absolute concentration of the syntaxin-1B<sup>Open</sup>/Munc18-1 complex is decreased in the syntaxin-1B<sup>Open</sup> mice to <<5% of wild type levels. Note that this experiment cannot provide insight into the assembly of SNARE complexes because the homogenates were prepared under conditions that favor complete formation of SNARE complexes.

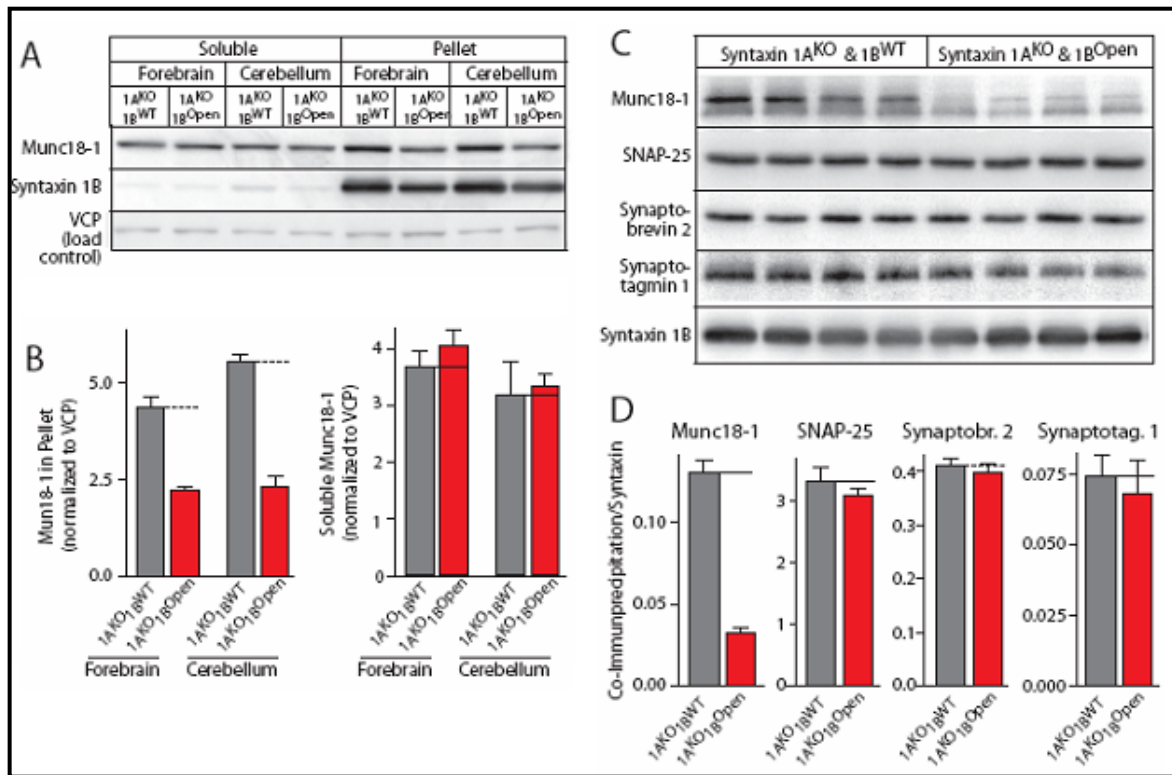


**Figure 1.4. Interaction of the open form of syntaxin-1B (1B<sup>Open</sup>) with Munc18-1.** (A) and (B). Representative immunoblot (A) and quantitation (B) of subcellular fractionation experiments analysing soluble vs. particulate Munc18-1 and syntaxin-1B protein. (C) and (D) Representative immunoblot (C) and quantitation (D) of immunoprecipitation experiments. Syntaxins 1A/1B were immunoprecipitated from Triton X-100 solubilized brain homogenates from syntaxin-1A<sup>KO</sup>/1B<sup>WT</sup> and syntaxin-1A<sup>KO</sup>/1B<sup>Open</sup> mice. Immunoprecipitated syntaxin and co-immunoprecipitated Munc18-1, SNAP-25, synaptobrevin-2, and synaptotagmin 1 were quantitated, and the co-immunoprecipitated proteins were normalized for the amount of syntaxin-1 present.

### Effect of syntaxin-1B<sup>Open</sup> mutation on vesicle docking

To determine whether syntaxin-1B<sup>Open</sup> synapses exhibit structural changes, I employed electron microscopy of neurons from littermate syntaxin-1B<sup>Open</sup> and -1B<sup>WT</sup> mice lacking syntaxin-1A (Figs. 1.5.A and B). Overall, syntaxin-1B<sup>Open</sup> mutant synapses did not exhibit overt changes, but quantitations revealed a significant increase in the number of docked vesicles (~25%; Figs. 1.5.C and D). This increase was confirmed by the large right shift in the frequency distribution of the number of docked vesicles per active zone (Fig. 1.5.E). In addition, the size of the postsynaptic density (which equals the size of the presynaptic active zone [Lisman and Harris, 1993]) was increased ~20% (Fig. 1.5.F); as a result, although the total number of vesicles per active zone is increased, the density of docked vesicles per active zone length is unchanged (Fig. 1.5.G). No other structural parameter differed between syntaxin-1B<sup>Open</sup> and -1B<sup>WT</sup> synapses; in particular, the number and intraterminal distribution of vesicles were unaltered (Figs. 1.5.H-K).

The increase in vesicle docking in syntaxin-1B<sup>Open</sup> synapses was surprising because deletion of Munc18-1 in mouse chromaffin cells (Voets et al., 2001), and of *unc-18* in *C. elegans* neurons (Weimer et al., 2003) impairs vesicle docking. Since in syntaxin-1B<sup>Open</sup> synapses the abundance of the Munc18-1/syntaxin complex is decreased to <5% (Fig. 1.4.B), a decrease in vesicle docking might have been expected based on the chromaffin cell phenotype. To explore this discrepancy, I performed electron microscopy on chromaffin cells from syntaxin-1B<sup>Open</sup> mutant mice, using wild type, Munc18-1 deficient mice and – in a separate experiment with a separate wild type control – synaptobrevin-2 deficient mice as controls (Figs. 1.5.L and M). The analyses were performed at embryonic day 18. I found that

different from synapses, syntaxin-1B<sup>Open</sup> mutant chromaffin cells exhibited a dramatic decrease in docking (>75%). This phenotype was similar to that of Munc18-1 deficient chromaffin cells, and both mutants did not exhibit a change in total vesicle numbers. In synaptobrevin-2 deficient chromaffin cells, by contrast, docking was not impaired, but total vesicle numbers were enhanced (Fig. 1.5.*L* and *M*).



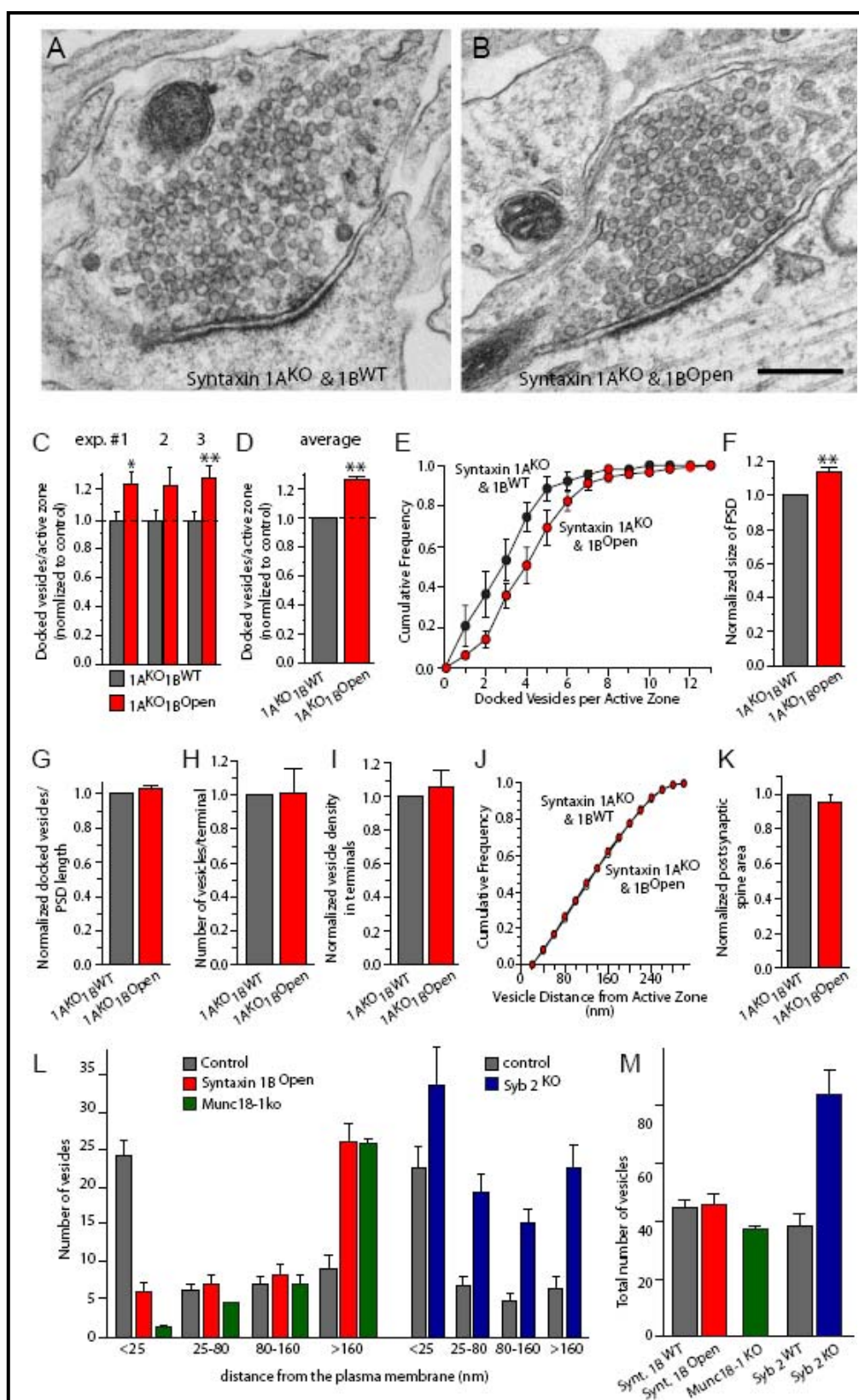


**Figure 1.5. Increased vesicle docking in syntaxin-1B<sup>Open</sup> synapses.** (A) and (B) Representative electron micrographs from cultured neurons from syntaxin-1A KO mice containing wildtype syntaxin-1B (A) or syntaxin-1B<sup>Open</sup> (B). (C) and (D) Number of docked vesicles per active zone obtained in three individual experiments (C; #1, n= 49 and 21 synapses from 1B<sup>WT</sup> and 1B<sup>Open</sup> mice; #2, n= 55 and 38 ; #3, n= 32 and 49 ) and summary graph of the three experiments,  $p < 0.01$  (D). (E) Plot of the cumulative distribution of the number of docked vesicles per active zone (statistical significance with Kolmogorov-Smirnov test  $p < 0.01$ ). (F) Size of the postsynaptic density ( $p < 0.05$ ); (G)-(H) normalized number of docked vesicles/length of postsynaptic density (which correlates with the length of the active zone) (G), number of vesicles per terminal (H) and density of vesicles in the terminal (I). (J) Plot of the cumulative distance of vesicles from the active zone. (K) normalized size of postsynaptic spines (as area); (L) and (M) Distribution of chromaffin granules in adrenal chromaffin cells from syntaxin-1B<sup>Open</sup> mice and from Munc18-1 and synaptobrevin-2 KO mice (each separately analyzed with wildtype control samples) as a function of their distance from the plasma membrane (L), and total number of chromaffin granules per cell (M; n = 60 chromaffin cells). Secretory vesicles were categorized in four bins according to their distance from the plasma membrane. All data shown are means  $\pm$  SEMs; asteriks indicate statistically significant differences of  $p < 0.001$  as assessed with Student's t test.

### Spontaneous neurotransmitter release in syntaxin mutant synapses

To examine synaptic transmission in syntaxin-mutant synapses, synaptic responses in autapses formed by single hippocampal neurons cultured on microislands of glia cells were recorded (Bekkers and Stevens, 1991). In all of these experiments, neurons from two sets of littermate mice were compared: syntaxin-1A<sup>WT</sup> or -1A<sup>KO</sup> mice on a syntaxin-1B<sup>WT</sup> background (to test the effect of the syntaxin-1A deletion on synaptic transmission), and syntaxin-1B<sup>WT</sup> or -1B<sup>Open</sup> mice on a syntaxin-1A<sup>KO</sup> background (to test the effect of opening syntaxin-1B on synaptic transmission).

First, spontaneous synaptic events (mEPSCs for miniature excitatory postsynaptic currents) were investigated in the presence of 0.3  $\mu$ M tetrodotoxin (TTX). Syntaxin-1A<sup>KO</sup> synapses displayed no significant change in the frequency, amplitude, or charge of mEPSCs compared to syntaxin-1A<sup>WT</sup> synapses (data not shown). In contrast, syntaxin-1B<sup>Open</sup> synapses exhibited a ~40% increase in mEPSC frequency with no significant difference in the charge or amplitude of mEPSCs (Figs. 1.6.A-C). As the RRP size in the same synapses was determined (see below), the ‘spontaneous vesicular release rate’ could be calculated by dividing the mEPSC frequency by the number of vesicles in the RRP. The spontaneous vesicular release rate was not altered in syntaxin-1A<sup>KO</sup> neurons, but increased >2-fold in syntaxin-1B<sup>Open</sup> synapses (Fig. 1.6.D).

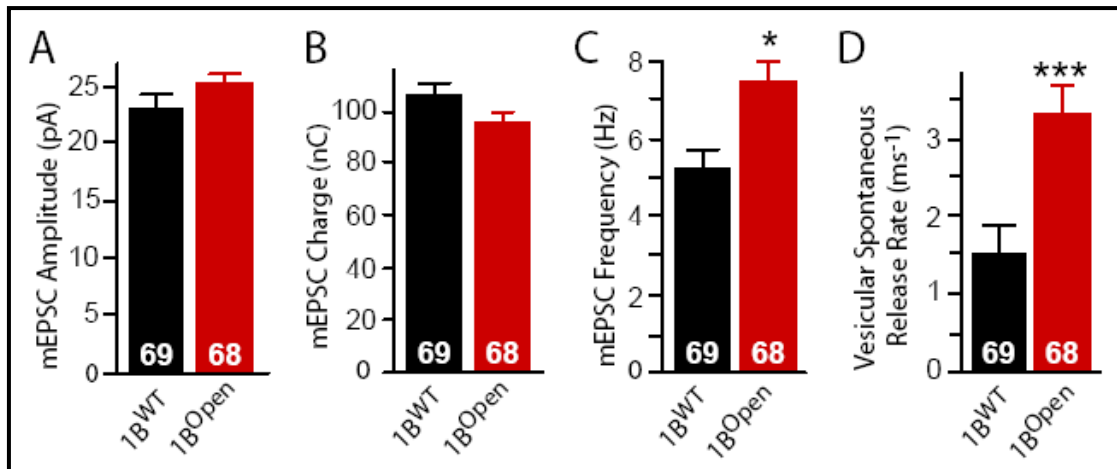


**Figure 1.6. Spontaneous neurotransmitter release and hypertonic sucrose-evoked release in syntaxin-1-mutant synapses.** (A)- (D) Summary graphs of the properties of spontaneous synaptic events.

### Increased sensitivity to hypertonic sucrose of primed vesicles in syntaxin 1B<sup>Open</sup> synapses

Hypertonic sucrose triggers exocytosis of primed vesicles by a  $\text{Ca}^{2+}$ -independent mechanism, and is commonly used to measure the size of the readily-releasable pool (RRP) of vesicles (Rosenmund and Stevens, 1996). When a pulse of hypertonic sucrose (usually 0.5 M) is applied onto a synaptic terminal, the hypertonic solution shrinks the intracellular volume by withdrawing water, resulting in an increasing transmembrane pressure that induces vesicle exocytosis and a large transient postsynaptic inward current (Fig. 1.7.A). The current transient is thought to reflect the size of the RRP, and is followed by a smaller steady-state current that corresponds to the exocytosis of vesicles as they are being reprimed into the RRP, and that is maintained as long as the hypertonic solution is present. Sucrose triggers the

current transient with a latent period because the sucrose has to diffuse to the terminals and to effect a pressure change in order to induce exocytosis.

Application of a 4 sec pulse of 0.5 M sucrose revealed no significant difference in the size of the RRP between littermate syntaxin 1A<sup>WT</sup> and 1A<sup>KO</sup> mice (data not shown), but uncovered a ~40% decrease in the RRP in syntaxin 1B<sup>Open</sup> synapses (Figs. 1.7.A and B). Thus, the RRP in syntaxin 1B<sup>Open</sup> synapses is decreased even though the number of docked vesicles was increased, arguing against the notion that the number of docked vesicles at a synapse reflects the size of the RRP (Schikorski and Stevens, 2001).

The kinetics of sucrose-triggered release was examined because sucrose-induced responses apparently set in earlier in syntaxin-1B<sup>Open</sup> synapses than in syntaxin-1B<sup>WT</sup> synapses (Fig. 1.7.A). Indeed, integrating the EPSC transients showed that sucrose-induced release was initiated in syntaxin-1B<sup>Open</sup> synapses before it started in syntaxin-1B<sup>WT</sup> synapses, independent of whether release was plotted in absolute values or after normalization for the total RRP charge (Fig. 1.7.C). Sucrose release began after a shorter latent period in the syntaxin-1B<sup>Open</sup> synapses with a significantly decreased time-to-peak (time-of-onset: 1B<sup>WT</sup>=0.59 ± 0.02 s [n=53]; 1B<sup>Open</sup>=0.52 ± 0.02s [68] ( $p=0.032$ ); Fig. 1.7.D; time-to-peak: 1B<sup>WT</sup>=1.01 ± 0.03 s [53]; 1B<sup>Open</sup>=0.91 ± 0.02 s [68];  $p=0.008$ ; responses with a time-to-onset of >1 s were excluded). In contrast, the half-widths of the responses were significantly smaller in syntaxin-1B<sup>Open</sup> synapses (1B<sup>WT</sup>=0.38 ± 0.02 s [53]; 1B<sup>Open</sup>=0.31 ± 0.01 s [68];  $p=0.003$ ), confirming the decrease in RRP size (Fig. 1.7.D).

A plausible explanation for the earlier onset of sucrose-triggered release is that the effective ‘triggering’ concentration of sucrose is decreased, i.e. the energy barrier to fusion is

lowered by the syntaxin-1B<sup>Open</sup> mutation. To test this hypothesis, vesicle release at lower sucrose concentrations was measured (Fig. 1.7.E). The relative sucrose response, measured as the fraction of the RRP released, that was triggered by 250 mM and 350 mM sucrose was increased by 270% and 156%, respectively, in syntaxin-1B<sup>Open</sup> synapses compared to syntaxin-1B<sup>WT</sup> synapses (Fig. 1.7.F). To further characterize this effect, the maximal release rates for each sucrose concentration were calculated. The transient component of each response was integrated, normalized for the synaptic charge induced by standard 0.5 M sucrose solution (e.g., see Fig. 1.7.C), and the maximal slope was fitted. At all sucrose concentrations, the syntaxin-1B<sup>Open</sup> mutation significantly boosted the fractional release rate (350 mM sucrose: 1B<sup>WT</sup>=0.40 ± 0.04 pool unit/s [17]; 1B<sup>Open</sup>= 0.90 ± 0.10 pool unit/s [18];  $p=0.0010$ ; 250 mM sucrose: 1B<sup>WT</sup>=0.10 ± 0.02 pool unit/s [17], 1B<sup>Open</sup>=0.37 ± 0.07 pool unit/s [18];  $p<0.0001$ ; Fig. 1.7.G). These data demonstrate that primed vesicles exhibit a decreased energy barrier for fusion in syntaxin 1B<sup>Open</sup> synapses.

A different approach to testing whether vesicles in syntaxin 1B<sup>Open</sup> synapses are hypersensitive to sucrose is to measure the steady-state component of the sucrose-induced response that follows the initial transient component (Fig. 1.7.H). The steady-state current component is thought to reflect the continuous repriming and re-exocytosis of vesicles that re-enter the RRP (Rosenmund and Stevens, 1996). No difference between syntaxin-1A<sup>WT</sup> and -1A<sup>KO</sup> synapses was observed in the amplitude of the sustained component, or in the RRP turnover rate (the mean amplitude divided by the charge of the RRP) during the sustained component (data not shown). In syntaxin-1B<sup>Open</sup> synapses, however, the absolute size of the steady-state component was slightly but not significantly larger than in syntaxin-1B<sup>WT</sup>

synapses (Fig. 1.7.I), whereas the fractional RRP turnover rate was enhanced >3-fold (Fig. 1.7.J). Since the effective sucrose concentration at wild type and mutant synapses is the same, this result confirms that on average, a primed vesicle is significantly more sensitive to hypertonic sucrose in syntaxin-1B<sup>Open</sup> synapses than in syntaxin-1B<sup>WT</sup> synapses. Thus in syntaxin-1B<sup>Open</sup> synapses, there are fewer slots for readily-releasable vesicles, but these vesicles are more sensitive to osmotic pressures than in syntaxin-1B<sup>WT</sup> synapses.

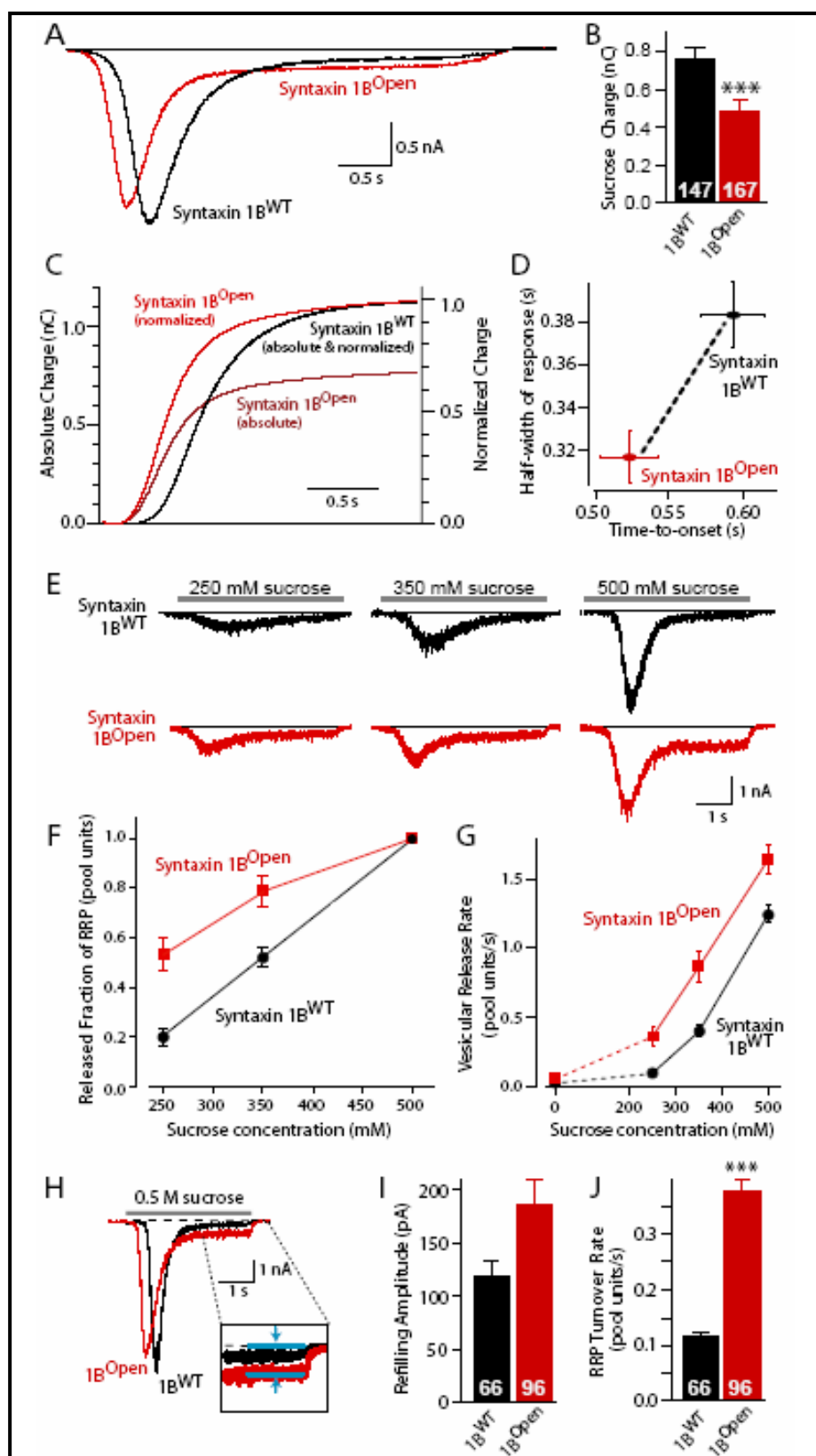




**Figure 1.7. Release evoked by hypertonic sucrose in syntaxin-1B<sup>Open</sup> synapses.** (A) Representative traces of postsynaptic responses elicited by application of 0.5 M sucrose in syntaxin-1B<sup>WT</sup> and 1B<sup>Open</sup> synapses. (B) Mean size of the transient EPSC induced by hypertonic sucrose. (C) Integration; (D) Plot of the half-width vs. time-to-onset of the sucrose responses. (E) Representative traces of responses induced by distinct sucrose concentrations. (F) Plot of the fraction of the RRP released by different concentrations of sucrose (the RRP being defined as the response to 0.5 M sucrose). (G) Plot of the vesicular release rate as a function of sucrose concentration. (H) illustration of the measurements of steady-state sucrose responses. (I) absolute steady-state sucrose responses. (J) vesicular turnover rate during the steady-state sucrose responses.

## Evoked synaptic responses

To study  $\text{Ca}^{2+}$ -triggered release in syntaxin-mutant neurons, EPSCs induced by 2 ms somatic depolarizations (from -70 to 0 mV) were measured. There was no difference in the EPSC amplitude or EPSC charge between syntaxin-1A<sup>WT</sup> and -1A<sup>KO</sup> neurons (data not shown), or between syntaxin-1B<sup>WT</sup> and -1B<sup>Open</sup> neurons (Figs. 1.8.A-C). I then determined for each neuron the RRP size, and calculated the fraction of the RRP that is released by a single depolarization (defined as the vesicular release probability  $P_{\text{vr}}$ ). I also observed no difference in  $P_{\text{vr}}$  between syntaxin-1A<sup>WT</sup> and -1A<sup>KO</sup> neurons (data not shown), but detected a >2-fold increase in the  $P_{\text{vr}}$  in syntaxin-1B<sup>Open</sup> neurons (Figs. 1.8.D), indicating that the percentage of RRP released by an action potential increased in syntaxin-1B<sup>Open</sup> synapses from ~10% to ~20%.

To test with an independent approach whether the syntaxin-1B<sup>Open</sup> mutation increases the  $P_{\text{vr}}$ , I monitored use-dependent synaptic depression during high-frequency stimulus trains. Use-dependent depression depends mainly on the  $P_{\text{vr}}$ , although parameters such as  $\text{Ca}^{2+}$ -influx and  $\text{Ca}^{2+}$ -accumulation also contribute (Zucker and Regehr, 2002). Use-dependent depression manifests in two phases: a fast phase lasting 5-10 action potentials that reflects the rate of RRP depletion (and therefore the  $P_{\text{vr}}$ ), and a slow phase that dominates after the fast phase is exhausted and corresponds to the steady-state balance between RRP depletion and refilling (Fig. 1.8.E and F). I detected no difference in use-dependent depression between syntaxin-1A<sup>WT</sup> and -1A<sup>KO</sup> neurons (data not shown), but observed a massive increase in the fast phase of use-dependent depression in syntaxin-1B<sup>Open</sup> neurons (Figs. 1.8.E and F).

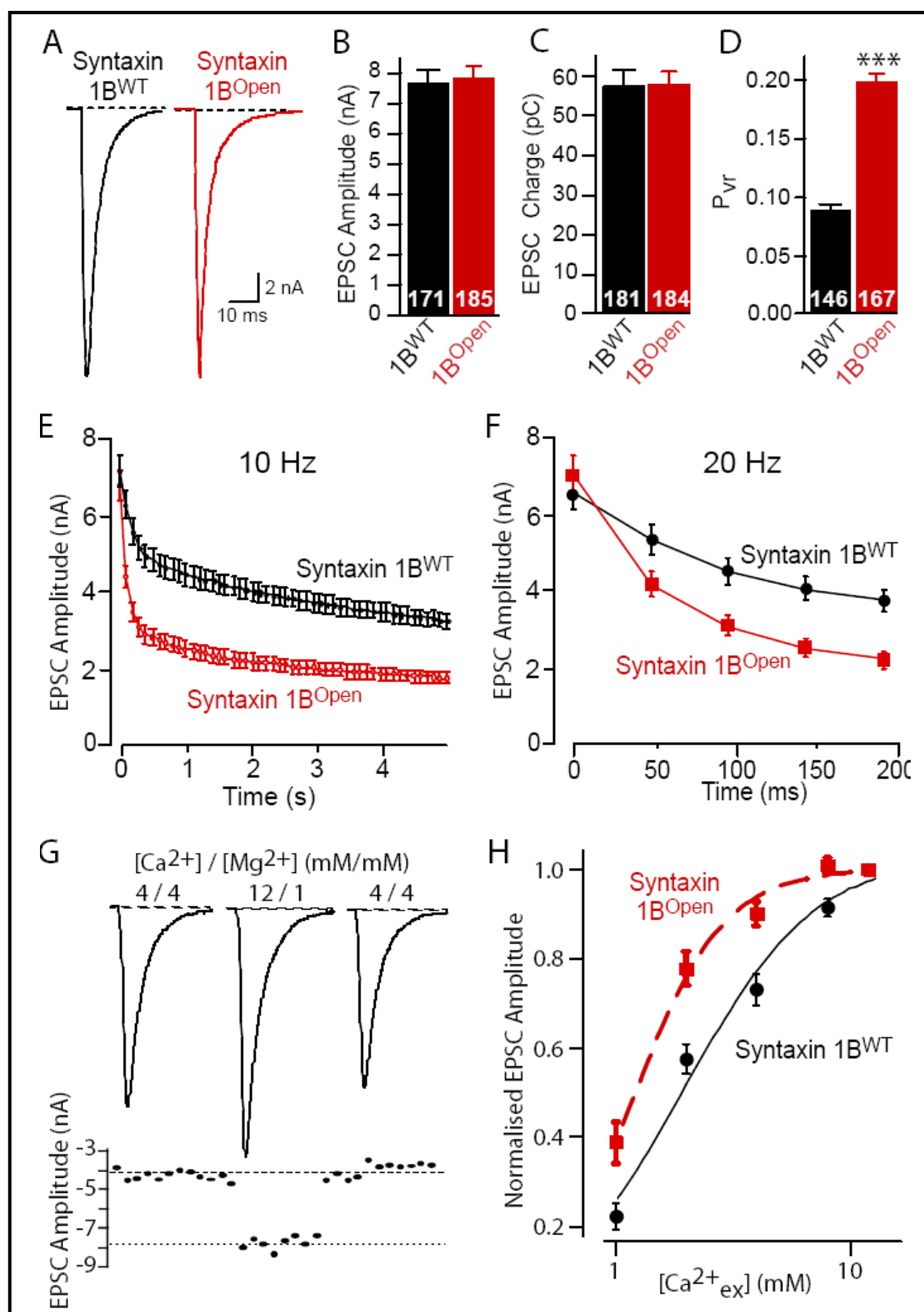


**Figure 1.8. Effect of syntaxin-1B<sup>Open</sup> mutation on Ca<sup>2+</sup>-triggered release.** (A) – (D) Properties of synaptic responses elicited by isolated action potentials (APs). (E) and (F) Properties of synaptic responses elicited by 10 and 20 Hz AP trains. (G) and (H) Determination of the apparent Ca<sup>2+</sup>-affinity of release. Representative traces (G) and amplitudes (H) recorded during the experimental paradigm used in which EPSCs were monitored first in the standard ambient Ca/Mg concentration (4 mM Ca/4 mM Mg), then in the test ambient Ca/Mg concentration (12 mM Ca/1 mM Mg in this example), and finally again in the standard ambient Ca/Mg concentration to control for rundown of responses. (B) Plot of the EPSC amplitudes (normalized to the response in 12 mM Ca<sup>2+</sup>) as a function of ambient Ca-concentration (all in 1 mM Mg). The data were fitted to the equation  $y = m1/(1+(m2/m0)^{m3})$  ( $m1$  = maximal potentiation;  $M2$  = affinity in mM; and  $m3$  = cooperativity of Ca-action), resulting in the following parameters:  $m1$  for 1B<sup>WT</sup> = 1.78, 1B<sup>Open</sup> = 1.38;  $m2$  = 1B<sup>WT</sup> = 2.13, 1B<sup>Open</sup> = 1.24 mM Ca;  $m3$  for 1B<sup>WT</sup> = 1.51; 1B<sup>Open</sup> = 2.16.

Next, the synaptic release probability  $P_r$  (i.e., the probability that a synapse will release neurotransmitters in response to an action potential) was measured in syntaxin-1B<sup>Open</sup> synapses, using the activity-dependent block of NMDA-receptor dependent EPSCs by the irreversible NMDA-receptor antagonist MK-801 (Hessler et al., 1993; Rosenmund et al., 1993; Fig. 1.9). There was no significant difference between syntaxin-1B<sup>WT</sup> and syntaxin-1B<sup>Open</sup> synapses, indicating that although the  $P_{vr}$  is increased in syntaxin-1B<sup>Open</sup> synapses, the synaptic  $P_r$  is not altered, presumably because during low-frequency stimulation, the increase in  $P_{vr}$  compensates for the decrease in the RRP.

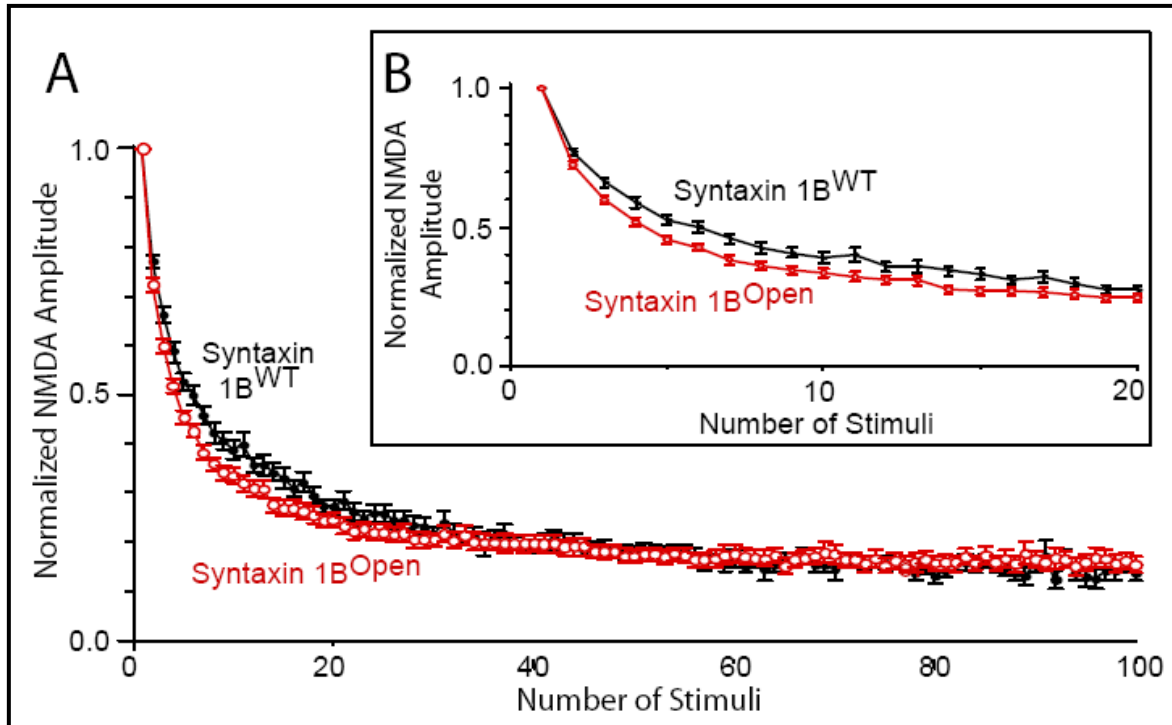


**Figure 1.9. Comparative analysis of the synaptic release probability  $P_r$  in syntaxin 1B<sup>WT</sup> and 1B<sup>Open</sup> synapses using the irreversible NMDA-receptor blocker MK-801.** The size of the normalized NMDA receptor-dependent EPSC is plotted as a function of the stimulus number after addition of MK-801. The inset shows the initial responses expanded in scale.

### **Ca<sup>2+</sup>-dependence of neurotransmitter release**

The release data suggest that the syntaxin-1B<sup>Open</sup> mutation simultaneously decreases the size of the RRP and increases the releasability of primed vesicles in the RRP. Then it was tested whether this extends to the apparent Ca<sup>2+</sup>-sensitivity of release. In these experiments, I measured EPSCs at external Ca<sup>2+</sup>-concentrations of 1-12 mM (with a constant 1 mM extracellular Mg<sup>2+</sup>-concentration). To control for possible run-down of EPSC amplitudes during the experiment, I determined control EPSCs in the standard external solution (4 mM Ca<sup>2+</sup>/4 mM Mg<sup>2+</sup>) before and after every test Ca<sup>2+</sup>-concentration, and normalized the test EPSC amplitudes for the control responses (Fig. 1.8.F).

Examination of syntaxin-1A<sup>KO</sup> and 1A<sup>WT</sup> neurons at a single test Ca<sup>2+</sup>-concentration (12 mM Ca<sup>2+</sup>/1 mM Mg<sup>2+</sup>) showed the same 1.6-fold potentiation of the EPSCs in syntaxin-1A<sup>WT</sup> and 1A<sup>KO</sup> neurons (data not shown), indicating that the Ca<sup>2+</sup> sensitivity of neurotransmitter release is not significantly altered in syntaxin-1A<sup>KO</sup> neurons. In syntaxin-1B<sup>Open</sup> synapses, however, the apparent Ca<sup>2+</sup>-sensitivity of synaptic responses was significantly enhanced (Fig. 1.8.G). For example, the EPSC amplitudes were relatively increased in the syntaxin-1B<sup>Open</sup> mutant at 1 mM extracellular Ca<sup>2+</sup> (EPSC ratio in 1 Ca<sup>2+</sup>/1 Mg<sup>2+</sup> vs. standard 4 Ca<sup>2+</sup>/4 Mg<sup>2+</sup>: 1B<sup>WT</sup>=0.36 ± 0.03 [16]; 1B<sup>Open</sup>=0.52 ± 0.04 [19] *p*=0.010), whereas at 12 mM extracellular Ca<sup>2+</sup>, the EPSC amplitudes were relatively decreased (EPSC ratio in 12 Ca<sup>2+</sup>/1 Mg<sup>2+</sup> vs. standard 4 Ca<sup>2+</sup>/4 Mg<sup>2+</sup>: 1B<sup>WT</sup>=1.70 ± 0.09 [15]; 1B<sup>Open</sup>=1.38 ± 0.04 [15], *p*=0.014). This increase was probably not due to more Ca<sup>2+</sup>-influx because somatic Ca<sup>2+</sup>-current in the hippocampal neurons (data not shown) was not altered in syntaxin-1B<sup>Open</sup> neurons.

### Potentialiation of synaptic responses by phorbol esters

A current hypothesis (Sudhof, 2004) suggests that Munc18-1 initiates and catalyses vesicle priming by binding to syntaxin-1 in the closed conformation and mediating its conversion into an open conformation in collaboration with Munc13-1, another essential priming factor for synaptic vesicle exocytosis (Augustin et al., 1999). This hypothesis was supported by the striking finding that in *C. elegans*, deletions of *unc13* and of RIM (which binds to Munc13; Betz et al., 2001) can be reversed by overexpression of syntaxin-1<sup>Open</sup> (Richmond et al., 2001; Koushika et al., 2001). To test whether the syntaxin-1B<sup>Open</sup> mutation affects Munc13-1 functionally, I measured phorbol ester-induced augmentation of synaptic responses in syntaxin-1B<sup>Open</sup>-mutant mice. This augmentation is mediated by phorbol ester-binding to Munc13's (Rhee et al., 2002); thus, if Munc13 acts by opening up syntaxin, stimulation of Munc13 by phorbol esters should have a decreased effect on release in syntaxin-1B<sup>Open</sup> synapses. To test this hypothesis, I monitored the potentiation of synaptic responses by 1  $\mu$ M  $\beta$ -phorbol ester dibutyrate (PDBu) during continuous low-frequency stimulation. After obtaining stable baseline responses, I applied PDBu for 1 min, and subsequently washed out the PDBu for 5 min (Fig. 1.10.A). Amplitudes of EPSCs in PDBu were normalized to the initial baseline, and the degree of potentiation was measured after augmented responses reached steady state. PDBu caused a smaller degree of potentiation in syntaxin-1B<sup>Open</sup> synapses ( $1.45 \pm 0.05$ -fold [ $n=43$ ]) than in control synapses ( $2.44 \pm 0.13$  fold [ $n=45$ ];  $p<0.0001$ ). To determine whether the reduced potentiation in the syntaxin-1B<sup>Open</sup> synapses correlated with their increased release probability, I also measured the  $P_{vr}$ , in the

same cells, and found that the PDBu response was inversely related to the initial  $P_{vr}$  (Fig. 1.10.B).

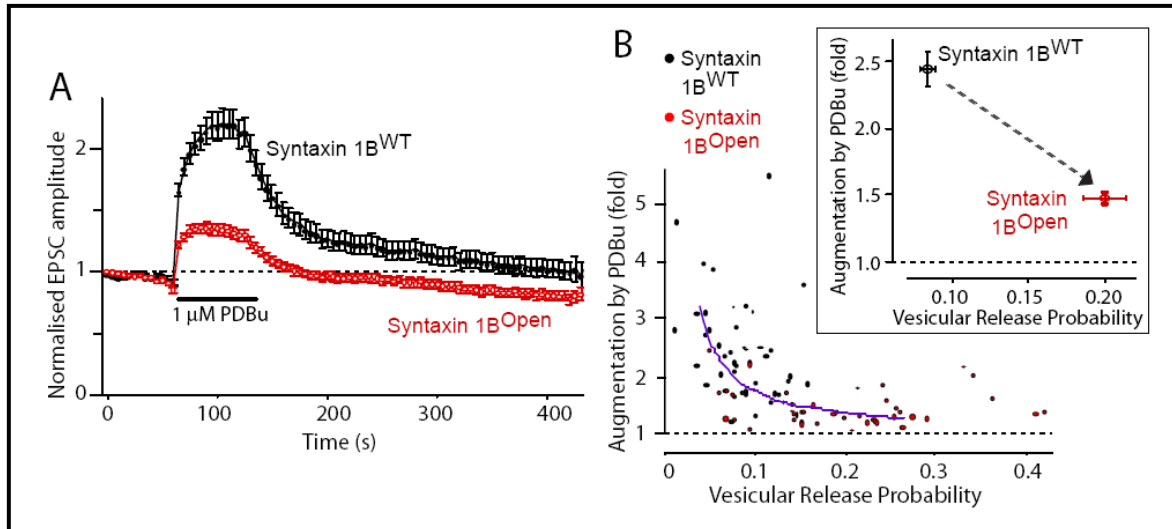


**Figure 1.10. Syntaxin-1B<sup>Open</sup> mutation reduces potentiation of synaptic responses by phorbol esters.** (A) Normalized synaptic responses before, during, and after application of 1  $\mu$ M PDBu. (B) Plot of the degree of potentiation of synaptic responses in a given neuron (y-axis) as a function of the vesicular release probability  $P_{vr}$  in the synapses of the same neuron (x-axis). The inset shows the mean values for these two parameters ( $1B^{WT} = 45$  neurons;  $1B^{Open} = 43$  neurons).



## Discussion

Synaptic exocytosis involves a reaction cascade that starts with vesicle docking which is independent of SNARE proteins, followed by vesicle priming which requires SNARE proteins, and ending in  $\text{Ca}^{2+}$ -triggered opening of the fusion pore which depends on the  $\text{Ca}^{2+}$ -binding protein synaptotagmin 1 or 2 (reviewed in Sudhof, 2004). In the present study, I have used a combined biophysical, genetic, and electrophysiological approach to investigate the physiological significance of the conformational switch of syntaxin-1 from a closed to an open form. My results confirm a critical role for syntaxin-1 in exocytosis that extends beyond its function as a SNARE protein, and involves a role in preparing vesicles for priming as well as in triggering fusion-pore opening of primed vesicles. Arguably my most important result was the finding that opening syntaxin-1 directly enhances triggering of exocytosis by  $\text{Ca}^{2+}$  or by hypertonic sucrose. Thus, although the open conformation of syntaxin-1 clearly alters steps upstream of SNARE complex assembly and priming as shown by the change in docked vesicles in chromaffin cells, rendering syntaxin-1 predominantly open also dramatically alters steps downstream of priming, as opening of syntaxin-1 lowers the energy barrier to  $\text{Ca}^{2+}$ -triggered fusion. To explain this finding, a model was proposed whereby priming is initiated by the Munc18/syntaxin-1 complex and executed by SNARE complex assembly such that it results in the variable assembly of SNARE complexes associated with individual vesicles, with the number of assembled SNARE complexes inversely proportional to the energy required to open the fusion pore. In conjunction with previous studies, my findings thus lead to a picture of syntaxin function in synaptic exocytosis suggesting that SNARE complex assembly is intimately linked both with the initiation of exocytosis (as reflected in

the docking defect in neuroendocrine syntaxin-1B<sup>Open</sup> cells) and with the final step in exocytosis (as reflected in the increase in Ca<sup>2+</sup>-triggering in syntaxin-1B<sup>Open</sup> synapses).

### **Properties of the syntaxin-1B<sup>Open</sup> mutation**

The 'LE' mutation introduced to generate syntaxin-1B<sup>Open</sup> mice likely alters the conformational equilibrium of syntaxin-1 without altering other properties of syntaxin-1. The 'LE' mutation in syntaxin-1B<sup>Open</sup> replaces only two residues in the linker sequence that connects the two functional cytoplasmic domains of syntaxin-1, i.e., the H<sub>abc</sub>-domain and the SNARE motif. Structurally, the linker sequence acts as a hinge that controls the intramolecular interactions between the H<sub>abc</sub>-domain and the SNARE motif, and the two linker residues that I mutated in syntaxin-1B<sup>Open</sup> stabilize these interactions (Dulubova et al, 1999; Misura et al., 2000). While my previous qualitative analysis indicated that this mutation disrupts the closed conformation of syntaxin-1 and prevents Munc18-1 binding (Dulubova et al., 1999), the more quantitative data presented here show that this mutation does not abolish the closed conformation, and does not negate Munc18-1 binding (Fig. 1.2 - 1.4). Instead, the syntaxin-1B<sup>Open</sup> mutation shifts the equilibrium from the closed towards the open conformation of syntaxin-1, suggesting that it decreases the abundance of Munc18/syntaxin-1 complexes and favors SNARE complex assembly.

### **Role of closed syntaxin-1 in vesicle docking**

I find that in syntaxin-1B<sup>Open</sup> synapses, ~25% more synaptic vesicles are docked at the active zone (Fig. 1.5.D), and the size of synaptic contacts is increased by ~20% (Fig.

1.5.F). The moderate increase in the number of docked vesicle and the size of syntaxin-1B<sup>Open</sup> synapses is unlikely to be a compensatory effect because synaptobrevin-2 and RIM1 $\alpha$  KO mice exhibit even larger decrease in the RRP but display no changes in either vesicle docking or synapse size (e.g., sy; Schoch et al., 2002; Calakos et al., 2004; Deak et al., 2005). Thus the increase in vesicle docking and synapse size is a specific consequence of opening syntaxin-1B. In syntaxin-1B<sup>Open</sup> chromaffin cells, by contrast, vesicle docking was decreased by ~75% (Fig. 1.5.L). In agreement with previous studies showing that Munc18-1 is not required for vesicle docking in synapses (Verhage et al., 2000) but is required for vesicle docking in chromaffin cells (Voets et al., 2001; see also Fig. 1.5.L), these results reveal that vesicle docking, as defined morphologically, involves distinct mechanisms in synapses and chromaffin cells. My results differ, however, from those obtained in *C. elegans* synapses suggesting where synaptic vesicle docking was prevented by unc-18 mutations (Weimer et al., 2003), indicating that synaptic vesicle docking in *C. elegans* may be more similar to chromaffin cells than to vertebrate synapses.

It seems likely that in synapses, the active zone protein scaffold captures vesicles before the function of Munc18-1 prepares vesicles for priming, and that as a result Munc18-1 is not required for synaptic vesicle docking. Such a mechanism – that would be absent from chromaffin cells which lack active zone proteins – would allow synapses to efficiently recruit vesicles during high-frequency stimulus trains. In the absence of such a mechanism in chromaffin cells, the function of Munc18-1 bound to syntaxin-1 appears to be a nucleating event in recruiting and docking vesicles. However, the function of Munc18-1 in chromaffin cell exocytosis, and by extension in all exocytosis, does not depend on assembly of SNARE

complexes because in chromaffin cells, as in synapses, deletion of synaptobrevin (VAMP) – the vesicular SNARE protein with which syntaxin forms a complex during fusion – does not interfere with vesicle docking. These results thus show that in chromaffin cells, and by extension in all fusion reactions, closed syntaxin-1 and Munc18-1 are required for a step in fusion that operates upstream of SNARE complex assembly.

### **Munc18/syntaxin complex in vesicle priming**

My data show that opening syntaxin-1 decreases the concentration of Munc18/syntaxin complexes to <5% of wildtype levels (Fig. 1.4), and lowers the number of primed vesicles in the RRP by ~45% (Fig. 1.7.B). This observation is consistent with previous results suggesting that Munc18 initiates vesicle priming and provides evidence for the hypothesis that the amount of Munc18/syntaxin-1 complexes determines the number of slots for primed vesicles in the RRP. Since the number of docked vesicles is slightly increased, and not decreased, in syntaxin-1B<sup>Open</sup> synapses, our results argue against the notion that the RRP corresponds precisely to docked vesicles (Schikorski and Stevens, 2001), but agrees with studies in cerebellar synapses that documented a similar lack of a correlation (Xu-Friedman et al., 2001). The fact that the RRP decrease is much less than the decline in the levels of the Munc18/syntaxin-1 complexes agrees with the observation that 50% changes in SNAP-25, synaptobrevin 2, or Munc18-1 in the corresponding heterozygous KO mice do not in themselves induce a major change in the RRP (data not shown).

### **The closed conformation of syntaxin-1B controls fusion pore opening**

Although syntaxin-1B<sup>Open</sup> synapses contain ~45% fewer release-ready vesicles (Fig. 1.7.B), these vesicles exhibit a >2-fold increase in spontaneous fusion (Figs. 1.6.C and D), are hypersensitive to sucrose (Figs. 1.7.C, F, G, and J), and are more responsive to Ca<sup>2+</sup>. The latter effect manifests in a >2-fold increase in the vesicular release probability  $P_{vr}$  (Fig. 1.8.D), an almost 2-fold enhanced apparent Ca<sup>2+</sup>-affinity of release (Fig. 1.8.G), and a ~2-fold increase in use-dependent synaptic depression (Figs. 1.8.E and F). The striking fusion phenotype of syntaxin-1B<sup>Open</sup> synapses is not an indirect consequence of the decrease in SNARE proteins and/or of the decline in the RRP in syntaxin-1B<sup>Open</sup> synapses because KO mice lacking SNARE proteins, RIM1 $\alpha$ , or Munc13-1 exhibit more severe changes in the levels of SNARE proteins and/or vesicle priming, but rather display a decrease in spontaneous and evoked fusion (Augustin et al., 1999; Schoch et al., 2001; Verhage et al., 2000; Washbourne et al., 2001). The fusion phenotype of the syntaxin-1B<sup>Open</sup> mice is not caused by an impairment of Munc18-1 function or Munc18-1 binding to syntaxin-1 because inactivation of Munc18-1 also produces a phenotype in synaptic vesicle fusion opposite to that of the syntaxin-1B<sup>Open</sup> mutation (Verhage et al., 2000). Thus, the increased ease with which vesicles in syntaxin-1B<sup>Open</sup> synapses fuse is a direct consequence of the mutation.

Primed synaptic vesicles can be thought of as being suspended in an intermediate energy state in which fusion was initiated, but an energy barrier prevents the progression of fusion to fusion-pore opening. According to this view, Ca<sup>2+</sup> and hypertonic solutions induce complete fusion by providing energy to overcome the barrier; when the barrier is lowered, more primed vesicles fuse spontaneously, and lower amounts of energy are required to evoke fusion. Our results demonstrate that opening up syntaxin-1 lowers the energy barrier of

synaptic vesicles to fusion, i.e., the energy barrier to fusion is provided, at least in part, by the closed conformation of syntaxin. Since – as revealed in the docking defect in syntaxin-1B<sup>Open</sup> chromaffin cells – syntaxin-1B<sup>Open</sup> acts upstream of SNARE complex assembly, the effect of this mutation has on triggering fusion-pore opening, downstream of SNARE complex assembly, was unexpected. How is it possible that such an upstream acting mutation alters the downstream Ca<sup>2+</sup>-triggering of synaptic vesicle exocytosis? At least three hypotheses can be envisioned to explain this effect:

*1. Primed vesicles lack assembled SNARE complexes, and Ca<sup>2+</sup> or hypertonic sucrose triggers fusion by opening up syntaxin-1 and inducing SNARE complex assembly.* The simplicity of this model is attractive, but existing evidence argues against it. It is difficult to envision a molecular mechanism that would allow such a dramatic conformational change in syntaxin-1 and assembly of the SNARE complex on the time scale of Ca<sup>2+</sup>-triggered release (ca. 100  $\mu$ s). Experimentally, it is known that complexins are required for Ca<sup>2+</sup>-triggering of fusion (Reim et al., 2001). Since complexins only bind to assembled SNARE complexes (McMahon et al., 1995), this observation indicated that SNARE complex assembly must occur prior to Ca<sup>2+</sup>-triggering. A variation of this model would be that primed vesicles are associated with pre-assembled syntaxin/SNAP-25 heterodimers that would allow very rapid SNARE complex assembly with free synaptobrevin on synaptic vesicles (Rickman et al., 2006). However, for syntaxin/SNAP-25 heterodimers to assemble in this model, closed syntaxin-1 would have to be opened, and thus the triggering step should not be altered by the syntaxin-1B<sup>Open</sup> mutation.

2. *Primed vesicles are composed of two subpopulations, more excitable primed vesicles with a lower energy barrier to fusion that are associated with 'open' syntaxin, and less excitable primed vesicles with 'closed' syntaxin and a higher energy barrier to fusion.* In syntaxin-1B<sup>Open</sup> synapses, vesicles would thus be shifted from the less excitable to the more excitable subpopulation, causing an overall increase in excitability. However, this hypothesis has a major experimental and a major conceptual problem. Experimentally, this hypothesis does not account for the fact that the syntaxin-1B<sup>Open</sup> mutation not only shifts vesicles to a greater degree of excitability within a preexisting range, but increases vesicle excitability in absolute terms (Figs. 1.7.C, F, and G). Conceptually, although subpopulations of "superprimed" or "immediately releasable" vesicles have been postulated in studies of chromaffin cells and synapses in the Calyx of Held and the hippocampus (Voets et al., 1999; Trommershäuser et al., 2003; Schlüter et al., 2006), this hypothesis would predict a much more profound division of readily-releasable vesicles into two separate classes. The vesicles in the RRP are heterogeneous in that they are triggered by different  $\text{Ca}^{2+}$ -concentrations, but fall into a continuum of responsiveness, not into distinct classes. The heterogeneity of vesicles is not only due to differences in the distance of the vesicles from  $\text{Ca}^{2+}$ -channels, but also due to an intrinsic heterogeneity in terms of their 'fusability', as revealed by the fact that some vesicles are more susceptible to sucrose than others. To rephrase the same argument in different terms, the  $\text{Ca}^{2+}$ -dependence of the vesicular release probability  $P_{\text{vr}}$  means that there is no physically defined subpool.

3. *A primed vesicle is linked to the active zone by multiple copies of SNARE proteins that are in different states of SNARE complex assembly, creating partially fused states that*

*depend on the number of assembled SNARE complexes.* The phenotype of the syntaxin-1B<sup>Open</sup> synapses would then be explained by the fact that the relative proportion of assembled SNAREs shifts to a larger number. Again, 'assembled SNARE complexes' could mean here either truly assembled SNARE complexes, and/or assembled syntaxin/SNAP-25 heterodimers. This would create a continuum of vesicles in the RRP, and explain how shifting to an open syntaxin lowers the energy barrier to fusion. Only this model fits the available data, suggesting that it may be the most appropriate at present.

### **Lowered phorbol ester response in syntaxin-1B<sup>Open</sup> synapses**

The ~3-fold reduction in synaptic potentiation by phorbol esters in syntaxin-1B<sup>Open</sup> synapses (Fig. 1.10.A) correlates precisely with the increase in vesicular release probability in these synapses (Fig. 1.10.B). The decreased phorbol ester response is not a direct consequence of the ~45% reduction in the RRP because RIM1 $\alpha$ -deficient synapses exhibit a similar decline in the RRP but display an increase, not a decrease, in phorbol ester-induced potentiation of synaptic responses (Calakos et al., 2004). The most parsimonious explanation for the occlusion of phorbol ester responses in syntaxin-1B<sup>Open</sup> synapses is that phorbol esters facilitate the opening of syntaxin-1, which would agree with the fact that the syntaxin-1B<sup>Open</sup> mutation does not completely open syntaxin-1 (Figs. 1.2 and 1.3) or abolish the phorbol ester response (Fig. 1.10.A). Since the major receptor for the phorbol ester-dependent potentiation of release is Munc13 (Rhee et al., 2001), the occlusion of the phorbol ester response by syntaxin-1B<sup>Open</sup> provides further evidence for the hypothesis that Munc13 acts on assembly of SNARE complexes. This hypothesis is consistent with the observation that overexpression



of syntaxin-1B<sup>Open</sup> by-passes the deletion of unc-13 in *C. elegans* (Richmond et al., 2001), and that Munc13 is required for the SNARE-dependent priming of synaptic vesicles (Augustin et al., 1999). In terms of our model 3 described above, this hypothesis implies that phorbol esters acting on Munc13 normally increase the number of assembled SNARE complexes associated with a primed vesicle, and that this effect is partially occluded in the syntaxin-1B<sup>Open</sup> mutant synapses because the opening of syntaxin-1 has already achieved such an effect.

## References

- Araç, D., Chen, X., Khant, H.A., Ubach, J., Ludtke, S.J., Kikkawa, M., Johnson, A.E., Chiu, W., Südhof, T.C., and Rizo, J.** (2006) Close membrane-membrane proximity induced by  $\text{Ca}^{2+}$ -dependent multivalent binding of synaptotagmin 1 to phospholipids. *Nature Struct. Mol. Biol.* **13**: 209-217.
- Arien H, Wiser O, Arkin IT, Leonov H, and Atlas D.** (2003) Syntaxin-1A modulates the voltage-gated L-type calcium channel (Ca(v)1.2) in a cooperative manner. *J. Biol. Chem.* **278**: 29231-29239.
- Augustin, I., Rosenmund, C., Südhof, T.C., and Brose, N.** (1999) Munc-13 is essential for fusion competence of glutamatergic synaptic vesicles. *Nature* **400**: 457-461.
- Bekkers, J.M., and Stevens, C.F.** (1991) Excitatory and inhibitory autaptic currents in isolated hippocampal neurons maintained in cell culture. *Proc. Natl. Acad. Sci. U.S.A.* **88**: 7834-7838.
- Bennett, M.K., Calakos, N., and Scheller, R.H.** (1992) Syntaxin: a synaptic protein implicated in docking of synaptic vesicles at presynaptic active zones. *Science* **257**: 255-259.
- Betz, A., Thakur, P., Junge, H.J., Ashery, U., Rhee, J.S., Scheuss, V., Rosenmund, C., Rettig, J., and Brose, N.** (2001) Functional interaction of the active zone proteins Munc13-1 and RIM1 in synaptic vesicle priming. *Neuron* **30**: 183-196.
- Bezprozvanny, I., Scheller, R.H., and Tsien, R.W.** (1995) Functional impact of syntaxin on gating of N-type and Q-type calcium channels. *Nature* **378**: 623-626.
- Borisovska, M., Zhao, Y., Tsytsyura, Y., Glyvuk, N., Takamori, S., Matti, U., Rettig, J., Südhof T, and Bruns D.** (2005) v-SNAREs control exocytosis of vesicles from priming to fusion. *EMBO J.* **24**: 2114-2126.
- Brunger, A.T.** (2005) Structure and function of SNARE and SNARE-interacting proteins. *Q. Rev. Biophys.* **9**, 1-47
- Bryant, N.J., and James, D.E. (2001) Vps45p stabilizes the syntaxin homologue Tlg2p and positively regulates SNARE complex formation. *EMBO J.* **20**: 3380-3388.
- Calakos, N., Schoch, S., Südhof, T.C., and Malenka R.C.** (2004) Multiple Roles for the Active Zone Protein RIM1 $\alpha$  in Late Stages of Neurotransmitter Release. *Neuron* **42**: 889-896.
- Carr, C.M., Grote, E., Munson, M., Hughson, F.M., and Novick, P.J.** (1999) Sec1p binds to SNARE complexes and concentrates at sites of secretion. *J. Cell Biol.* **146**: 333-344.

**Chandra, S., Gallardo, G., Fernández-Chacón, R., Schlüter, O.M., and Südhof, T.C.** (2005)  $\alpha$ -Synuclein Cooperates with CSP $\alpha$  in Preventing Neurodegeneration. *Cell* **123**: 383-396.

**Chen, Y.A., and Scheller RH.** (2001) SNARE-mediated membrane fusion. *Nat. Rev. Mol. Cell Biol.* **2**: 98-106.

**Collins, K.M., Thorngren, N.L., Fratti, R.A., and Wickner, W.T.** (2002) Sec17p and HOPS, in distinct SNARE complexes, mediate SNARE complex disruption or assembly for fusion. *EMBO J.* **24**: 1775-1786.

**Condliffe, S.B., Zhang, H., Frizzell, R.A.** (2004) Syntaxin-1A regulates ENaC channel activity. *J. Biol. Chem.* **279**: 10085-10092.

**Deák, F., Schoch, S., Liu, X., Südhof, T.C., and Kavalali, E.T.** (2004) Synaptobrevin/VAMP is Essential for Fast Synaptic Vesicle Endocytosis. *Nature Cell Biol.* **6**: 1102-1108.

**Deken, S.L., Beckman, M.L., Boos, L., and Quick, M.W.** (2000) Transport rates of GABA transporters: regulation by the N-terminal domain and syntaxin-1A. *Nat. Neurosci.* **3**: 998-1003.

**Dulubova I, Sugita S, Hill S, Hosaka M, Fernandez I, Südhof TC, and Rizo J.** (1999) A conformational switch in syntaxin during exocytosis. *EMBO J.* **18**: 4372-4382.

**Dulubova, I., Yamaguchi, T., Min, S.W., Gao, Y., Südhof, T.C., and Rizo, J.** (2002) How Tlg2p/syntaxin16 "snares" Vps45. *EMBO J.* **21**: 3620-3631.

**Fernandez, I., Ubach, J., Dulubova, I., Zhang, X., Südhof, T.C., and Rizo, J.** (1998) Three-dimensional structure of an evolutionarily conserved N-terminal domain of syntaxin 1A. *Cell* **94**: 841-849.

**Foletti, D.L., Lin, R., Finley, M.A., and Scheller, R.H.** (2000) Phosphorylated syntaxin-1 is localized to discrete domains along a subset of axons. *J. Neurosci.* **20**: 4535-4544.

**Garcia, E.P., Gatti, E., Butler, M., Burton, J., De Camilli, P.** (1994) A rat brain Sec1 homologue related to Rop and UNC18 interacts with syntaxin. *Proc. Natl. Acad. Sci. U.S.A.* **91**: 2003-2007.

**Harrison, S.D., Broadie, K., van de Goor, J., Rubin, G.M.** (1994) Mutations in the Drosophila Rop gene suggest a function in general secretion and synaptic transmission. *Neuron* **13**: 555-566.

**Hata, Y., Slaughter, C.A., and Südhof, T.C.** (1993) Synaptic vesicle fusion complex contains unc-18 homologue bound to syntaxin. *Nature* **366**: 347-351

**Hessler, N.A., Shirke, A.M., and Malinow, R.** (1993) The probability of transmitter release at a mammalian central synapse. *Nature* **366**: 569-572.

**Hurley, J.H., Cahill, A.L., Wang, M., and Fox, A.P.** (2004) Syntaxin-1A regulation of weakly inactivating N-type  $\text{Ca}^{2+}$  channels. *J. Physiol.* **560**: 351-363.

**Inoue, A., Obata, K., and Akagawa, K.** (1992) Cloning and sequence analysis of cDNA for a neuronal cell membrane antigen, HPC-1. *J. Biol. Chem.* **267**: 10613-10619.

**Jahn, R., Lang, T., and Südhof, T.C.** (2003) Membrane fusion. *Cell* **112**: 519-533.

**Katz, B.** (1969). The release of neural transmitter substances. *Liverpool: Liverpool University Press.*

**Kosodo, Y., Noda, Y., Adachi, H., and Yoda, K.** (2002) Binding of Sly1 to Sed5 enhances formation of the yeast early Golgi SNARE complex. *J. Cell Sci.* **115**: 3683-3691.

**Koushika, S.P., Richmond, J.E., Hadwiger, G., Weimer, R.M., Jorgensen, E.M., and Nonet, M.L.** (2001) Apoptotic-docking role for active zone protein Rim. *Nat. Neurosci.* **4**: 997-1005.

**Leung, Y.M., Kang, Y., Gao, X., Xia, F., Xie, H., Sheu, L., Tsuk, S., Lotan, I., Tsushima, R.G., and Gaisano, H.Y.** (2003) Syntaxin-1A binds to the cytoplasmic C terminus of Kv2.1 to regulate channel gating and trafficking. *J. Biol. Chem.* **278**: 17532-17538.

**Lisman, J.E., and Harris, K.M.** (1993) Quantal analysis and synaptic anatomy--integrating two views of hippocampal plasticity. *Trends Neurosci.* **16**: 141-147.

**Misura, K.M., Scheller, R.H., and Weis, W.I.** (2000) Three-dimensional structure of the neuronal-Sec1-syntaxin1a complex. *Nature* **404**: 355-362.

**Naren, A.P., Nelson, D.J., Xie, W., Jovov, B., Pevsner, J., Bennett, M.K., Benos, D.J., Quick, M.W., and Kirk, K.L.** (1997) Regulation of CFTR chloride channels by syntaxin and Munc18 isoforms. *Nature* **390**: 302-305

**Pevsner, J., Hsu, S.C., and Scheller, R.H.** (1994) n-Sec1: a neural-specific syntaxin-binding protein. *Proc. Natl. Acad. Sci. U.S.A.* **91**: 1445-1449.

**Reim, K., Mansour, M., Varoqueaux, F., McMahon, H.T., Südhof, T.C., Brose, N., and**

**Rosenmund, C.** (2001) Complexins regulate a late step in  $\text{Ca}^{2+}$ -dependent neurotransmitter release. *Cell* **104**: 71-81.

**Rhee, S.-R., Betz, A., Pyott, S., Reim, K., Varoqueaux, F., Augustin, I., Hesse, D., Südhof, T.C. Takahashi, M., Rosenmund, and Brose, N.** (2002) Phorbol ester- and diacylglycerol-induced augmentation of neurotransmitter release from hippocampal neurons is mediated by Munc13s and not by PKCs. *Cell* **108**: 121-133.

**Richmond, J.E., Weimer, R.M., and Jorgensen ,E.M.** (2001) An open form of syntaxin bypasses the requirement for UNC-13 in vesicle priming. *Nature* **412**: 338-341.

**Richmond, J.E., and Broadie, K.S.** (2002) The synaptic vesicle cycle: exocytosis and endocytosis in *Drosophila* and *C. elegans*. *Curr. Opin. Neurobiol.* **12**: 499-507.

**Rickman, C., Jimenez, J.L., Graham, M.E., Archer, D.A., Soloviev, M., Burgoyne, R.D., and Davletov, B.** (2006) Conserved prefusion protein assembly in regulated exocytosis. *Mol. Biol. Cell* **17**: 283-294.

**Rosenmund, C., Clements, J.D., and Westbrook, G.L.** (1993) Nonuniform probability of glutamate release at a hippocampal synapse. *Science* **262**: 754-757.

**Rosenmund, C., and Stevens, C.F.** (1996) Definition of the readily releasable pool of vesicles at hippocampal synapses. *Neuron* **16**: 1197-1201.

**Saifee, O., Wei, L., Nonet, M.L.** (1998) The *Caenorhabditis elegans* unc-64 locus encodes a syntaxin that interacts genetically with synaptobrevin. *Mol. Biol. Cell* **9**: 1235-1252.

**Schikorski, T., and Stevens, C.F.** (2001) Morphological correlates of functionally defined synaptic vesicle populations. *Nat. Neurosci.* **4**: 391-395.

**Schlüter, O., Südhof, T.C., and Rosenmund, C.** (2006) Rab3 Superprimes Synaptic Vesicles for Release: Implications for Short Term Synaptic Plasticity. *J. Neurosci.* **26**: 1239-1246.

**Schoch, S., Castillo, P.E., Jo, T., Mukherjee, K., Geppert, M., Wang, Y., Schmitz, F., Malenka, R.C., and Südhof, T.C.** (2002) RIM1 $\alpha$  forms a protein scaffold for regulating neurotransmitter release at the active zone. *Nature* **415**: 321-326.

**Schulze, K.L., Broadie, K., Perin, M.S., and Bellen, H.J.** (1995) Genetic and electrophysiological studies of *Drosophila* syntaxin-1A demonstrate its role in nonneuronal secretion and neurotransmission. *Cell* **80**: 311-320.

**Sheng, Z.H., Rettig, J., Cook, T., Catterall, W.A.** (1996) Calcium-dependent interaction of N-type calcium channels with the synaptic core complex. *Nature* **379**: 451-454.

**Söllner, T., Whiteheart, S.W., Brunner, M., Erdjument-Bromage, H., Geromanos, S., Tempst, P., Rothman, J.E.** (1993b) SNAP receptors implicated in vesicle targeting and fusion. *Nature* **362**: 318-324.

**Sorensen, J.B.** (2005) SNARE complexes prepare for membrane fusion. *Trends Neurosci.* **28**: 453-455.

**Südhof, T.C.** (2004) The synaptic vesicle cycle. *Annu. Rev. Neurosci.* **27**: 509-547.

**Sung, U., Apparsundaram, S., Galli, A., Kahlig, K.M., Savchenko, V., Schroeter, S., Quick, M.W., Blakely, R.D.** (2003) A regulated interaction of syntaxin-1A with the antidepressant-sensitive norepinephrine transporter establishes catecholamine clearance capacity. *J. Neurosci.* **23**: 1697-1709.

**Sutton, K.G., McRory, J.E., Guthrie, H., Murphy, T.H., Snutch, T.P.** (1999) P/Q-type calcium channels mediate the activity-dependent feedback of syntaxin-1A. *Nature* **401**: 800-804.

**Sutton, R.B., Fasshauer, D., Jahn, R., and Brunger, A.T.** (1998) Crystal structure of a SNARE complex involved in synaptic exocytosis at 2.4 Å resolution. *Nature* **395**: 347-353.

**Trommershauser, J., Schneggenburger, R., Zippelius, A., and Neher, E.** (2003) Heterogeneous presynaptic release probabilities: functional relevance for short-term plasticity. *Biophys. J.* **84**: 1563-1579.

**Verhage, M., Maia, A.S., Plomp, J.J., Brussaard, A.B., and Heeroma, J.H.** (2000) Synaptic assembly of the brain in the absence of neurotransmitter secretion. *Science* **287**: 864-69.

**Voets, T., Neher, E., and Moser, T.** (1999) Mechanisms underlying phasic and sustained secretion in chromaffin cells from mouse adrenal slices. *Neuron* **23**: 607-615.

**Voets, T., Toonen, R.F., Brian, E.C., de Wit, H., Moser, T., Rettig, J., Südhof, T.C., Neher, E., and Verhage, M.** (2001) Munc18-1 promotes large dense-core vesicle docking. *Neuron* **31**: 581-591.

**Weber, T., Zemelman, B.V., McNew, J.A., Westermann, B., Gmachl, M., Parlati, F., Sollner, T.H., and Rothman, J.E.** (1998) SNAREpins: minimal machinery for membrane fusion. *Cell* **92**: 759-772.

**Weimer, R.M., Richmond, J.E., Davis, W.S., Hadwiger, G., Nonet, M.L., and**

**Jorgensen, E.M.** (2003) Defects in synaptic vesicle docking in unc-18 mutants. *Nat. Neurosci.* **6**: 1023-1030.

**Xu-Friedman, M.A., Harris, K.M., Regehr, W.G.** (2001) Three-dimensional comparison of ultrastructural characteristics at depressing and facilitating synapses onto cerebellar Purkinje cells. *J. Neurosci.* **21**: 6666-6672.

**Yamaguchi, T., Dulubova, I., Min, S.W., Chen, X., Rizo, J., and Südhof, T.C.** (2002) Sly1 binds to Golgi and ER syntaxins via a conserved N-terminal peptide motif. *Developmental Cell* **2**: 295-305.

**Zucker, R.S., and Regehr, W.G.** (2002) Short-term synaptic plasticity. *Annu. Rev. Physiol.* **64**: 355-405.

## **Chapter II**

### **Genetic approach to analyze the differential function of syntaxin-1A and 1B**



## Introduction

A general mechanism, driven by specific interactions between N-ethylmaleimide-sensitive factor (NSF), soluble NSF attachment proteins (SNAP) and the soluble N-ethylmaleimide-sensitive fusion protein attachment protein receptor (SNARE) proteins has been proposed for membrane fusion in eukaryotic cells (1, 2). There are three SNARE proteins, synaptobrevin-2, synaptosomal-associated protein of 25kDa (SNAP-25) and syntaxin-1 (2, 3). While synaptobrevin-2 is associated with synaptic vesicle, SNAP-25 and syntaxin-1 are with plasma membrane mostly in presynaptic active zone. In hypothesis, one helix from synaptobrevin-2, two from SNAP-25 and one from syntaxin-1 form 4  $\alpha$ -helical bundles called as ternary SNARE complex in order to catalyze the formation of fusion pore, which causes to release the contents of synaptic vesicle, called chemical neurotransmitters (4). While other SNARE proteins form  $\alpha$ -helical bundles using most of their sequences, syntaxin-1 has a relatively long N-terminal region, where three helices, called H<sub>a</sub>, H<sub>b</sub> and H<sub>c</sub>, reside (4).

Isoforms of the three SNAREs, SNAP-25 (a, b), synaptobrevin (I, II) and syntaxin 1(1A, 1B) have been identified in neurons (5-7). In nerve terminals, those isoforms of SNAREs show differential distribution patterns in some areas of central and peripheral nervous system. Interestingly, syntaxin-1A and syntaxin-1B are usually co-localized with synaptobrevin-1 and synaptobrevin-2, respectively, suggesting their differential / overlapping roles in nervous system (8, 9). Also there have been some reports indicating differential / overlapping expression pattern for syntaxin-1A and 1B (8, 9). Therefore, it is interesting to pursue the research whether these two proteins play a redundant / distinctive role *in vivo*.

Munc18-1 (also known as nSec1, Munc18-a, and rbSec 1) is a cytosolic protein of 68 kDa, a mammalian member of the Sec1/Munc18-related proteins (SM proteins) that shows a specific expression in brain (10). Munc18-1 was first identified in brain based on its ability to bind syntaxin with high affinity and was later cloned by homology screening based on its similarity to *Drosophila* rop and *C. elegans* Unc18 (11-13). Most of known SM proteins appear to interact specifically with syntaxin family members, raising the possibility that perhaps SM protein is essential for the function of syntaxin family members (11, 14-16). Since syntaxin-Munc18-1 complex is mutually exclusive of SNARE complex formation in most species (14, 17, 18), although that hypothesis is still debating (19), it has been suggested that Munc18-1 is a negative regulator for neurotransmission. In agreement with this idea are studies showing a reduction of neurotransmitter release in *Drosophila* and squid after introduction of the respective Munc18-1 orthologs Rop and s-Sec1 (20, 21). In contrast, secretion is blocked in *S. cerevisiae* Sec1p mutants and in *Drosophila* Rop null mutants and synaptic transmission is completely inhibited in mouse Munc18-1 null mutants (22-24), suggesting a positive role for SM proteins in neurotransmission. Therefore, their exact molecular function still remains elusive. In order to study the differential functions of syntaxin-1A and 1B, it is essential to study their binding properties to Munc18-1 and other SNARE proteins *in vivo*.

In this study, syntaxin-1A and 1B GFP-knock-in mice were generated and studied in order to identify their distinct, but overlapping role in membrane traffic and neurotransmission. However, unexpectedly, both GFP knock-in proteins become non-functional, suggesting the mimics of knock-out. While it was recently reported there is a

specific defect in long-term potentiation, consolidation of conditioned fear memory in syntaxin-1A KO mice, we still do not understand the phenotype of syntaxin-1B knock-out mice. Using advantages of syntaxin-1B GFP knock-in mice, I studied both the effect of syntaxin-1B knock-out and differential functions of syntaxin-1A and 1B. Since syntaxin-1B open-conformation mutant mice also shows the reduction of syntaxin-1B protein, but epileptic seizure phenotype (see Chapter I), it is interesting to know what the relationship between these two knock-in mice is: open-conformation mice and loss-of-function mice of syntaxin-1B.

## **Materials and Methods**

### **Generation of syntaxin-1A- and 1B GFP-KI mice**

Targeting strategy to generate syntaxin-1A and -1B GFP-KI mice was described in Chapter I.

### **Weight and survival analyses**

The offspring from each breeding were toe-tagged at postnatal day 7 (P7) and weight measurements and survival analyses were performed on P7, P14, P21 and P28.

### **Densimetric quantitation**

Total brains were collected from each mouse at the same age and homogenated using detergent-free buffer. After complete homogenization, SDS sampling buffer was added to the homogenized sample and boiled for 10 minutes. After boiling, the samples were passed through the 27-gauge, 0.5-inch needle (BD Biosciences) for at least five times.

Once SDS-PAGE analysis is done, primary antibody was added accompanied with antibody, such as VCP and GDI as a loading control. I<sup>125</sup>-conjugated secondary antibody was used and image was read and quantitated by phosphorimager.

### **Morphological analysis of brain**

Anesthetized mice were perfused with 4% paraformaldehyde in phosphate buffer. Brains were cryoprotected and cut on a cryostat (30- $\mu$ m sections). Sections were incubated with the primary antibodies overnight at 4 °C, followed by secondary and secondary

antibody-labeled PAP (peroxidase-antiperoxidase). Free-floating sections were mounted on gelatin-coated slides with permount. Images were taken using standard microscope.

### **Morphological analysis of neuromuscular junction**

Mice were sacrificed and diaphragm muscle was collected. Muscles were teased into fine muscle and incubated with the primary antibodies, followed by secondary antibody and Texas-red-conjugated  $\alpha$ -bungarotoxin. After wash, muscle was whole-mounted using permount. Images were taken using confocal-microscope.

### **Immunoprecipitation**

Mouse brain homogenates with 0.5% Triton X-100 was pre-mixed with GFP polyclonal antibody followed by protein A/G beads (Santa Cruz). Wash 6 times with phosphate buffered saline and the bead binding proteins were analyzed by SDS-PAGE and immunoblot and densimetric quantitation (described previously).

## Results

### Generation of syntaxin-1A- and 1B GFP-KI mice and expression level of syntaxin-1A and 1B proteins

To investigate the differential expression patterns of syntaxin-1A and -1B, ECFP or EYFP cassette was introduced within exon 2 of syntaxin-1A or exon 7 of syntaxin-1B by homologous recombination, so as to have the integrated cassette fused to N-terminus or C-terminus of proteins, respectively (Fig. 2.1). For syntaxin-1B targeting construct, neomycin cassette is not removed, because deletion of neomycin cassette did not recover expression level of fusion protein (Fig. 2.1.B).

In order to evaluate the syntaxin-1 protein levels in syntaxin-1A<sup>KO</sup> and 1A<sup>KO</sup>/1B<sup>GFP</sup> lines, I prepared brain homogenates of WT, syntaxin-1A<sup>KO</sup> and 1A<sup>KO</sup>/1B<sup>GFP</sup> mice. Most of syntaxin-1 antibodies detect both syntaxin-1A and 1B but T3748, which specifically detects syntaxin-1A (Fig. 2.2.A). Indeed, syntaxin-1A protein is not detected in syntaxin-1A KO mouse brain and syntaxin-1B protein is almost not detected in syntaxin-1B GFP-KI mouse brain (Fig. 2.2.A). Next, I immunoquantitated the protein levels of GFP-syntaxin-1 fusion protein and WT syntaxin-1 protein independently. While GFP-syntaxin-1A fusion protein level is more than three fold increased compared to WT syntaxin-1A protein, GFP-syntaxin-1B fusion protein level is only about 10% of WT syntaxin-1B protein (Fig. 2.2.B). Since GFP-syntaxin-1B fusion protein level is greatly decreased, this mouse line was also called as 'hypomorph of syntaxin-1B' line. Note that the residual protein in GFP-KI syntaxin-1B homozygous mice is syntaxin-1A due to lack of specificity of antibody.

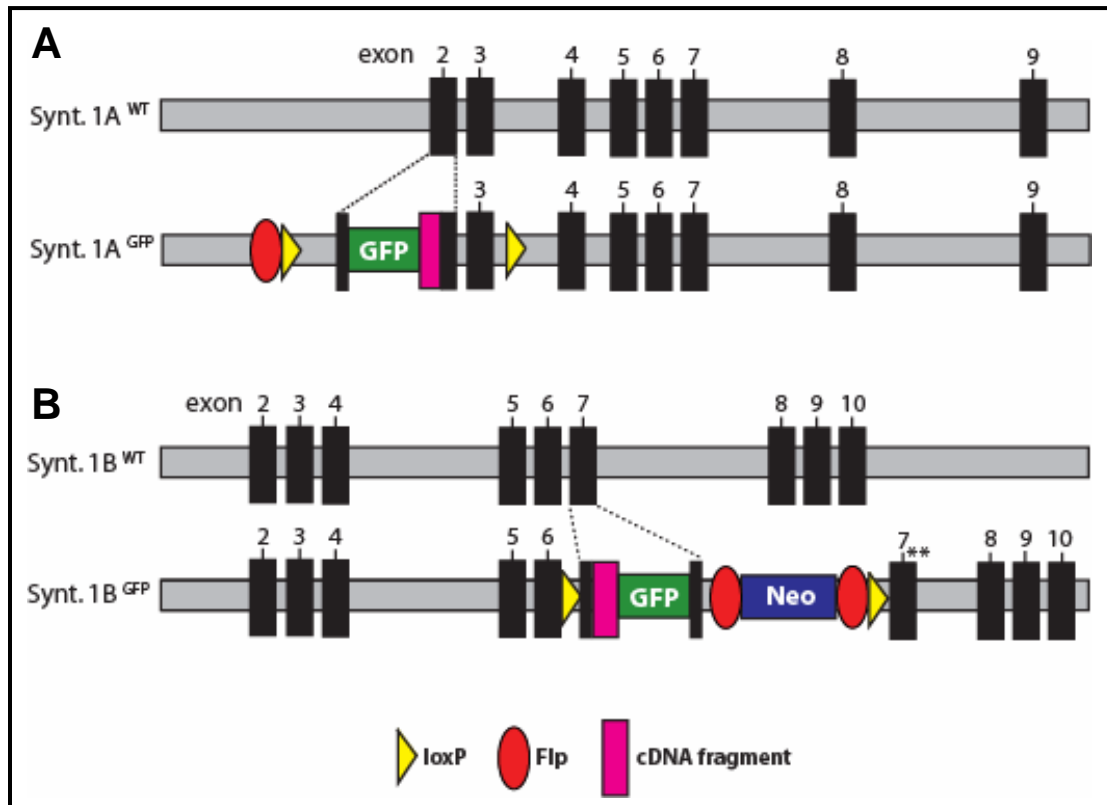


**Figure 2.1. Schematic diagram of targeting strategy to generate syntaxin-1A and syntaxin-1B GFP-KI (syntaxin-1A<sup>GFP</sup> and syntaxin-1B<sup>GFP</sup>) mice.** Numbered black rectangles illustrate coding exons; yellow and red triangles denote loxP and flp recombination sites, respectively.

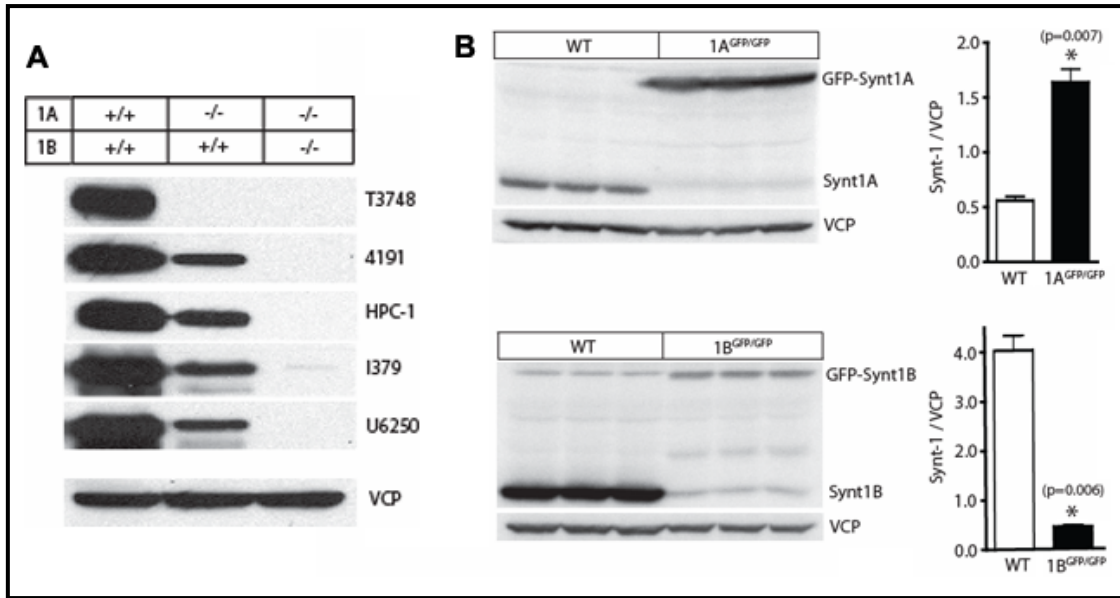


**Figure 2.2. Expression of syntaxin-1 and GFP-syntaxin fusion protein in syntaxin-1A<sup>GFP</sup> and syntaxin-1B<sup>GFP</sup> mice.** (A) Immunoblot analysis of total brain homogenates from wt, syntaxin-1A<sup>KO</sup> and double KO (1A<sup>KO</sup>/1B<sup>GFP</sup>) animals at E18.5 stage (30  $\mu$ g protein/lane) was performed. Blots were probed with various antibodies to syntaxin-1 and VCP (as a loading control). (B) GFP-syntaxin-1A fusion protein is more stabilized than GFP-syntaxin-1B fusion protein *in vivo*. Quantitative immunoblot analysis of total brain homogenates from 3 GFP-KI mice and 3 littermate wt mice was performed. Brain sample was collected at P30 from GFP-syntaxin1A KI line and collected at P14 from GFP-syntaxin 1B KI line. Blots were probed with antibodies to syntaxin-1 and VCP (as a loading control).



**Postnatal lethality of Syntaxin-1B<sup>GFP</sup> mice**

I checked the survival of offspring on postnatal day 7, 14, 21 and 28 days from intercrosses of double heterozygous mice for syntaxin-1A<sup>KO</sup> and syntaxin-1B<sup>GFP</sup> alleles. Double homozygous mice are not included in this study due to perinatal lethality. Except for double homozygous mice, the survival ratio from double heterozygous breeding is similar to Mendelian ratio (Fig. 2.3.A). However, while syntaxin-1A knock-out mice shows no obvious lethality, syntaxin-1B GFP knock-in mice start showing lethality on postnatal day 14 and no longer survive until postnatal day 21 (Fig. 2.3.A). Syntaxin-1B GFP knock-in mice also show severe growth retardation as shown in weight curve (Fig. 2.3.B). In accordance with survival data, they show severe motor incoordination and unbalanced movement behavior at P14 (data not shown).

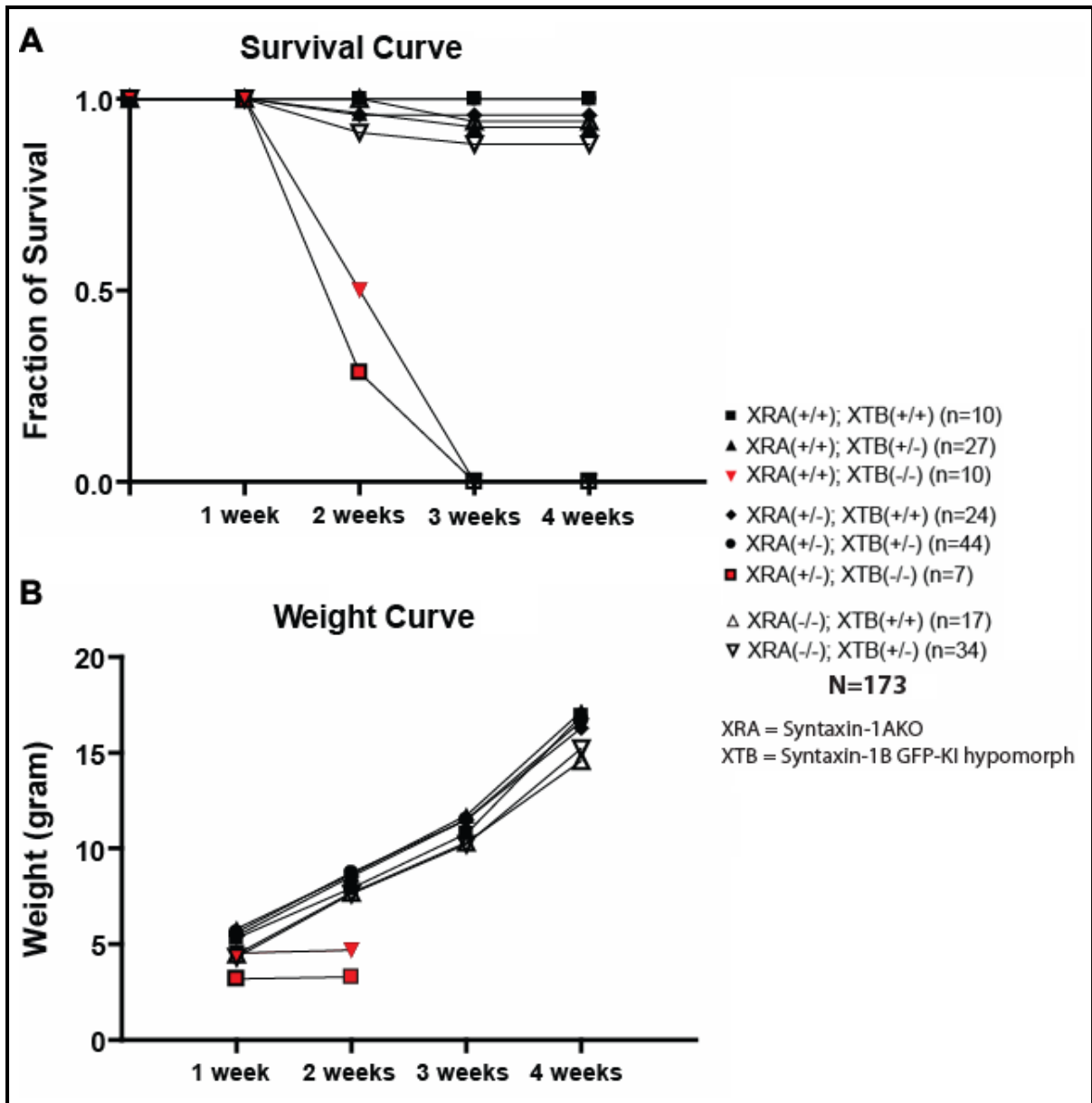


**Figure 2.3. Survival and weight studies of syntaxin-1A<sup>KO</sup> / syntaxin-1B<sup>GFP</sup> mice.** (A) Survival and (B) body weight analyses of double line mice of syntaxin-1A<sup>KO</sup> (XRA) / 1B<sup>GFP</sup> (XTB) were performed as a function of age at 1 week, 2 weeks, 3 weeks and 4 weeks after birth (Double homozygous mouse is not included in this graph, because it died on the date of birth).

**Functional redundancy between syntaxin-1A and 1B protein and failure of GFP-syntaxin-1A fusion protein to rescue perinatal lethality of syntaxin-1A<sup>KO</sup>/1B<sup>GFP</sup>**

In order to test the effects of loss of both syntaxin-1A and 1B proteins on mice survival, the survival for litters from double heterozygous breeding of syntaxin-1A<sup>KO</sup>/1B<sup>GFP</sup> mice at P7 was counted and compared to the Mendelian ratio. Again, while loss of syntaxin-1A protein alone does not affect the observed lethality of mice, the absence of both syntaxin-1A and 1B protein greatly reduced the postnatal survival of mice (Table 2.1). Interestingly, while in the presence of syntaxin-1A protein, loss of syntaxin-1B protein does not affect the survival ratio at P7, in the absence of syntaxin-1A protein, decrease in syntaxin-1B protein significantly reduced the survival ratio at P7 (Table 2.1). These results suggest there might be a functional redundancy between syntaxin-1A and 1B proteins.

Since syntaxin-1A<sup>KO</sup>/1B<sup>GFP</sup> mice showed a perinatal lethality, I tested whether GFP-Syntaxin-1A fusion protein can rescue that lethality. To investigate that, the double line of syntaxin-1A<sup>GFP</sup>/1B<sup>GFP</sup> was generated and the survival ratio at P7 from the double heterozygous breeding was counted and compared to the results from line of syntaxin-1A<sup>KO</sup>/1B<sup>GFP</sup> breedings. Unexpectedly, the survival results from both lines are not significantly different each other (Table 2.1), suggesting that N-terminal GFP-fusion makes syntaxin-1A protein non-functional *in vivo*.

**Table 2.1. Survival tables of mice of syntaxin-1A<sup>KO</sup> / 1B<sup>GFP</sup> and syntaxin-1A<sup>GFP</sup> / 1B<sup>GFP</sup> lines.** Survival analysis was performed from double heterozygous breeding of syntaxin-1A<sup>KO</sup> / 1B<sup>GFP</sup> (A) and syntaxin-1A<sup>GFP</sup> / 1B<sup>GFP</sup> (B) at 1 week after birth.

**A**

	XRA(+/-) XTB(+/-)	XRA(+/-) XTB(+/-)	XRA(-/-) XTB(+/-)	XRA(+/-) XTB(+/-)	XRA(+/-) XTB(+/-)	XRA(-/-) XTB(+/-)	XRA(+/-) XTB(+/-)	XRA(+/-) XTB(+/-)	XRA(-/-) XTB(+/-)
<b>Expected Ratio</b>	6.25%	12.5%	6.25%	12.5%	25%	12.5%	6.25%	12.5%	6.25%
<b>Observed Ratio</b>	5.78%	13.9%	9.8%	15.6%	25.4%	19.6%	5.78%	<b>4.0%</b>	<b>0%</b>

\* N=173

**B**

	XFA(+/-) XTB(+/-)	XFA(+/-) XTB(+/-)	XFA(-/-) XTB(+/-)	XFA(+/-) XTB(+/-)	XFA(+/-) XTB(+/-)	XFA(-/-) XTB(+/-)	XFA(+/-) XTB(+/-)	XFA(+/-) XTB(+/-)	XFA(-/-) XTB(+/-)
<b>Expected Ratio</b>	6.25%	12.5%	6.25%	12.5%	25%	12.5%	6.25%	12.5%	6.25%
<b>Observed Ratio</b>	13.2%	21.5%	8.3%	11.8%	27.1%	10.4%	4.2%	<b>2.8%</b>	<b>0%</b>

\* N=144

**Protein quantitation of syntaxin-1A<sup>KO</sup> /1B<sup>GFP</sup> mice**

The severe lethality of syntaxin-1B GFP-KI line intrigues me to try to check the changes of other synaptic marker protein levels. In order to investigate this question, at least three whole brain homogenates were prepared from WT, syntaxin-1A<sup>KO</sup>, and syntaxin-1B<sup>GFP</sup> mice at P14 and immunoquantitation experiment was performed using antibodies to a variety of synaptic marker proteins, such as SNARE proteins, active zone proteins etc. In contrast to the results from open-conformation mice, which show the reduced protein level of SNAP-25 (see Chapter I), SNARE protein levels are not disturbed in syntaxin-1B<sup>GFP</sup> mice (Fig. 2.4, Table 2.2). However, the protein level of Munc18-1, which is the major binding partner of syntaxin-1, is decreased about 50% (Fig. 2.4, Table 2.2). Therefore, it was noticed that the level of Munc18-1 protein is more decreased in syntaxin-1B GFP-KI than that of syntaxin-1B open-conformation mice (unpublished data).

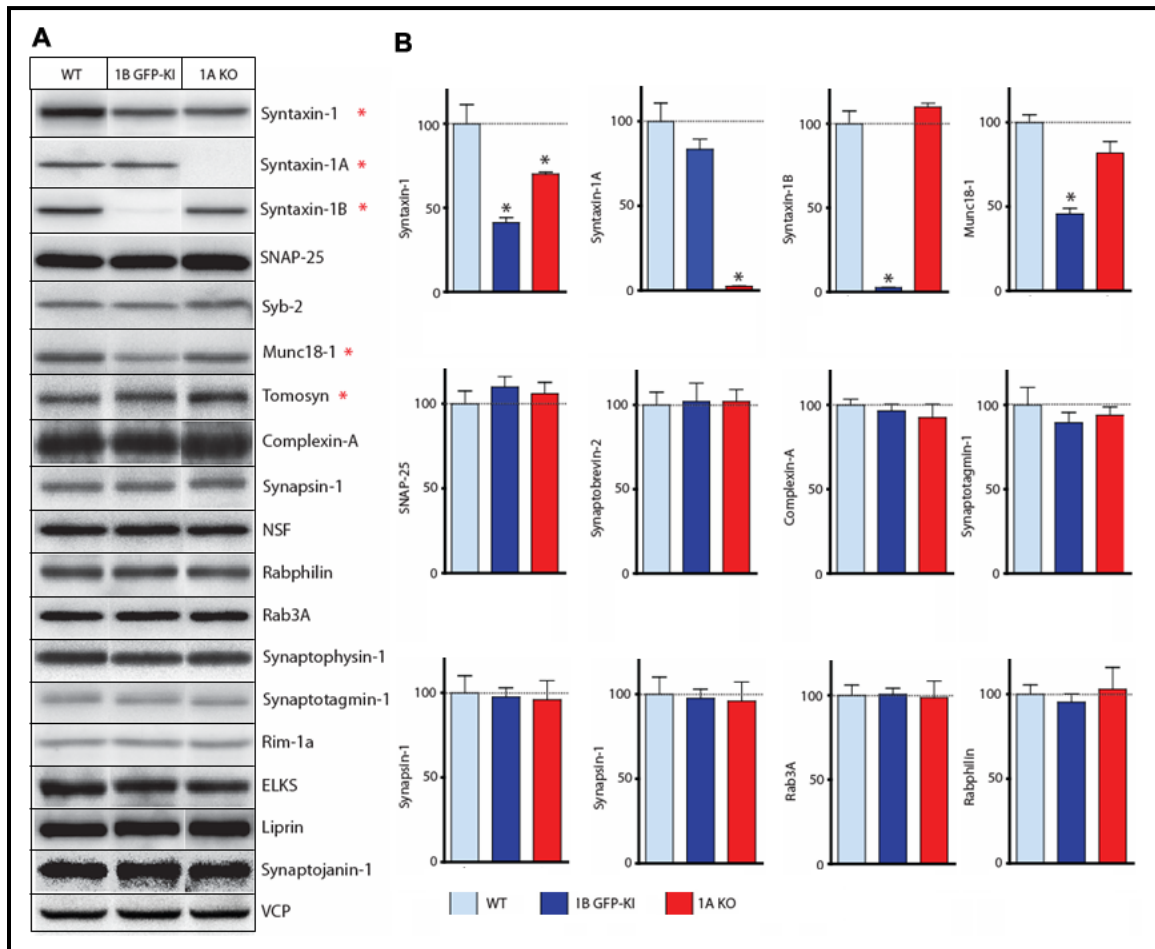


**Figure 2.4. Protein quantitation of syntaxin-1A<sup>KO</sup> / syntaxin-1B<sup>GFP</sup> mice.** (A) At least 3 of total brain extracts were prepared at P14 for each genotype and quantitative western blot analyses were performed using a variety of antibodies, which are related to synapse. Panel (B) shows representative diagram of quantitation.

Table 2.2. Protein quantitation table of syntaxin-1A<sup>KO</sup> / 1B<sup>GFP</sup> mice line.

	1A <sup>WT</sup> 1B <sup>WT</sup>	1A <sup>WT</sup> 1B <sup>GFP</sup>	1A <sup>KO</sup> 1B <sup>WT</sup>	p-value: A <sup>WT</sup> B <sup>WT</sup> vs. A <sup>WT</sup> B <sup>GFP</sup>	p-value: A <sup>WT</sup> B <sup>WT</sup> vs. A <sup>KO</sup> B <sup>WT</sup>
Syntaxin-1A T3748	100 ± 10.8	83.6 ± 6.0	2.6 ± 0.1	0.154	<b>0.007</b>
Syntaxin-1B 4191	100 ± 7.6	2.7 ± 0.1	110 ± 2.1	<b>0.003</b>	0.105
Syntaxin-1 HPC-1	100 ± 11.4	41.2 ± 3.1	70.2 ± 1.1	<b>0.004</b>	<b>0.034</b>
Syntaxin-1 I-379	100 ± 6.1	67.5 ± 3.7	70.5 ± 3.2	<b>0.004</b>	<b>0.005</b>
Syntaxin-1 U6250	100 ± 4.3	89.7 ± 2.8	39.9 ± 3.0	<b>0.058</b>	<b>0.003</b>
SNAP-25	100 ± 7.7	110 ± 6.0	106 ± 6.7	0.255	0.505
Synaptobrevin-2	100 ± 7.6	102 ± 10.9	102 ± 7.2	0.861	0.827
Munc18-1 Monoc1	100 ± 4.7	45.8 ± 3.3	81.8 ± 6.9	<b>0.0001</b>	<b>0.053</b>
Munc18-1 B70	100 ± 12.8	74.4 ± 5.6	97.8 ± 6.3	<b>0.072</b>	0.855
Munc18-1 B71	100 ± 8.0	70.9 ± 3.6	96.0 ± 8.2	<b>0.014</b>	0.700
Munc18-1 K329	100 ± 14.7	70.3 ± 1.1	91.9 ± 1.5	<b>0.056</b>	0.510
Munc18-1 PS92	100 ± 12.1	71.9 ± 6.8	91.6 ± 9.0	<b>0.058</b>	0.511
Complexin-A	100 ± 3.6	96.4 ± 4.2	92.5 ± 8.0	0.462	0.364
Synaptotagmin 1	100 ± 10.5	89.6 ± 6.0	93.9 ± 5.0	0.346	0.571
Rab3A	100 ± 6.2	100.7 ± 3.6	98.7 ± 9.8	0.911	0.901
Rabphilin	100 ± 5.5	95.4 ± 4.9	103 ± 12.8	0.474	0.795
Synapsin	100 ± 10.2	97.6 ± 5.5	96.1 ± 11.2	0.820	0.767
Synaptophysin 1	100 ± 4.9	87.2 ± 6.8	87.8 ± 9.2	0.114	0.233
NSF	100 ± 7.4	105 ± 8.8	116 ± 16.6	0.602	0.310
Synaptotagmin 1	100 ± 6.3	89.1 ± 6.1	97.1 ± 5.5	0.204	0.683
RIM1α	100 ± 4.6	102 ± 4.9	94.7 ± 6.1	0.718	0.417
ELKS	100 ± 8.7	116 ± 11.9	104.2 ± 6.6	0.266	0.655
Liprin	100 ± 3.5	93.2 ± 8.3	99.9 ± 4.2	0.377	0.983
Synaptogyrin-1	100 ± 8.2	92.2 ± 9.2	112 ± 6.5	0.476	0.245
Vglut 1	100 ± 16.1	100 ± 10.9	102.7 ± 11.1	0.999	0.878
CASK	100 ± 6.4	109 ± 2.9	104 ± 5.1	0.182	0.571

### **Differential binding of GFP-syntaxin-1A and -1B fusion proteins to other SNAREs and Munc18-1**

The fact that N-terminal GFP-syntaxin-1A fusion protein is non-functional is surprising, because I have already shown that GFP-syntaxin-1A fusion protein level is increased compared to WT syntaxin-1A. One possibility to explain this problem is that the GFP-fusion might inhibit the interaction of other binding partners, such as other SNAREs and Munc18-1, to syntaxin-1 *in vivo* and followed by observed non-functionality of proteins. In order to solve this question, immunoprecipitation experiment was performed using the whole brain homogenates from either syntaxin1A-GFP KI or syntaxin-1B-GFP KI mice line. Both GFP-syntaxin-1A and 1B fusion proteins still shows the interaction with other SNAREs and Munc18-1 *in vivo* (Fig. 2.5.A-B). However, it was shown that the binding property of GFP-fusion proteins between 1A and 1B is different. GFP-syntaxin-1B fusion protein shows significantly reduced binding affinity to synaptobrevin-2 and Munc18-1, while shows slightly increased binding property to SNAP-25 compared to GFP-syntaxin-1A fusion protein (Fig. 2.5.C).



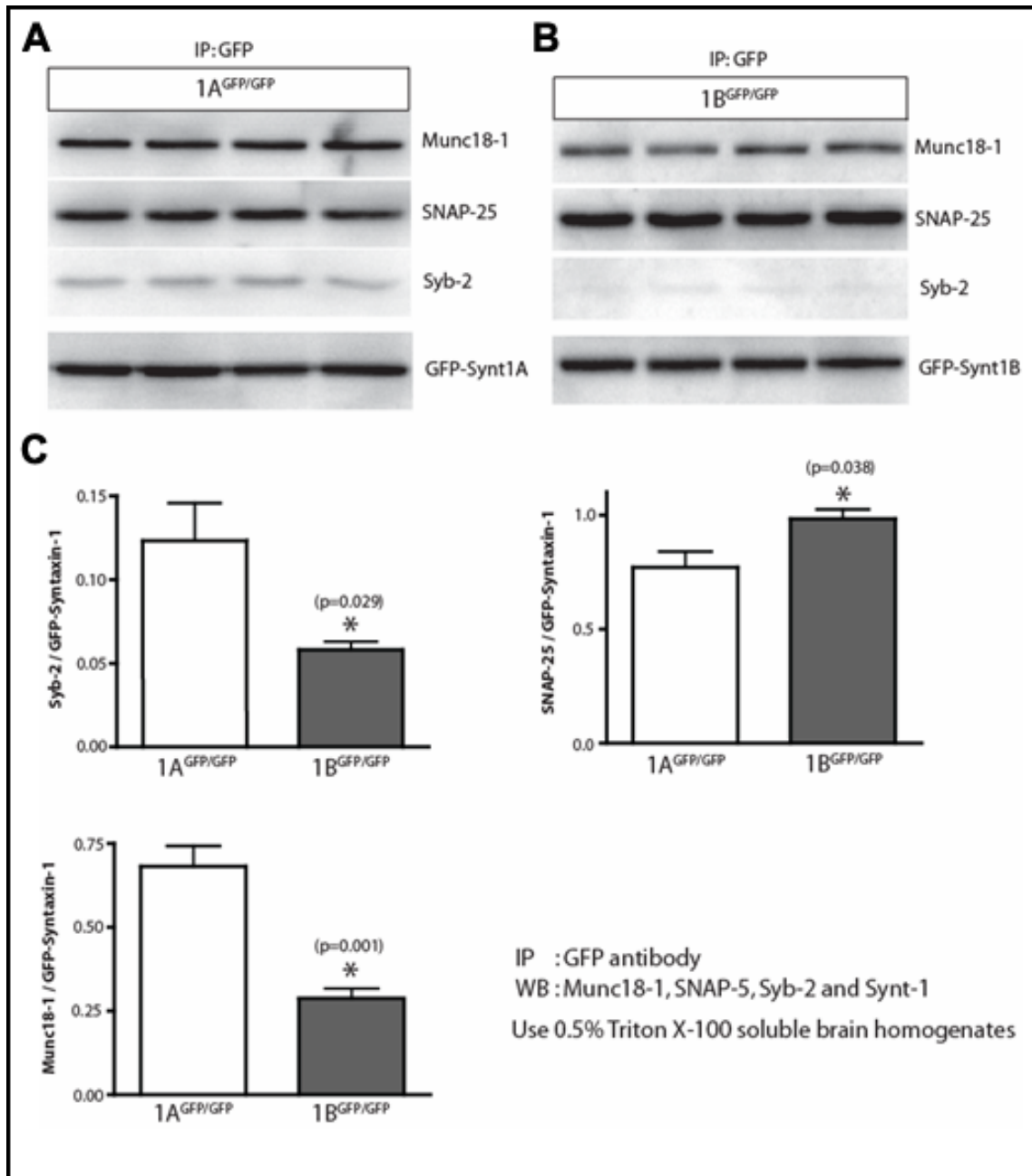


**Figure 2.5. Binding experiment using GFP-syntaxin-1 fusion protein.**

Immunoprecipitation experiment against GFP antibody was performed using 0.5% Triton X-100 soluble brain homogenates from GFP-KI syntaxin-1A (A) and 1B (B) homozygous line. (C) Quantitative immunoblot analyses against antibodies to munc18-1, SNAP-25 and synaptobrevin-2 were performed.

**GFP-syntaxin-1 fusion proteins show normal synaptic staining**

The one possibility for observed non-functionality of GFP-syntaxin-1 fusion proteins might be due to aberrant localization of fusion proteins *in vivo*. To test this possibility, immunostaining on brain sagittal section was performed using antibodies to synaptic markers, such as synaptotagmin-1, Rab3A and the signal pattern was compared to staining for GFP antibody. Pre-immune serum for GFP antibody was used as a negative control. The immunostaining pattern and comparison to synaptic markers indicate that both GFP-syntaxin-1A and 1B fusion proteins show normal synaptic staining (Fig. 2.6), suggesting that the observed non-functionality of fusion proteins are not due to aberrant localization.

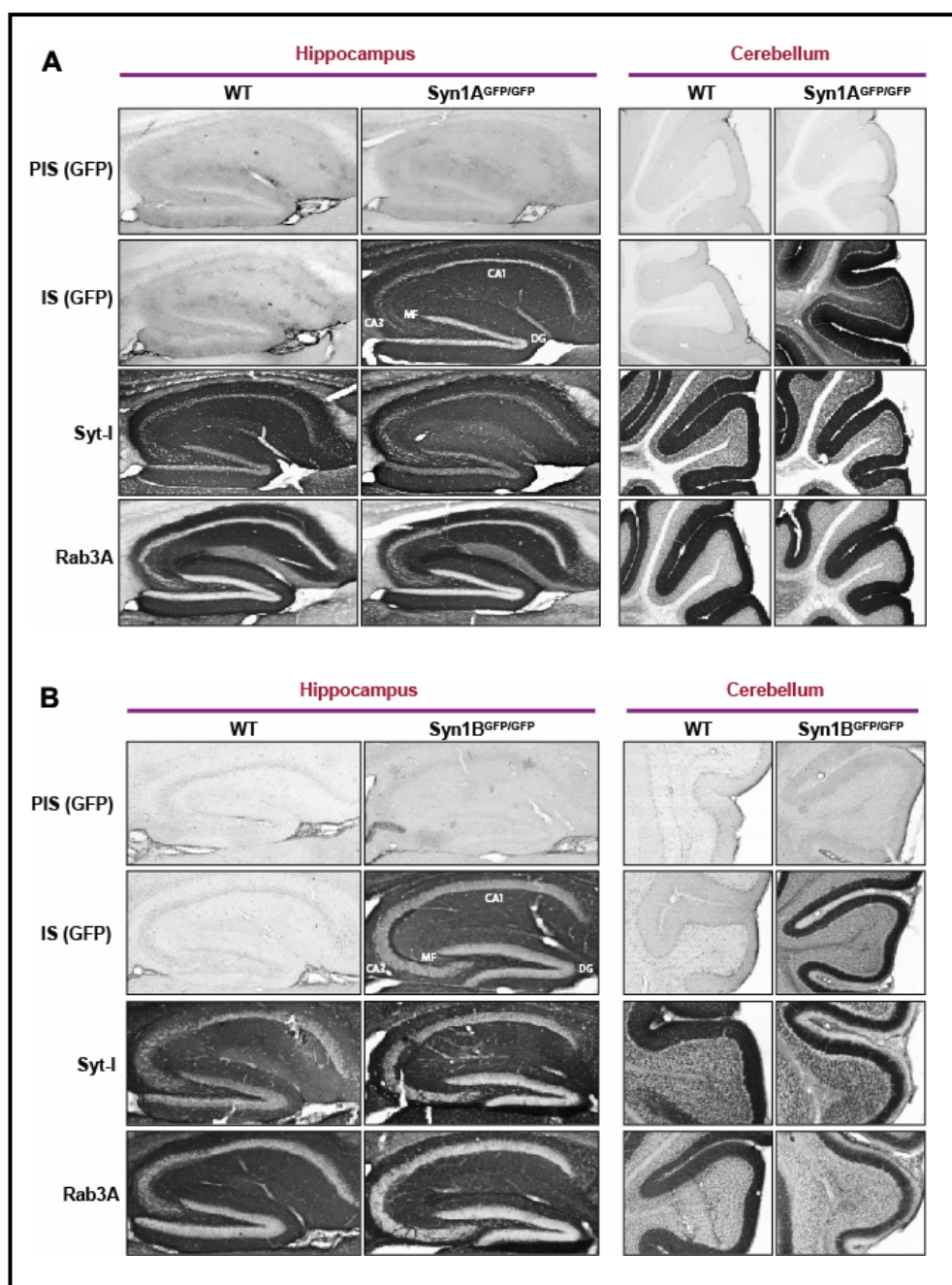


**Figure 2.6. Brain structure analysis and morphological analysis of GFP-fusion protein expression of syntaxin-1A<sup>KO</sup> / syntaxin-1B<sup>GFP</sup> mice.** Hippocampal and cerebellar immunostaining from GFP fusion Syntaxin-1A (A) and -1B (B) KI mice were performed. Brain sagittal sections were collected for peroxidase immunostaining for each syntaxin-1A<sup>GFP</sup> and syntaxin-1B<sup>GFP</sup> mice and their WT littermate control. The antibodies to synaptotagmin-I and rab3A were used as a positive control, while antibody to PIS was used as a negative control. DG = dentate gyrus; MF = hippocampal mossy fiber synapse; GL = granular layer; PL = purkinje cell layer; ML = molecular layer

### Decrease in cerebellar purkinje cell layer in syntaxin-1B<sup>GFP</sup> mice

Since cerebellum plays a pivotal role in movement and balancing of whole body and also syntaxin-1B<sup>GFP</sup> mice shows fragile movement and balance, I decided to look at morphology of cerebellum more carefully, especially morphology of purkinje cell, because it was reported that human inherited ataxia is related to disorders of purkinje cell degeneration (25). Brain sagittal section of syntaxin-1B<sup>GFP</sup> mice were prepared and stained with antibodies to calbindin, one of markers of cerebellar purkinje cell, and compared to WT littermate control. While there is no obvious change in terms of overall size of cerebellum, the layer of cerebellar purkinje cell was significantly decreased compared to WT littermate (Fig. 2.7).

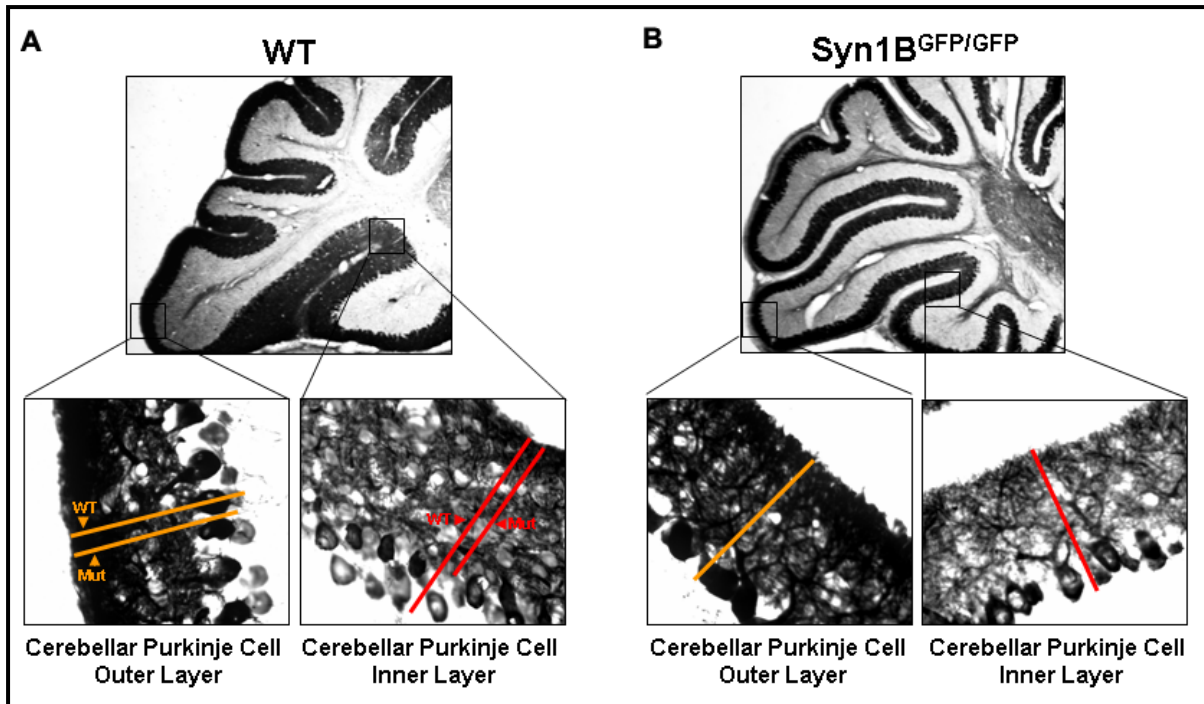


**Figure 2.7. Abnormal morphology of purkinje cell of syntaxin-1B<sup>GFP</sup> mice.** Immunoperoxidase staining was performed on syntaxin-1B<sup>GFP</sup> knock-in mice using antibody to calbindin, specific marker of cerebellar purkinje cell.

## Morphology of neuromuscular junction (NMJ) of syntaxin-1A<sup>GFP</sup> and syntaxin-1B<sup>GFP</sup> mice

Since neuromuscular junction synapse is ideal system for identification of individual synaptic terminal, I tested whether GFP-syntaxin-1A or 1B fusion protein is targeted / localized in synaptic terminal of NMJ by using immunostaining of GFP. Immunostaining for syntaxin-1 showed a typical synaptic terminal staining as a control in both WT and GFP-syntaxin-1A knock-in mice, as expected (Fig. 2.8). However, surprisingly, while GFP-syntaxin-1B fusion protein is innervated well in the synaptic terminal of NMJ, GFP-syntaxin-1A fusion protein is not (Fig. 2.8). This suggests syntaxin-1B, not syntaxin-1A plays an essential role in at least synapse of NMJ.

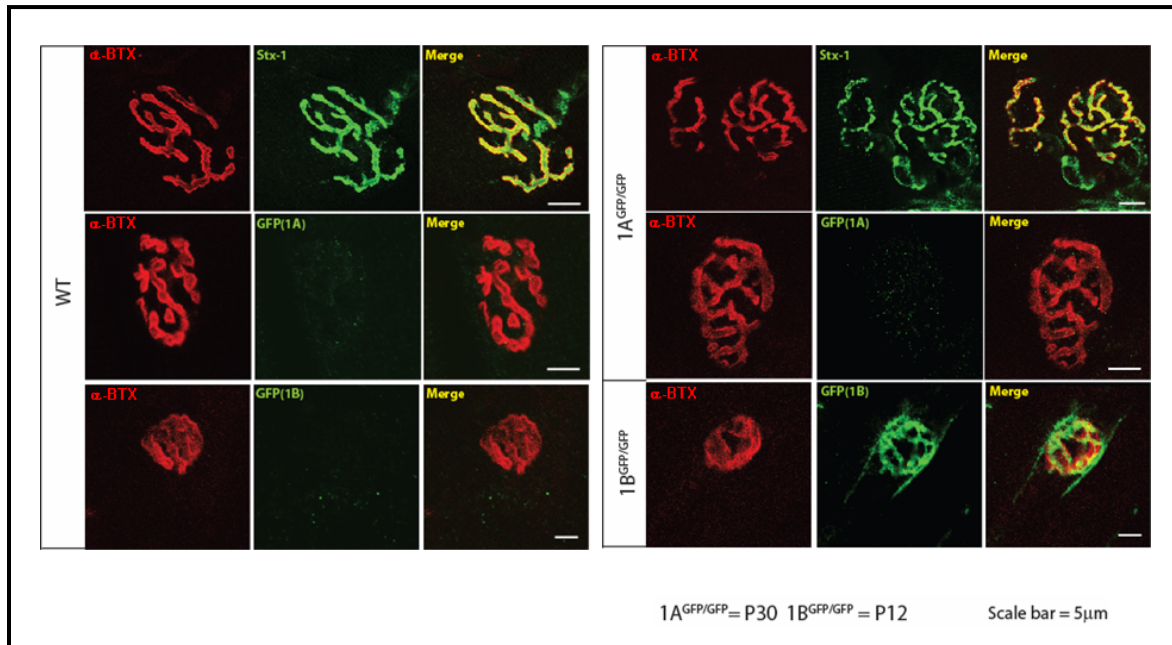


**Figure 2.8. Exclusive expression of GFP-syntaxin-1B fusion protein in synapse of neuromuscular junction.** Immunofluorescent staining against GFP antibody of neuromuscular junction synapse using diaphragm muscle was performed on syntaxin-1B<sup>GFP</sup> knock-in mice. Scale bar at the right column depicts 5 μm and applies to all sections.

## Discussion

Synaptic exocytosis is executed by a series of processes, such as vesicle docking, priming,  $\text{Ca}^{2+}$ -evoked fusion and endocytosis for recycling of vesicles (26). It was originally reported that syntaxin-1 plays a pivotal role specifically in  $\text{Ca}^{2+}$ -evoked fusion by participating SNARE core-complex (1-4). In this study, I used GFP-fusion syntaxin-1A/1B knock-in mice in order to understand their distinct/ overlapping roles in synapse/brain *in vivo*. Originally, I introduced this knock-in gene in hope of mimicking/ rescuing WT syntaxin-1. However, it turns out that both N-terminal fusion GFP-syntaxin-1A and C-terminal fusion GFP-syntaxin-1B are at least not fully-functional compared to WT (Table 2.1), suggesting that adding GFP-tag interferes the normal function of syntaxin-1.

### Lethality of syntaxin-1B<sup>GFP</sup>

Syntaxin-1B<sup>GFP</sup> mice died around P14 (Fig. 2.3A) and showed an unbalanced movement. This lethality is somewhat surprising, because syntaxin-1A<sup>KO</sup> mice do not show any phenotype in terms of survival and basic electrophysiological properties (27) and I thought this non-lethality of syntaxin-1A<sup>KO</sup> is due to redundancy of syntaxin-1A and 1B. This differential lethality between syntaxin-1A<sup>KO</sup> and 1B<sup>GFP</sup> line suggests either their differential localization or their differential basic properties, such as differential interaction affinity to other binding partners so on.

### Non-functionality of GFP-syntaxin-1 fusion protein

As previously discussed, I found out that adding GFP-tag on N-terminal syntaxin-1A causes syntaxin-1A non-functional (Table 2.1). There can be several explanations for this question. Firstly, GFP-fusion protein can be mis-localized *in vivo*. Secondly, there might reside very important sequences for normal function of syntaxin-1 in N-terminal part. The first hypothesis does not seem true, because as shown in immunostaining experiment on brain section, both N-terminal GFP fusion of syntaxin-1A and C-terminal GFP fusion of syntaxin-1B show normal synaptic staining (Fig. 2.6). Therefore, I think the second hypothesis can be at least one of the explanations for non-functionality of GFP-fusion protein. Because there seems that N-terminal part of syntaxin-1A is important for phosphorylation of syntaxin-1A and also this part is essential for the interaction with Munc18-1 confirmed by *in vitro* binding analysis and FRET analysis (unpublished data).

### **Impaired morphology of cerebellar purkinje cell**

I found that the length of layer of cerebellar purkinje cell is significantly decreased in syntaxin-1B<sup>GFP</sup> (Fig. 2.7). The resolution for standard microscopic level can not confirm whether that phenomenon is due to shortening of dendritic length or to other reason. However, since cerebellar purkinje cells send inhibitory projections to the deep cerebellar nuclei, and constitute the sole output of all motor coordination in the cerebellar cortex, this shortening of cerebellar purkinje cell layer should affect the electrophysiological properties, associated with motor coordination and balance of body.



Therefore, even though I don't know the mechanism of this shortening of purkinje cell layer yet, this change of morphology should be one of the reason why syntaxin-1B<sup>GFP</sup> mice show motor incoordination, fragile movement and balance.

### **Lack of innervation of GFP-syntaxin-1A fusion protein into NMJ**

Neuromuscular junction (NMJ) development is regulated by reciprocal interaction between presynaptic (nerve terminal and Schwann cell) and postsynaptic (muscle cell) components (28). In order to identify whether GFP-syntaxin-1A/B fusion proteins are innervated into nerve terminal or not, GFP-immunostaining experiment was performed on both knock-in mice. I found out only GFP-syntaxin-1B fusion protein is innervated into NMJ, not syntaxin-1A (Fig. 2.8). Since lack of innervation might cause the deficiency in communication with muscle cell, the specific innervation of syntaxin-1B into NMJ suggests that abnormality of GFP-fusion protein in NMJ might be one of the reasons for observed phenotype of syntaxin-1B<sup>GFP</sup> mice. However, in order to pursue this question more specifically, the NMJ electrophysiology might be required.

## References

1. Söllner T., Whiteheart S. W., Brunner M., Erdjument-Bromage H., Geromanos S., Tempst P., and Rothman J. E. (1993) SNAP receptors implicated in vesicle targeting and fusion. *Nature* **362**, 318-324.
2. Rizo J., and Südhof, T. C. (2002) Snares and Munc18 in synaptic vesicle fusion. *Nat Rev Neurosci.* **8**, 641-653
3. Jahn, R., and Südhof, T. C. (1999) Membrane fusion and exocytosis. *Annu. Rev. Biochem.* **68**, 863-911.
4. Rizo J., and Südhof, T. C. (1998) Mechanics of membrane fusion. *Nature* **5**, 839-842.
5. Bark I. C. (1995) Structure of the chicken gene for SNAP-25 reveals duplicated exons encoding distinct isoforms of the protein. *J. Mol.Biol.* **233**, 67-76.
6. Bennet M. K., Garcia-Ararras J. E., Elferink L. A., Peterson K., Fleming A. M., Hazuka C. D., and Scheller R. H. (1993) The syntaxin family of vesicular transport receptors. *Cell* **74**, 863-873.
7. Elferink L. A., Trimble W. S., and Scheller R. H. (1989) Two vesicle-associated membrane protein genes are differentially expressed in the rat central nervous system. *J. Biol. Chem.* **264**, 11,061-11,064.
8. Aguado, F., Majo, G., Ruiz-Montasell, B., Llorens, J., Marsal, J., and Blasi, J. (1999) Syntaxin 1A and 1B display distinct distribution patterns in the rat peripheral nervous system. *Neuroscience* **88**, 437-446.
9. Ruiz-Montasell, B., Aguado, F., Majo, G., Chapman, E. R., Canals, J. M., Marsal, J., and Blasi, J. (1996) Differential distribution of syntaxin isoforms 1A and 1B in the rat central nervous system. *Eur. J. Neurosci.* **8**: 2544-2552.
10. Jahn, R. (2000) Sec1/Munc18 proteins: mediators of membrane fusion moving to center stage. *Neuron* **27**, 201-204.
11. Hata, Y., Slaughter, C. A., and Südhof, T. C. (1993) Synaptic vesicle fusion complex contains unc-18 homologue bound to syntaxin. *Nature* **366**, 347-351.
12. Katagiri, H., Terasaki, J., Murata, T., Ishihara, H., Ogihara, T., Inukai, K., Fukushima, Y., Anai, M., Kikuchi, M., and Miyazaki, J. (1995). A novel isoform of syntaxin-binding protein homologous to yeast Sec1 expressed ubiquitously in mammalian cells. *J. Biol. Chem.* **270**, 4963-4966.

13. Salzberg, A., Cohen, N., Halachmi, N., Kimchie, Z., and Lev, Z. (1993). The *Drosophila* Ras2 and Rop gene pair: A dual homology with a yeast Ras-like gene and a suppressor of its loss-of-function phenotype. *Development* **117**, 1309–1319.
14. Pevsner J., Hsu, S. C., and Scheller, R. H. (1994). n-Sec1: a neural-specific syntaxin-binding protein. *Proc. Natl. Acad. Sci. USA* **91**, 1445–1449.
15. Grabowski R., and Gallwitz, D. (1997). High-affinity binding of the yeast cis-Golgi t-SNARE, Sed5p, to wild-type and mutant Sly1p, a modulator of transport vesicle docking. *FEBS Lett.* **411**, 169–172.
16. Nichols, B. J., Holthuis, J. C., and Pelham, H. R. (1998). The Sec1p homologue Vps45p binds to the syntaxin Tlg2p. *Eur. J. Cell Biol.* **77**, 263–268.
17. Dulubova, I., Sugita, S., Hill, S., Hosaka, M., Fernandez, I., Sudhof, T. C., and Rizo, J. (1999). A conformational switch in syntaxin during exocytosis: role of munc18. *EMBO J.* **18**, 4372–4382.
18. Yang, B., Steegmaier, M., Gonzalez Jr., L. C., and Scheller, R. H. (2000). nSec1 binds a closed conformation of syntaxin1A. *J. Cell Biol.* **148**, 247–252.
19. Carr, C. M., Grote, E., Munson, M., Hughson, F. M., and Novick, P.J. (1999). Sec1p binds to SNARE complexes and concentrates at sites of secretion. *J. Cell Biol.* **146**, 333–344.
20. Schulze, K. L., Littleton, J. T., Salzberg, A., Halachmi, N., Stern, M., Lev, Z., and Bellen, H. J. (1994). rop, a *Drosophila* homolog of yeast Sec1 and vertebrate n-Sec1/Munc-18 proteins, is a negative regulator of neurotransmitter release in vivo. *Neuron* **13**, 1099–1108.
21. Dresbach, T., Burns, M. E., O'Connor, V., DeBello, W. M., Betz, H., and Augustine, G. J. (1998). A neuronal Sec1 homolog regulates neurotransmitter release at the squid giant synapse. *J. Neurosci.* **18**, 2923–2932.
22. Novick, P., Field, C., and Schekman, R. (1980). Identification of 23 complementation groups required for post-translational events in the yeast secretory pathway. *Cell* **21**, 205–215.
23. Harrison, S. D., Broadie, K., van de Goor, J., and Rubin, G.M. (1994). Mutations in the *Drosophila* Rop gene suggest a function in general secretion and synaptic transmission. *Neuron* **13**, 555–566.

24. Verhage, M., Maia, A. S., Plomp, J. J., Brussaard, A. B., Heeroma, J. H., Vermeer, H., Toonen, R. F., Hammer, R. E., van den Berg, T. K., Missler, M. *et al.* (2000). Synaptic assembly of the brain in the absence of neurotransmitter secretion. *Science* **287**, 864–869.
25. Lim, J. *et al.* (2006). A protein-protein interaction network for human inherited ataxias and disorders of Purkinje cell degeneration. *Cell* **125**, 801–814.
26. Südhof, T. C. (2004). The synaptic vesicle cycle. *Annu Rev Neurosci.* **27**, 509–547.
27. Fujiwara, T., Mishima, T., Kofuji, T., Chiba, T., Tanaka, K., Yamamoto, A., and Akagawa, K. (2006). Analysis of knock-out mice to determine the role of HPC-1/syntaxin 1A in expressing synaptic plasticity. *J. Neurosci.* **26**, 5767–5776.
28. Lin, W., Sanchez, H. B., Deerinck, T., Morris, J. K., Ellisman, M., and Lee K. F. (2000). Aberrant development of motor axons and neuromuscular synapses in erbB2-deficient mice. *Proc. Natl. Acad. Sci. USA* **97**, 1299–1304.

## **Chapter III**

### **E-Syts: A Family of Plasma Membrane C<sub>2</sub>-domain**

### **Proteins with an Unusual Targeting Mechanism**

## Introduction

C<sub>2</sub>-domains were identified as a conserved sequence motif in protein kinase C isoforms (1), and shown to represent autonomously folded Ca<sup>2+</sup>-binding domains in synaptotagmin-1 (2, 3). C<sub>2</sub>-domains are now recognized as the second most common Ca<sup>2+</sup>-binding module in the proteome after the much smaller, but more frequently occurring EF-hand module (4). All C<sub>2</sub>-domains are composed of a stable 8-stranded  $\beta$ -sandwich that contains flexible loops at the top and bottom, with ‘top’ and ‘bottom’ defined by reference to the synaptotagmin-1 C<sub>2</sub>A-domain, the first C<sub>2</sub>-domain whose atomic structure and Ca<sup>2+</sup>-binding mode were determined (5, 6).

C<sub>2</sub>-domains come in two topological variations that are circular permutations of each other (reviewed in Ref. 6). In type I C<sub>2</sub>-domains, e.g. those of synaptotagmin-1, the  $\beta$ -strands are arranged in a linear manner and the C- and N-termini emerge at the top of the domain (5). In contrast, in type II C<sub>2</sub>-domains as first found in the phospholipase C $\delta$  C<sub>2</sub>-domain (7), the N-terminus of the C<sub>2</sub>-domain is formed by  $\beta$ -strand #2, and the C-terminus by  $\beta$ -strand #1, and the N- and C-termini emerge at the bottom of the C<sub>2</sub>-domain. In all C<sub>2</sub>-domains that bind Ca<sup>2+</sup>, Ca<sup>2+</sup> binds exclusively to the top loops, coordinated by a set of five conserved aspartate or asparagine residues (8). Although the Ca<sup>2+</sup>-binding modes of all C<sub>2</sub>-domains are the same, their precise Ca<sup>2+</sup>-binding properties differ, with some C<sub>2</sub>-domains such as those of synaptotagmin-1 exhibiting a low intrinsic Ca<sup>2+</sup>-affinity that is boosted several orders of magnitude by the presence of phospholipids (2, 8). In contrast, other C<sub>2</sub>-domains such as those of rabphilin display a high intrinsic Ca<sup>2+</sup>-affinity even in the absence of phospholipids (9). Not all C<sub>2</sub>-domains bind Ca<sup>2+</sup>. A subset of C<sub>2</sub>-domains lacks the residues involved in Ca<sup>2+</sup>-binding, making Ca<sup>2+</sup>-binding impossible (e.g., see refs. 10, 11). More surprisingly, in some C<sub>2</sub>-domains the canonical Ca<sup>2+</sup>-binding residues are present, but the domains nevertheless do not bind Ca<sup>2+</sup> because a subtle change in the orientation of the  $\beta$ -strands makes it impossible for the top loops to actually coordinate Ca<sup>2+</sup> (e.g., see the C<sub>2</sub>B-domain of synaptotagmins 4 and 11; ref. 12).

Most  $\text{Ca}^{2+}$ -dependent and even some  $\text{Ca}^{2+}$ -independent  $\text{C}_2$ -domains bind to phospholipids as first described for the synaptotagmin-1  $\text{C}_2\text{A}$ -domain (2, 3) and the Pten  $\text{C}_2$ -domain (10). However, not all  $\text{C}_2$ -domains interact with phospholipids. Several  $\text{Ca}^{2+}$ -independent  $\text{C}_2$ -domains constitute protein interaction domains, as revealed in the crystal structure of the Munc13-1  $\text{C}_2\text{A}$ -domain in a complex with the RIM zinc finger domain (13). Moreover, at least in synaptotagmin-1,  $\text{Ca}^{2+}$ -binding to the  $\text{C}_2$ -domains triggers their interaction not only with phospholipids, but also with SNARE complexes as a target protein, suggesting a multifaceted functional activity at the phospholipid/protein interface (14, 15) and demonstrating that the same  $\text{C}_2$ -domain can bind to both a protein and phospholipids simultaneously.

$\text{C}_2$ -domains are primarily found in proteins that function in membrane traffic and/or signal transduction, with synaptotagmins and protein kinase C as the prime examples. In membrane trafficking proteins,  $\text{C}_2$ -domains are generally present in multiple copies (although there are some proteins with only a single  $\text{C}_2$ -domain), whereas signal transduction proteins usually have a single  $\text{C}_2$ -domain. Membrane-trafficking  $\text{C}_2$ -domain proteins are often attached to membranes by a mechanism that is independent of the  $\text{C}_2$ -domain, either directly via a transmembrane region (TMR), as most clearly demonstrated for synaptotagmins (14), or indirectly via a binding protein, as shown for rabphilin (16). In contrast, in signal transduction proteins the  $\text{C}_2$ -domains generally appear to function to localize the protein to the membrane, as shown, for example, for protein kinase C (17) or Pten (10). Few  $\text{C}_2$ -domain proteins are conserved in yeast, for example the phosphatidylserine decarboxylase Psd2p (reviewed in Ref. 18), protein kinase C (19), and the ubiquitin ligase Rsp5p (20).

Three families of putative trafficking proteins containing multiple  $\text{C}_2$ -domains and a single transmembrane region have been described: synaptotagmins, ferlins, and MCTPs (21-23). In addition, the sequence of a fourth type of protein with multiple  $\text{C}_2$ -domains and a single TMR was reported from rat adipocytes (25). Interestingly, this adipocyte protein is evolutionarily related to a family of

membrane proteins in yeast containing three C<sub>2</sub>-domains that were called tricalbins (24). Tricalbins may thus be noteworthy because they may represent the only proteins resembling synaptotagmins that are conserved in yeast, although the properties and expression of these proteins and their mammalian counterparts have not been examined.

In the present study, I follow up on these observations, and define a family of homologous proteins that I refer to as E-Syts for extended synaptotagmins because of their similarity to synaptotagmins. E-Syts differ from yeast tricalbins to which they are related in that they are Ca<sup>2+</sup>-binding proteins. E-Syt1 contains five C<sub>2</sub>-domains and is localized to intracellular membranes, whereas E-Syt2 and E-Syt3 contain three C<sub>2</sub>-domains and are localized to the plasma membrane. The most interesting property of E-Syts, however, may be the mechanism by which E-Syt2 and E-Syt3 are targeted to the plasma membrane because this targeting does not depend on their TMR. Instead, it is determined by the Ca<sup>2+</sup>-independent third C<sub>2</sub>C-domain of these proteins. Thus E-Syts represent a family of Ca<sup>2+</sup>-binding membrane proteins that form a heterogeneous group of proteins, two of which are targeted to the plasma membrane by a novel mechanism.



## **Materials and Methods**

### **Cloning, sequence analyses and Data Bank Searches**

E-Syts were first analyzed by databank searches of genomic and cDNA sequences. Their full-length human sequences were then assembled by sequencing of expressed-sequence tag (EST) clones, and submitted to GenBank (accession numbers DQ993200, DQ993201, and DQ993202).

### **Expression and purification of recombinant Glutathione S-Transferase (GST)-fusion Proteins**

The cDNA sequences encoding various domains of the human E-Syts were amplified by PCR, subcloned into pGEX-KG vector, and expressed and purified as recombinant GST-fusion proteins essentially as described (19). The following GST-fusion proteins were produced: E-Syt1 X C<sub>2</sub>AB (residues 91-600), E-Syt1 C<sub>2</sub>A (residues 278-449), E-Syt1 C<sub>2</sub>E (residues 918-1104), E-Syt2 X C<sub>2</sub>AB (residues 147-658), E-Syt2 X C<sub>2</sub>A (residues 147-511), E-Syt2 X (residues 147-387), E-Syt2 C<sub>2</sub>A (residues 340-511), E-Syt2 C<sub>2</sub>AB (residues 340-658), E-Syt2 C<sub>2</sub>B (residues 500-658), E-Syt2 C<sub>2</sub>C (residues 736-921).

### **Construction and expression of vectors encoding various myc-tagged E-Syt fusion proteins**

The following gene constructs were subcloned into pCMV5 vector with an N-terminal myc-tag, and transfected into HEK293 cells for subcellular localization experiments: E-Syt1 full-length (residues 1-1104), E-Syt2 full-length (residues 1-921), E-

Syt3 full-length (residues 1-886), E-Syt1  $\Delta$ TM (residues 92-1104), E-Syt2  $\Delta$ TM (residues 150-921), E-Syt3  $\Delta$ TM (residues 73-886), E-Syt2 deletion constructs (residues 1-810, 1-458, 1-240, 240-921, 458-921, 755-921), E-Syt1 deletion construct (residues 965-1104) and E-Syt3 deletion construct (residues 748-886).

### **RT-PCR analysis**

Human Normal Tissue cDNA Panel obtained from PrimGen was used for PCR reaction by several pairs of primers. For E-Syt1 PCR, GCTCACGCAAAGCCAGACCCAG and GAAGGGCCAGACCTGGGCCAC primers, for E-Syt2 PCR, GACCACCAACACTCA GCTCAAG and GCTTGTTTCTCTGCGAGCTG primers, for E-Syt3 PCR, CTCTGTAC CTCGTGGTGCG and GTCCTCAGGTGGATGCTC primers were used. PCR reaction of GAPDH was used as a loading control.

### **Phospholipid binding assay**

Phospholipid binding assays were carried out with purified soluble GST-fusion proteins in buffer A (50 mM HEPES-NaOH, pH 6.8, 0.1 M NaCl, and 4 mM sodium EGTA). The GST-fusion C<sub>2</sub> domain proteins were incubated with liposomes of defined phospholipid composition in buffer A containing variable amounts of CaCl<sub>2</sub> or MgCl<sub>2</sub> to provide defined concentrations of free Ca<sup>2+</sup>, Mg<sup>2+</sup> respectively (calculated using EqCal for Windows software from Biosoft, Ferguson, MO). In order to produce liposomes, dried phospholipids (obtained from Avanti Co.) were resuspended in buffer A containing 0.5 M sucrose and sonicated. The resulting "heavy" liposomes were then isolated by centrifugation. After the incubations of C<sub>2</sub>

domain proteins with liposomes, liposomes with bound C<sub>2</sub> domain proteins were re-isolated by centrifugation essentially as described (27, 28), and bound proteins were precipitated, resuspended in 30  $\mu$ l of 2x SDS sample buffer, and analyzed by SDS-PAGE and Coomassie-blue staining.

### **Immunostaining and confocal imaging**

HEK293 cells plated on cover slips in 12 well plates were transfected with E-Syt expression and control vectors using FuGENE (Roche Applied Science). Two days after transfection, cells were washed in PBS and fixed with 3.7 % formaldehyde in PBS. After fixation, cells were blocked and non-permeabilized or permeabilized by 3 % non-fat milk without or with 0.1 % NP-40 in PBS, respectively. Cells were then incubated with both monoclonal antibodies against the myc epitope (Santa Cruz Biotechnology) and FITC-conjugated phalloidin (Molecular Probes) for 1 hour, washed three times with PBS, and reacted with Alexa-488 labeled secondary antibody (Invitrogen) for 1 hour. After three time washes with PBS, cells were briefly immersed in water, and mounted with Vectashield (Vector Laboratories). Images were acquired on a Leica TCS2 laser-scanning confocal microscope using a 62 x oil objective.

### **Subcellular fractionation and drug treatment**

Transfected HEK293 cells were washed with PBS, collected, and homogenized two days after transfection. Homogenates were centrifuged at 500 x g for 20 min to obtain a postnuclear supernatant that was centrifuged at 100,000 x g for 1 hour to isolate the cytosolic fraction from pellet

fraction. The pellet was resuspended with buffer containing 1 % Triton X-100 and permeabilized with rocking for 1hr. After permeabilization, it was centrifuged at 100,000 x g for 1 hour to isolate Triton X-100 soluble fraction from Triton X-100 insoluble fraction. Latrunculin-A (Biomol), Nocodazole (Biomol) and DMSO were applied one day after transfection and cells were harvested 24 hours later.

### **Miscellaneous procedures**

SDS-PAGE and immunoblotting were performed using standard procedures (29, 30). Immunoblots were developed by enhanced chemiluminescence (Amersham Biosciences).

## Results

### Structure and expression of E-Syts

I identified E-Syts by databank searches for C<sub>2</sub>-domain proteins that contain a TMR (31). Analyses of vertebrate sequences revealed that mammals contain three evolutionarily conserved and closely related E-Syt proteins that are distantly homologous to yeast tricalbins (24). One of these proteins, named here E-Syt1, was originally described by Morris et al. (25) as an anonymous membrane protein isolated from intracellular vesicles. I employed expressed sequence-tag (EST) clones to assemble full-length sequences for E-Syt1, E-Syt2 and E-Syt3, and verified their primary structures by sequencing multiple independent clones and comparing the resulting sequences with database entries. The domain structures of E-Syts emerging from these analyses are shown in Fig. 3.1 and an alignment of the human E-Syt sequences and their worm and insect homologs is depicted in Fig. 3.2.

The domain structure of E-Syts consists of a short, non-conserved N-terminal sequence, a single N-terminal TMR, a conserved domain that is different from any other sequence in the databanks (here referred to as 'X'), and either five C<sub>2</sub>-domains (E-Syt1) or three C<sub>2</sub>-domains (E-Syt2 and E-Syt 3). The 'X-domain' exhibits no noticeable features or homologous domains. The TMR, X-domain, and C<sub>2</sub>A-domain closely follow each other without a discernable linker sequence separating them. In contrast, the C<sub>2</sub>A- and C<sub>2</sub>B-domains in all E-Syts are connected by a short variable linker sequence (~20 residues), and the C<sub>2</sub>B- and C<sub>2</sub>C-domains by a long variable linker sequence (>100 residues). Apart from the X-domain, the C<sub>2</sub>-domains, and the linker sequences, E-Syts have no recognizable domains, suggesting that their functions are mediated by the X- and C<sub>2</sub>-domains. In E-Syt1,

the third and fourth C<sub>2</sub>-domains (the C<sub>2</sub>C- and C<sub>2</sub>D-domains that are absent from E-Syt2 and E-Syt3) are highly homologous to the first and second C<sub>2</sub>-domains (the C<sub>2</sub>A- and C<sub>2</sub>B-domains), respectively (Fig. 3.2). This suggests that evolutionarily, the C<sub>2</sub>C- and C<sub>2</sub>D-domains were duplicated in E-Syt 1 (Figs. 3.1 and 3.2).

All E-Syt C<sub>2</sub>-domains are composed of a type 2 topology as defined originally for the phospholipase C $\delta$  C<sub>2</sub>-domain (7). In all mammalian, worm, and insect E-Syts, only the C<sub>2</sub>A-domain contains the canonical Ca<sup>2+</sup>-binding residues in the ‘top’ loops (the loops between  $\beta$ -strands #2/3, #4/5, and #6/7). In contrast, the other C<sub>2</sub>-domains lack several of the critical Ca<sup>2+</sup>-binding aspartate/asparagine residues in these loops, suggesting that they are unlikely to bind Ca<sup>2+</sup>. The sequences of the C<sub>2</sub>-domains do not otherwise contain a particularly noticeable feature except for the presence of a relatively long sequence in the ‘top’ loop between  $\beta$ -strands 2/3 in the C<sub>2</sub>B-domains of the vertebrate E-Syts, suggesting that this loop may have a more extensive structure. Interestingly, this long loop sequence is alternatively spliced at least in E-Syt1 and E-Syt2 (Fig. 3.2).

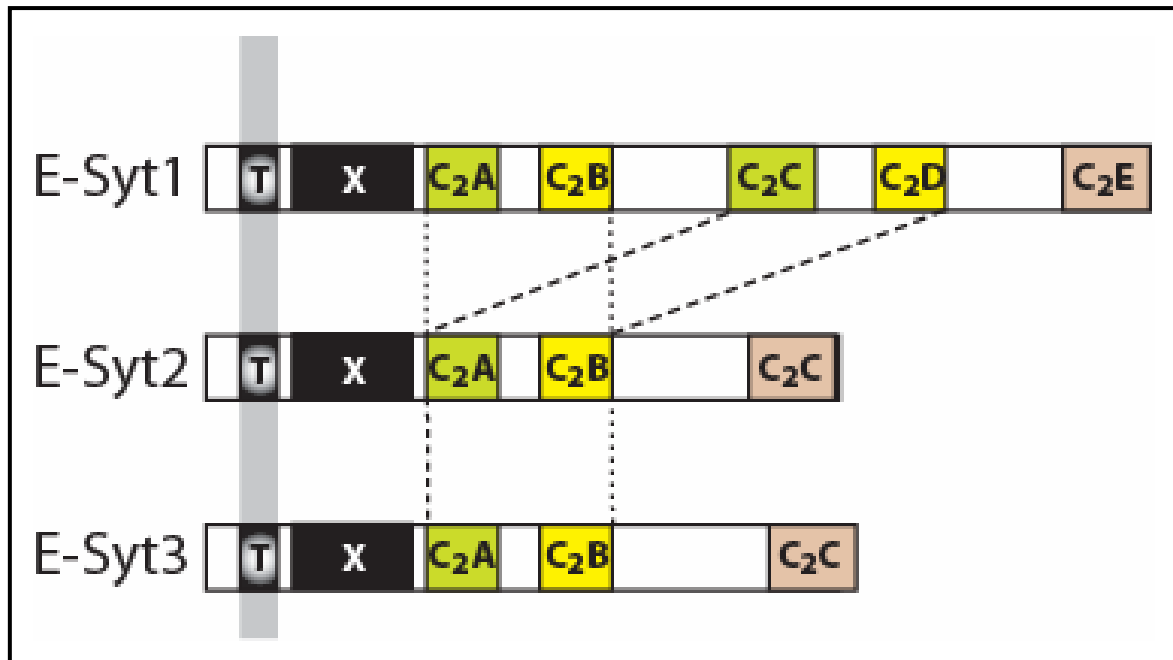


**Figure 3.1. Structures of E-Syts.** Note that the C<sub>2</sub>C- and C<sub>2</sub>D-domains of E-Syt1 are highly homologous to the C<sub>2</sub>A- and C<sub>2</sub>B-domains of all E-Syts (T = TMR).

E2	MTANRDAALSSHRHPGCAQRPTPTTFASSQRRSAFGFDGNGFPLGERSHAPGSRGLG	58
E1	MERSPGEGPSPMDQPSAPSDPTDQFAAHAKDPGSGGQAGPGAAGEALAVLTSFGRRLVLIPVYLAVAGLSVGFVFFGALYLGWRRV	94
E2	ARRRAKTARGLRGRQRGAGAGLSRPGSARAPSPRPGGPNPGVLSVELPGLLAQLARSFALLPVYALGYLGLSFSWVLALALAWQRRS	152
E3	MRAEPCAGGAPSALGAQRTGGEELRLSSQLLELCTFVVRVLFYLGPPVYAGYLGSLIITWLLGALLMMWARRN	75
Dm	MNESPVVTPPTPTGNGTPPTQTNGNSIVATKSVSDNSIIFSVFTLGGKVAIVGSIYLVGYTGSVAWLIAPVILSVARDQL	83
Ag	MAGASKELSPKQSAAPPESSEVAKTKDDSMITLYSFAKKVTVGIIVFVGYGGSVAWLIITPVILSVARESW	72
Ce	MSWQSYLVPVGSAILSTFTFELGKWDYSFVWVLIILIASVTK	43
E1	RDERSRRAARQLLDDEEQLTAKTLYMSHRELPAWVFPDVEKAELWNKIVAVWPFLGQYMERLLAETVAPVNR--SNHLLTFTFETRVEL	186
E2	RGLKALRLCRALALLEDEERV--VRLGVRACLLPAWVFPDTERAEWLNKIVKHWPPICQFIEKLFRETIEPAVRG--ANHLSTFSTFTRVDV	242
E3	RRGKLRLAAAFELDNREF--ISRELRGQHLPAWVFPDVERVEWANKIISQWPPYLSMIMESKFREKLEPKIRE--KSIHLTFTFTKLYF	165
Dm	AKTSEKKRDIKASALASEKD--VIL-ARIDELPAWVFPDVERCEWLNKIKQVWPANANHFARTLVKETIEPNVALALANVKMHGFFETRIIL	174
Ag	RKTNDTRRSVAKASALANDKE--VIL-ARLHDLPAWVFPDVERCEWLNKIKQVWPANANFYAKNLIKESTIEPNQAAAGYKLNGETFRDMIL	163
Ce	SYLWRKRERRLIARATALRERPVIM-AQLQLPAWVFPDTERVEWLNKVIHQWVPGVYTKTFMNDRIHPGVK-AQPMGMFKNFETIKMDM	135
E1	GEKPIRIIGVKVHFGQ-RKEQILLDINISYVGDVQIVVEVKKYFCKAGVKSQOLHGVLRVILEPLIEDIPVGVAVSMFFIRFPITLDINWGTMTN	279
E2	GOQPIRINGVKVYTVENVKRQIILDLQISEVNCIDDEIKRYFCRAGVKSQIHGTIRVILEPLIEDMPLVGALSIFFLRKPLINWGTMTN	336
E3	GQKCPRVNGVKAHNTCNRRRTVDLIIYIGDCISVLEOKI--CAGVNGIQGLGLRILEPLIVDRFVGVAVVFFLNNPNIDFNLGVID	257
Dm	GLIPPRIGGVKIYDKNVSRNEIIMDLDLYAGDCDINFYLSGM--KGKIKDQIHGVWVRVVMKPLIRSMPLVGGGLIFFLNNPNIDFNLGVID	266
Ag	GLIPPRIGGVKIYDKNVSRNEIIMDLDLYAGDCDISFALSGL--KGKIKDQIHGTIRVIMKPLISQMLVGGGLIFFLNNPNIDFNLGVID	255
Ce	GLIPPRVGGIKVYTVNVRDRIIVDDVAYAGDADFTVSCGF--TGMNNTQFSGRLRILKPLLPYFPVGGVSTFLEMPKMDFNLTGME	227
E1	LLDIPGLSSSLDTHIMDSIAAEVLVLPNRILVPLVPLDQDVAQLRSLPPIRGIIRIHLAARGLSKDKYVKGLEKSDPYALVRIGTQIFCSR	363
E1'	.....NPGRSSVDAPPRPCHTTPDSQFGEHTHTTPDSQFGEHTVIRIHLVLAQDLIAKDRFLGGLKGSDDPYVKKLAGRSRFSHV	701
E2	LLDVPLGLNGLSDTHIMDSINYLVLNRIITVPLVGE-VQIAQLRFPVPGVIRIHEIAQDLQKDTYLGKLAGRSDDPYGILFVGNQIFCSR	429
E3	LLDAPGINDVSDSLLEDLIAHLVLPNRITVFPVKKGIDLTNLRFPFPGVIRIHLLEAECLACKDNFL-GL-RGKSDPYAKVSIIGLCHFSRT	348
Dm	FMDVPLGSDLRRIITVBOIGNVVLPNRIISLSE--VSAVALKMPPEPGIRIHLVLEAKDLMKKDISVIG--KGKSDPYALINVGAGFEKTQI	357
Ag	LLDVPLGSDLRRIITVBOIGNVVLPNRIISLSDG-VSAVALKMPPEPGIRIHLVLEAKDLMKKDISVIG--KGKSDPYALISVGAQCFRTQI	346
Ce	MVELPGLIDAIRSVINSQIAALQVLNPIVPLAPD-VDTQLFPEPGVIRIHLLEAKLENRDISFIK--KGKSDPYALIVGSGFEKTRT	318
	-----β2-----β3-----β4-----	
E1	IDDELNPVWGETYVMMVHEVPGQIEVEVEDKD-IDKDDFLGRMKIDVGKVLQASVLDWFFLQGGQ-GOVHLRLEWLSILSDAEKLEQVLOWN	465
E1'	VREDLNPNVWVFPVIVTVSPGOELEVEVEDKD-IDKDDFLGRCKVRLITVLNSGFLDEMTLEDVPSGELHLRLRLFRPTAAELEEVLOWN	794
E2	IKENLSPMNWVEYEAIVYHEPGQELEIELEDED-IDKDDFLGSLMIDIEVEKERLLDEWFTLDEVPKGLHLRLLEWILMPNASNLDKVIDTI	522
E3	IYRNLNPNVWVVEFVYVHEPGQIELEVEDKD-IDKDDFLGSLQIGLIVMTNRVVDWVFNDDTSGELHLRLLEWLSILTD---QEVLTED	437
Dm	IDNNVNPWVWYCEATVFIEMGQFVEIQKDDSDSKDENLGRASIDIASVIKGVVDWVFNDDTLEDAKHGLHLRLVWYLTADPNLDQHLLET	451
Ag	IDNTVNPWVWYCEATVFIHAESGQTLVFINDED-AGEDELGRATVEISSVTKNGSIDWVLTLEDAKHGLHLRLVWYLTADPNLDQHLLET	439
Ce	IDDLNPNWVEYEAIVDQADGQKRIELEDED-QGKDEBLGRSLVDLKLIVQAKGIDWVFLBSCKHGLHLRIKATWMLSTELRLHEKQEWBA	411
	-----β5-----β6-----β7-----β8-----β1-----	
E1	WGV-SSRPDPFSAAILLVYIDRAQDL-----MVTSELYPQLKKNKEPNVYGLSIQDVT-QESKAVYSTNCPVWEEAEFFLQD	545
E1'	SLIQTKSAELAAALLSIYMERAEELP-----LRKGTKHLSPYATLTVGQSS-HKTKTISQTSAPVWDESASFLIRK	865
E2	KADKQDANGISSALLIYDSARNLPSNPLDFNPGVKKSAVORALKSGKKISSNPNVYVMSVGHRA-QESKIRYKTNVWVEENETFEIHN	615
E3	HG-----GLSTAILVFELESACNLPNPFYDLNGEYRAKKLSRFA--RNKYSKDPSSYKLSVGKKT-HTSKTCPHNKDPVWQVSEFFVHN	521
Dm	QL---LRVTSMSAWLSVETDSARHLK-----QARSSSKPDPYLVGSVNKOK-QATAMIMRDSVPVWQGGTFELVSN	519
Ag	QH---LRVTSMSAWLSVETDSARHLK-----QARQSQSDPYLVLSVGKKN-EQTSVQMRTDAPVWQGGTFELVSN	507
Ce	EW---GQADKPIHSAALLVYIDSVADLP-----YPRSKLEPSEFFVSLGKETQRTFVVKRVNPLFQSKLEFVVRH	480
	-----β2-----β3-----β4-----β5-----	
E1	PQSQELDVQVMDSRALTGLTLPARTLTAPEL-ILDQFOLSSSGNSRLYKLVMRILYLSSEICFPTVPGPCGAWVDSE	630
E1'	PHTSELELQVGEQGTG-VLGSLSLPLSELLVADCL-CLDRWFTLS-SGGQGVIL-LRACLILVQHSQVGAHSHSYSHSSSSLSLSE	946
E2	PKRQTLIEVEVEDQHQCSLGNLKVPLSOLLTSEDM-TVSQFOLSSSGNSRLYKLVMRILYLSSEICFPTVPGPCGAWVDSE	708
E3	VATERHLKIVDDQECALGMLEVPICQILPYADL-TLEQFOLDHSGLLSLISMLVLRSLQVEERELGSPYTGPEALKKGPLLKIKVATNQG	614
Dm	PONESLNKIYDQKTNIDGYYTYTLSTLLKQFNMEVIQCFQOLKSGPESKLYSLSLRLKPGEIDKDSALEQVALLTRSSSVKTPDVAAV	613
Ag	PONDYLQKLVDDQKTNIDGYYTYTLSTLLKQFNMEVIMSEFQOLKSGPESKLYSLSLRLKRRHQEPVATTPDKGPASEADSVLSRTSSIR	601
Ce	LEGQBLKFEAVDDCTRRSLGSLNIPITLLKEPNLEQNQMMHMTLGVHQSSEIVITTRIRMLRSDSQGSLNSHGRSNS	458
	-----β6-----β7-----β8-----β1-----	
E2	SHMSGSPGPGSNTAPSTFVIGGSDKPGMEKQAQPEAGPGLHDLGRSSSSLLA-	763
E3	PKAQPEEGPTDLPCPPDASDTKDVSRSTTTTATTVAETPTSETGPEPKGDSAKRFCEPIGEKKSPATIFLTVPGPHSPGPIKSPRPMK	708
Dm	SPPAFKESQASSKRLSAESPISSEDPVA-	641
Ag	TSASHGSGSGLTQQPSTGDSNAEEAALSHQGSVRKQDSRKSTTSAIMEQMSIQEFP-	660
E1	--EPELSG-----GPPHTS--SAPELRORLTHVDSPLEAPAGFLGVKLTLMYSEERKLVSIYHGCRSLRQ-NGRDEPDPPV--SLLLP	1026
E1'	--SEGHISVKEPTSIASDISLPIATQELRORLQLENGTTLQSPFLGQILTIRHSSORNKLVVWHACRNLIA-FSEDGSDPPV--RMVLLP	852
E2	CPASFPWPPKRLAFSSSLNLSASSCFLLADISLNIEGDLRRRLQGLTQITVRYVCLRRQLSVLINGCRNLPT-CTSSGADPPV--RVYLLP	799
Dm	--ATKISPAMSASTSEKPISEL-ATSVLTHRF--PDSTSSPGEHLGRMQLSIRYSARQKLVTHKIQKIPLDPSNIPDPV--KLYLLP	728
Ag	--VSTLNTVMATTPPSNLSLSD-GGTELLRS--PSTSSSGSAGLGRQILTIVYSVQORQLVTVHKINNIPLDPSNIPDPV--KLYLLP	747
Ce	-----RLGRFRRSKHEMKRETRADENRGEIEQIDFDLVNQLKIALIRCRILMTFDKDKQCNPPVSVKLVALLD	628
	-----β1-----β2-----β3-----	
E1'	DKNRGTKRRTSQRKRTLSPEFNERFEWELPLDEAQRRLDVSVKNS-SFMSRERELG--KVLDLAETDLSQGVARWYDLMNKKDGSS*	1114
E2	DKRRSGRRTIVSEKTLNPFVDSFDSVSLDEVQRRLDVAVK-NSGGLSKDKGLG--KVLVALASEELAKGWTQYDLDGTGPQAMT*	942
E3	ERKACRKRRTSVKRTKTLPLFDETFEFFVPMPEVKKRLDVAVK-NSRPLGSHRRKELG--KVLIDLKSKDLKGSQVYELTPNGQPRS*	886
Dm	GRTKESKRRTSVKRCNCPVYDASFYLLISIAELQTELVTVYVQTK-GLSSGSLIIGMLKILDBAETITQTLGNSLMDLQPIRHE*	816
Ag	GRSKESKRRTSVKRCNCPVYDITFEYIISNAELVNSLEPVYVQTK-GRF--GSPVLGMOKLSLSDPDISSGQGLKAWYDLHESKE*	833
Ce	GNKEVKKKKTPTAANTRHPPFDNHVEIDINPSDLNHHKVVINVKDDTNYGTFAKEVVLGCLERILDSLMNR--QLSQRIPLSVGRK*	713
	-----β4-----β5-----β6-----β7-----β8-----	



**Figure 3.2. Alignment of E-Syts.** Alignment of the human E-Syt1 (E1), E-Syt2 (E2), and E-Syt3 (E3) sequences with each other and with the *Drosophila* (Dm), mosquito (Ag), and *C. elegans* (Ce) E-Syt sequences. Residues shared by the majority of sequences are shaded in a domain-specific manner (yellow = extra-cytoplasmic sequence; gray = TMR; blue = juxtamembranous E-syt domain; red = C<sub>2</sub>-domains). In the C<sub>2</sub>-domains, the approximate locations of the  $\beta$ -strands are indicated below the sequence. Aspartate, asparagine, and glutamate residues that correspond to residues involved in ligating Ca<sup>2+</sup> in synaptotagmin-1 C<sub>2</sub>-domains are shown in white on a black background. Note that in E-Syt1, the C<sub>2</sub>A- and C<sub>2</sub>B-domains are duplicated, resulting in a total of five C<sub>2</sub>-domains in which the C<sub>2</sub>A- and C<sub>2</sub>C-, and the C<sub>2</sub>B- and C<sub>2</sub>D-domains are equivalent, and aligned with each other (E1' = E-Syt1 sequences starting with the C<sub>2</sub>C-domain aligned with the C<sub>2</sub>A-domains of the other E-Syts). The long N-terminal sequence of the Mosquito E-Syt is not shown. Sequences are numbered on the right.

To determine the tissue distribution of E-Syt expression, I performed RT-PCR analyses on various human tissues using E-Syt1-, E-Syt2-, and E-Syt3-specific primers and a normal human tissue cDNA panel (from PrimGen, Inc.). I observed ubiquitous expression of all E-Syts, with an enrichment of E-Syt2 and E-Syt3 in cerebellum (Fig. 3.3).

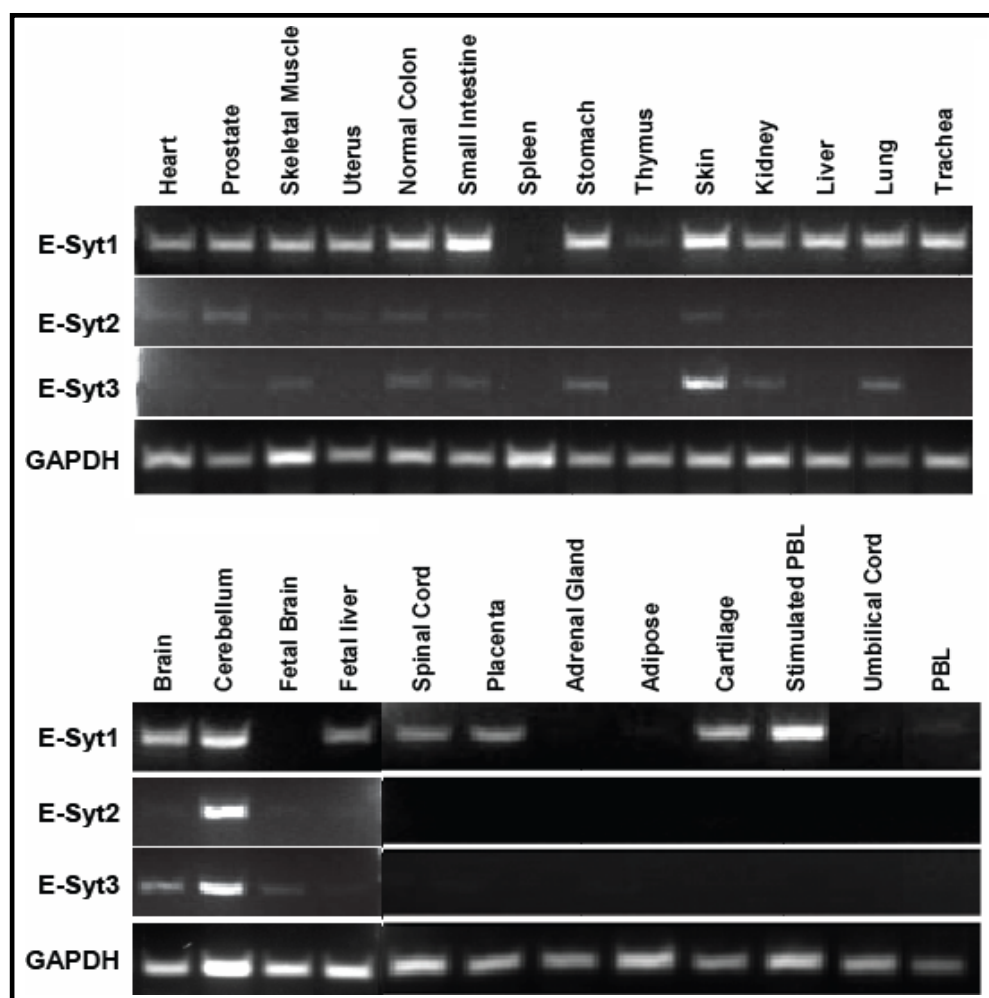


**Figure 3.3. Expression patterns of E-Syts determined by RT-PCR of RNA from human adult tissues.** RT-PCR analysis was performed for E-Syt1, E-Syt2 and E-Syt3 using single-stranded cDNA generated from various human adult tissue RNA samples as indicated (obtained from PrimGen). While E-Syt1 is expressed ubiquitously, E-Syt2 and E-Syt3 are expressed primarily in cerebellum. GAPDH was used as an RT-PCR control to ensure the integrity of the samples.

## Phospholipid binding by E-Syt2

Apart from the TMR, X-domain, and the C<sub>2</sub>-domains, E-Syts have no recognizable domains, suggesting that their function is mediated by their C<sub>2</sub>- and X-domains tethered to a membrane. Although the sequence analyses suggested that the C<sub>2</sub>A-domain of E-Syts can bind Ca<sup>2+</sup>, not all C<sub>2</sub>-domains with a typical Ca<sup>2+</sup>-binding motif in fact bind Ca<sup>2+</sup> (e.g., see ref. 11). Moreover, although most C<sub>2</sub>-domains that bind Ca<sup>2+</sup> also form Ca<sup>2+</sup>-dependent phospholipid complexes, not all Ca<sup>2+</sup>-binding C<sub>2</sub>-domains in fact do that, whereas some C<sub>2</sub>-domains that do not bind Ca<sup>2+</sup> bind phospholipids in a Ca<sup>2+</sup>-independent manner (e.g., see ref. 10). Thus, to investigate whether the E-Syt C<sub>2</sub>-domains have a potential for Ca<sup>2+</sup>-dependent and/or Ca<sup>2+</sup>-independent interactions with phospholipids, I produced a series of recombinant proteins containing various fragments from E-Syt2 expressed as GST-fusion proteins (Fig. 3.4). I tested the binding of these protein fragments to liposomes composed of 25% phosphatidylserine (PS) / 75% phosphatidylcholine (PC) in the absence or presence of divalent cations, using a sensitive centrifugation assay because the pull-down assay that we originally developed does not detect weak interactions, such as the binding of the synaptotagmin-1 C<sub>2</sub>B-domain (27). I detected no phospholipid binding in the absence of divalent cations or in the presence of Mg<sup>2+</sup> with any E-Syt2 fragments. In contrast, fusion proteins of the C<sub>2</sub>A-domain with either the X-domain, or the C<sub>2</sub>B-domain, or both, bound to liposomes in a Ca<sup>2+</sup>-specific manner. Although the only common denominator of these different E-Syt2 fragments was the presence of the C<sub>2</sub>A-domain (Fig. 3.4), the isolated C<sub>2</sub>A-domain by itself only weakly bound to phospholipids in a Ca<sup>2+</sup>-dependent manner (Fig.

3.5.A), possibly because the fragment used did not exactly include the precise domain boundaries.

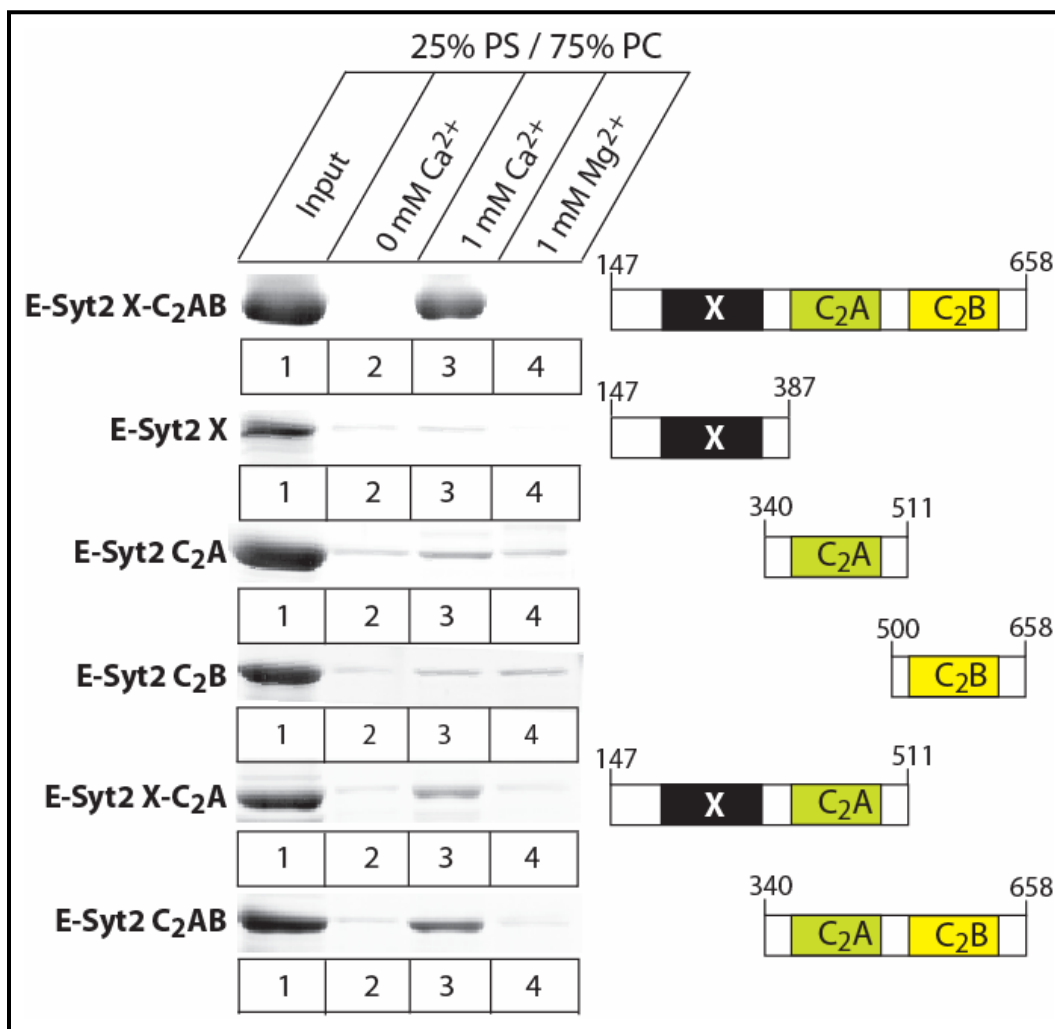


**Figure 3.4.  $\text{Ca}^{2+}$ -dependent phospholipid binding by various fragments from E-Syt2.** Recombinant GST-fusion proteins containing the parts of E-Syt2 indicated on the right were employed in phospholipid binding assays. The recombinant proteins were incubated in the absence of divalent cations, in 1 mM  $\text{Ca}^{2+}$ , or in 1 mM  $\text{Mg}^{2+}$  with liposomes composed of 25% phosphatidylserine (PS) / 75% phosphatidylcholine (PC) (w/w). Liposomes were pelleted by centrifugation, and bound proteins were analyzed by SDS-PAGE and Coomassie staining.

I next examined the apparent  $\text{Ca}^{2+}$ -affinity and the phospholipid-specificity of  $\text{Ca}^{2+}$ -dependent phospholipid binding by the E-Syt2 X C<sub>2</sub>AB-domain fragment (Fig. 3.5). Binding was observed between 1 to 10  $\mu\text{M}$  free  $\text{Ca}^{2+}$ , similar to that observed for the synaptotagmin-1 C<sub>2</sub>-domains. Different from the synaptotagmin-1 C<sub>2</sub>-domains, however, E-Syt2  $\text{Ca}^{2+}$ -dependent phospholipid binding was not specific for negatively charged phospholipid, but also detectable with liposomes composed of neutral phospholipids (PE and PC; Fig. 3.5.B), although negatively charged phospholipids exhibited a higher apparent  $\text{Ca}^{2+}$ -affinity.

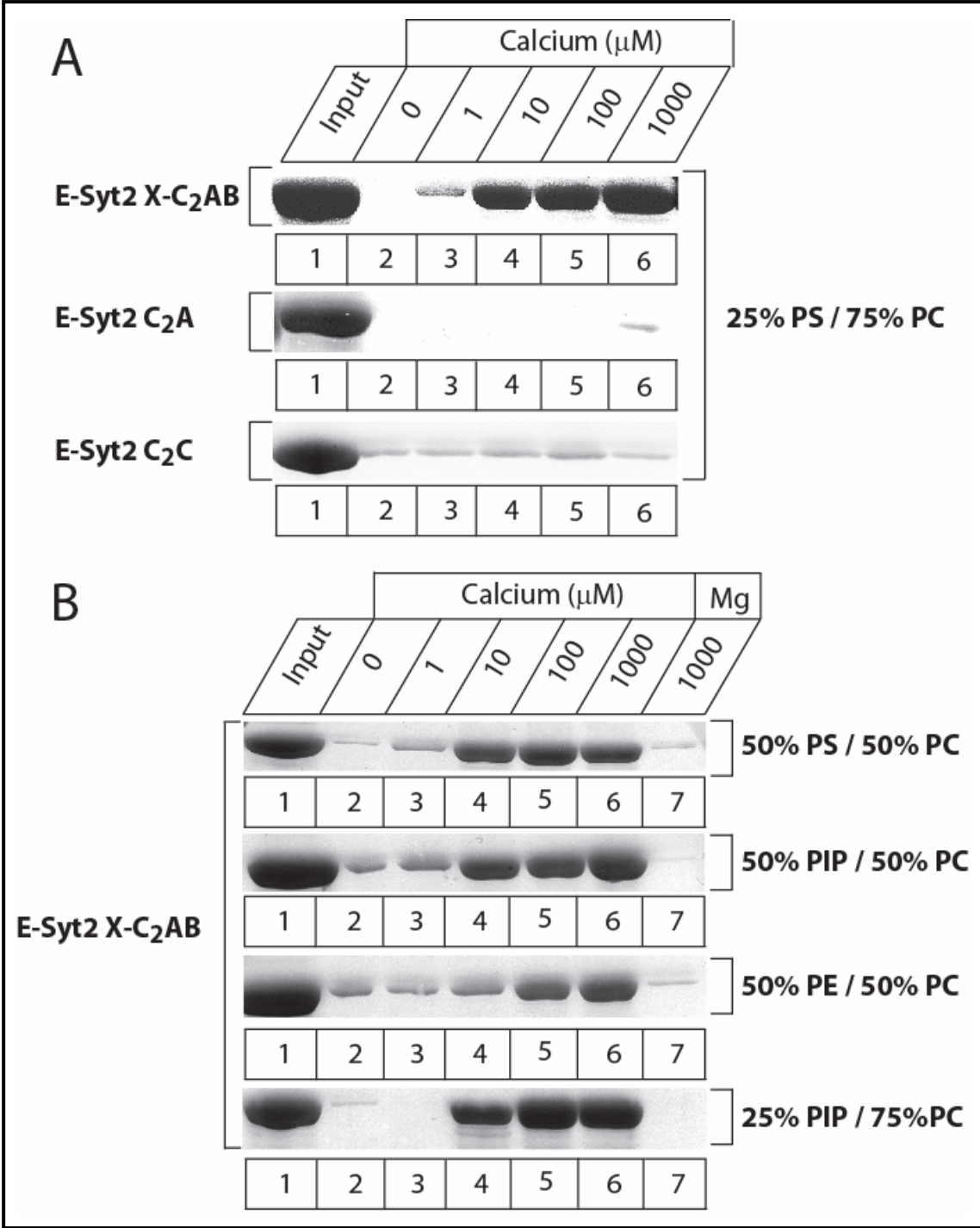


**Figure 3.5.  $\text{Ca}^{2+}$ - and phospholipid-dependence of membrane-binding of E-Syt2.** (A) To measure the  $\text{Ca}^{2+}$ -dependence of phospholipid binding, purified recombinant GST-fusion proteins containing either the E-Syt juxtamembranous 'X' domain together with the  $\text{C}_2\text{A}$ - and  $\text{C}_2\text{B}$ -domains (X- $\text{C}_2\text{AB}$ ), or only the  $\text{C}_2\text{A}$ - or  $\text{C}_2\text{C}$ -domain from E-Syt2, were incubated with liposomes composed of 25% phosphatidylserine (PS) / 75% phosphatidylcholine (PC) in the presence of the indicated concentrations of free  $\text{Ca}^{2+}$ . Proteins bound to the liposomes were analyzed by centrifugation followed by SDS-PAGE and Coomassie-blue staining. (B) Phospholipid-dependence of  $\text{Ca}^{2+}$ -dependent membrane binding of the E-Syt2 X- $\text{C}_2\text{AB}$ -domains. Phospholipid binding of a GST-fusion protein containing the E-Syt2 X- $\text{C}_2\text{AB}$ -domains was tested at the indicated  $\text{Ca}^{2+}$ -concentrations and in the presence of 1 mM  $\text{Mg}^{2+}$  (as a negative control) in liposomes with the four different phospholipid compositions shown on the right (PS, phosphatidylserine; PIP, phosphatidylinositol phosphate; PC, phosphatidylcholine; PE, phosphatidylethanolamine).

### **Subcellular localization of E-Syts**

To determine the subcellular localization of E-Syts, I raised antibodies to various E-Syts using recombinant protein fragments, but was unable to generate antibodies of sufficiently high affinity to detect endogenous E-Syt proteins in various tissues (data not shown). Thus, to circumvent this problem, I produced expression vectors for all three E-Syts in which the full-length coding region was subcloned into a pCMV5 vector with an N-terminal myc-epitope tag. In addition to vectors encoding full-length myc-tagged E-Syts, I also constructed vectors in which the N-terminal extracytoplasmic sequences and TMR were deleted from the coding region, resulting in the expression of myc-tagged E-Syt proteins that contained only the cytoplasmic sequences. Expression of all these proteins from the respective vectors was confirmed by immunoblotting in transfected HEK293 and COS cells (data not shown).

To immunolocalize the various E-Syts, I transfected HEK293 cells with the expression vectors and stained the cells with anti-myc epitope antibodies either without or with permeabilization (Fig. 3.6). This experiment was designed to test whether E-Syts are plasma membrane proteins because plasma membrane localization would expose their N-terminals, myc-tagged sequences on the cell surface, and thus make them accessible to immunolabeling without permeabilization. As a positive control, I transfected the cells with N-terminal myc-tagged synaptotagmin-7 that is quantitatively deposited into the plasma membrane (32); as a negative control, I used N-terminal myc-tagged filamin A, an intracellular protein. All samples were labeled with both anti-myc antibody and FITC-conjugated phalloidin that reacts with the actin cytoskeleton in cells.



I made three principal observations with this approach. First, E-Syt1 was not detected in transfected unpermeabilized cells, but became visible after permeabilization of the cells. In these cells, E-Syt1 was found to be localized in unidentified intracellular membranes that did not resemble the Golgi apparatus, endoplasmic reticulum, lysosomes, or mitochondria (Fig. 3.6).

Second, E-Syt2 and E-Syt3 were fully stained on the cell surface in unpermeabilized transfected cells, and appeared to be completely inserted into the plasma membrane because permeabilization did not uncover additional intracellular staining for these E-Syts (Fig. 3.6). This localization is striking for a transfected cell in which the transfected proteins must be massively overexpressed, suggesting that the transfected protein is not retained in the endoplasmic reticulum or Golgi apparatus but quantitatively transported to the cell surface.

Third, the apparent localization of E-Syts surprisingly did not change upon removal of the TMR. Although E-Syt2 and E-Syt3 without a TMR could no longer be detected on the cell surface in nonpermeabilized cells as expected, they were still found to be quantitatively associated with the plasma membrane (Fig. 3.6). Thus the localization of E-Syt2 and E-Syt3 into close proximity to the plasma membrane is not dependent on the TMR as in other proteins.

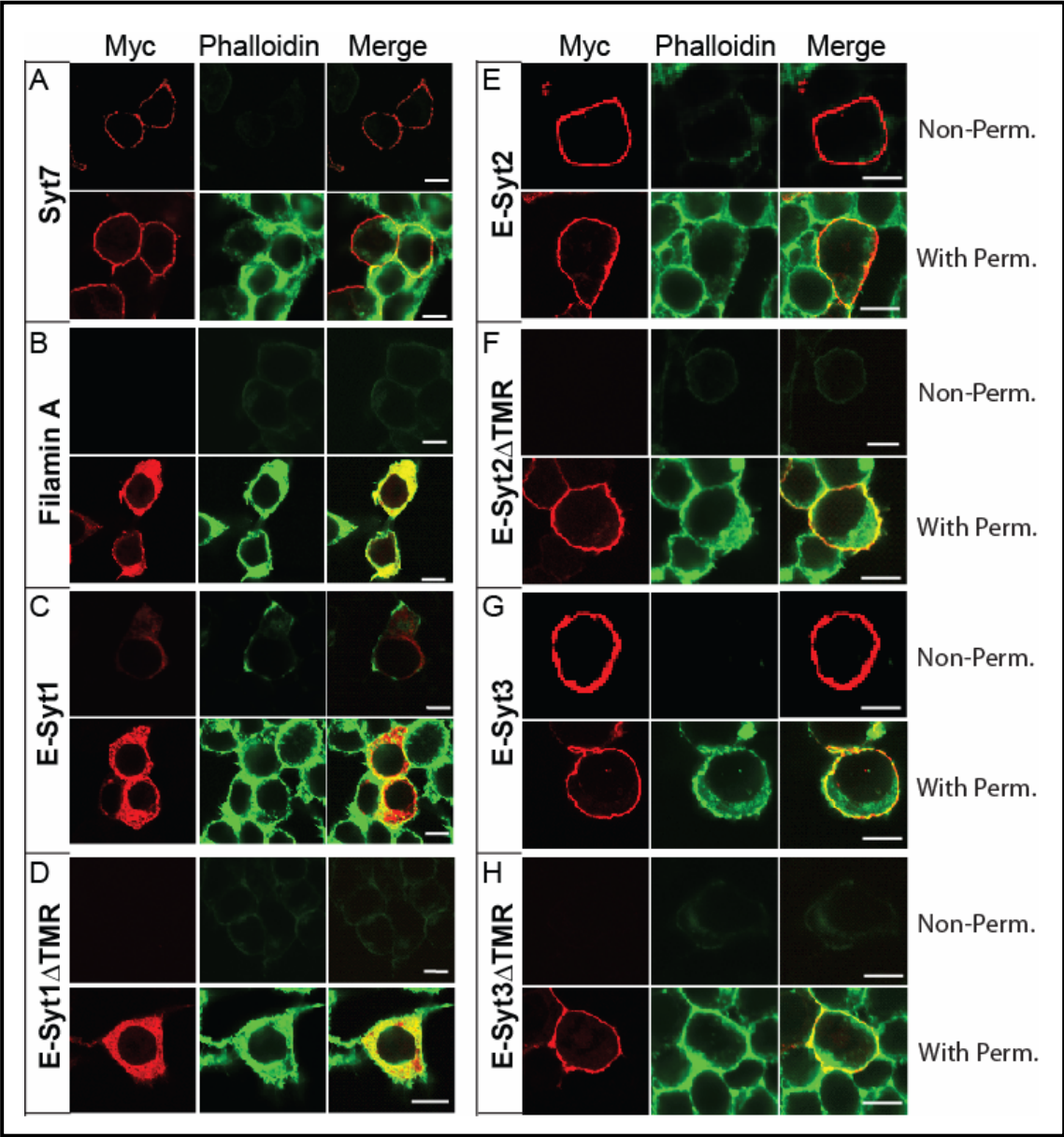


**Figure 3.6. Subcellular localization of E-Syts in HEK293 cells.** HEK293 cells transfected with expression vectors encoding the proteins indicated on the left of the panels were analyzed by anti-myc antibody (red) and phalloidin staining (green) and fluorescence microscopy. Cells were stained without permeabilization in buffer lacking detergents or in buffer containing 1% Triton X-100 (indicated as 'non-permeabilized' and 'permeabilized' on the right). Transfected proteins were: A, synaptotagmin-7 (Syt-7); B, filamin-A; C and D, E-Syt1 either as a full-length protein (E-Syt1) or as a truncated protein lacking the N-terminal TMR (E-Syt1 $\Delta$ TMR); E and F, E-Syt2 either as a full-length protein (E-Syt2) or as a truncated protein lacking the N-terminal TMR (E-Syt2 $\Delta$ TMR); and G and H, E-Syt3 either as a full-length protein (E-Syt3) or as a truncated protein lacking the N-terminal TMR (E-Syt3 $\Delta$ TMR). All expressed proteins contain an N-terminal myc-epitope tag, and all immunofluorescence labeling was performed with anti-myc antibodies. Images were captured by confocal microscopy; in each set, the right panel shows the merged image, with overlapping staining indicated in yellow (Non-Perm. = Non-Permeabilized, With Perm. = With Permeabilized; calibration bars = 5  $\mu$ m).

### **Plasma membrane targeting of E-Syt2 and E-Syt3 is mediated by its C-terminal C<sub>2</sub>-domain**

To investigate which sequences target E-Syt2 and E-Syt3 to the plasma membrane even in the absence of the TMR, I produced E-Syt2 deletion constructs that contained an N-terminal myc-epitope and were analyzed by transfection into HEK293 cells (Fig. 3.7). I found that deletion of only the C<sub>2</sub>C-domain abolished the plasma membrane localization of E-Syt2, even when E-Syt2 still contained a TMR. In contrast, partial or complete deletion of the X-domain or the C<sub>2</sub>A-domain had no effect on the plasma membrane localization of E-Syt2 (Fig. 6).

These results suggested that the C<sub>2</sub>C-domain of E-Syt2 is necessary for its plasma membrane localization, whereas the TMR, X-domain, and C<sub>2</sub>A-domain are not. To determine whether the C<sub>2</sub>C-domain of E-Syt2 is sufficient for plasma membrane localization, and whether this property is shared with the C-terminal C<sub>2</sub>-domains of other E-Syts, I examined the localization of isolated C-terminal C<sub>2</sub>-domains in transfected HEK293 cells (Fig. 3.8). Both the E-Syt2 and the E-Syt3 C<sub>2</sub>C-domains were localized to the plasma membrane, whereas the E-Syt1 C<sub>2</sub>E-domain was not, thus mirroring the localizations of the full-length proteins. It is thus unexpected that although the C-terminal C<sub>2</sub>-domains of E-Syt1, E-Syt2, and E-Syt3 share a high degree of sequence homology (Fig. 3.2), only the latter two include targeting information that deposits them on the intracellular surface of the plasma membrane.

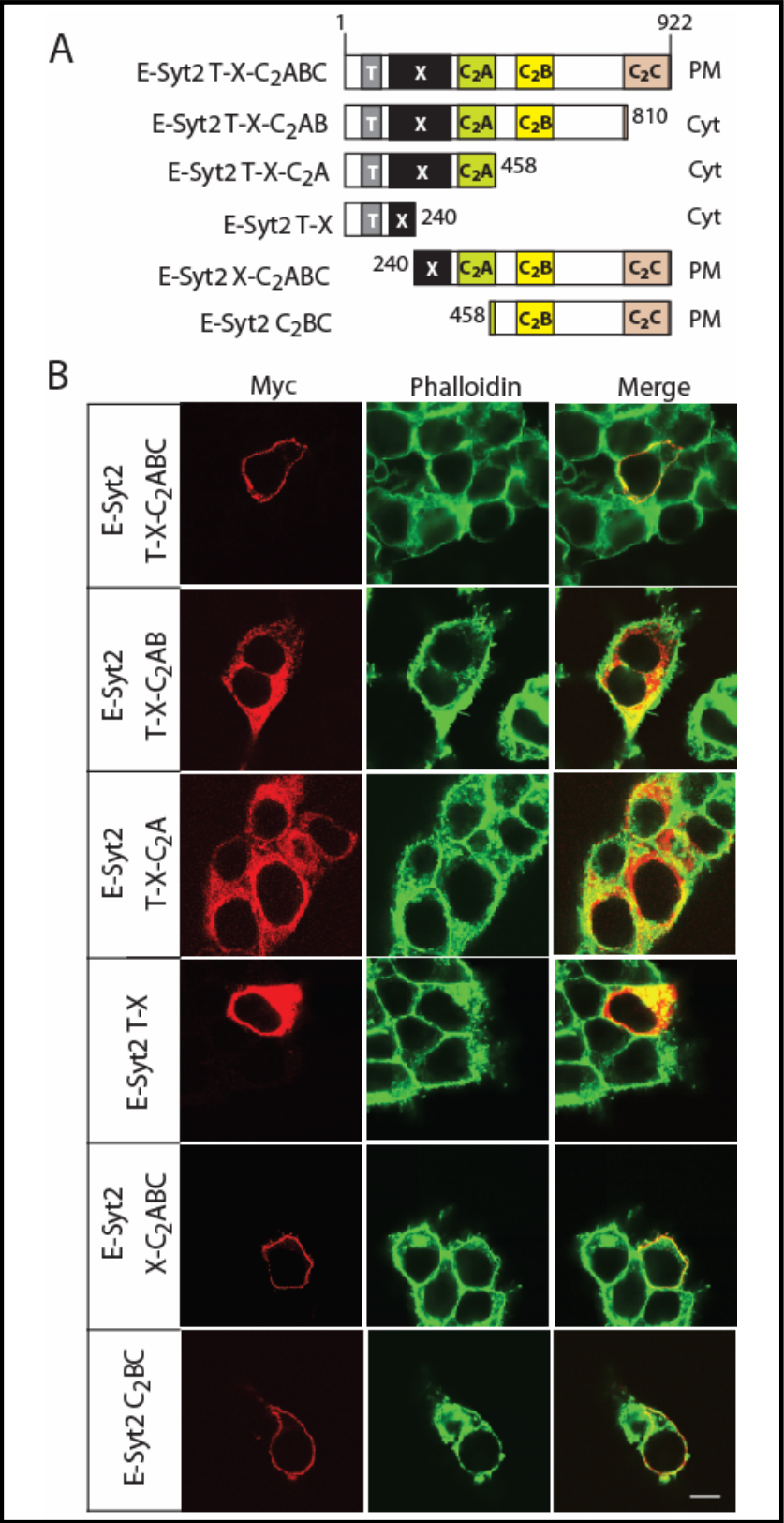


**Figure 3.7. Subcellular localization of E-Syt2 deletion mutants in transfected HEK293 cells.** (A) Schematic diagram of the E-Syt2 deletion constructs and summary of their subcellular localization in transfected HEK293 cells (on right; PM = plasma membrane; Cyt = cytoplasmic). Numbers display residue numbers at the N- and C-terminus of the various fragments. (B) Confocal images of HEK293 cells transfected with various constructs as indicated on the left, permeabilized, and stained with myc antibodies (red) and fluorescent phalloidin (green); merged images are depicted on the right (yellow = red/green overlap). Scale bar at the bottom of the right column depicts 5  $\mu$ m and applies to all sections.

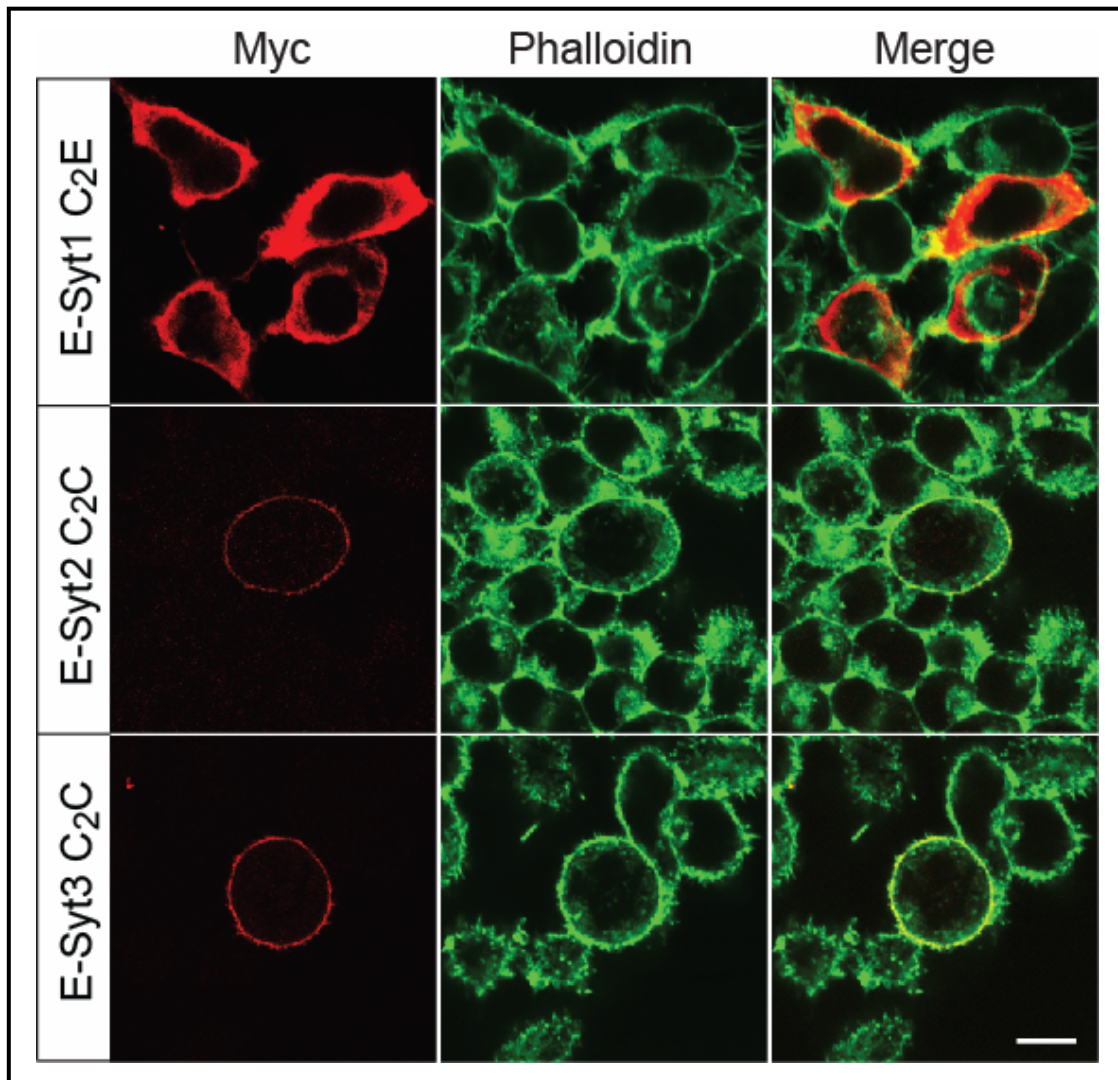


**Figure 3.8. The C-terminal C<sub>2</sub>-domain of E-Syt2 and E-Syt3 but not E-Syt1 is sufficient for plasma membrane localization.** Confocal images of HEK293 cells transfected with myc-tagged C-terminal C<sub>2</sub>-domains of E-Syt1, E-Syt2 and E-Syt3, permeabilized, and stained with myc antibodies (red) and fluorescent phalloidin (green); merged images are depicted on the right (yellow = red/green overlap). Scale bar at the bottom of the right column represents 5  $\mu$ m and applies to all sections.

## **Effects of disrupting the actin or microtubule cytoskeleton on the plasma membrane localization of E-Syt2**

To investigate how it is possible for the E-Syt2 and E-Syt3 C<sub>2</sub>C-domains to be localized to the plasma membrane, I evaluated their biochemical properties. For these experiments, I used the E-Syt2 fragment containing the C<sub>2</sub>B- and C<sub>2</sub>C-domains because this fragment is strongly expressed in HEK293 cell. Fractionation of transfected HEK293 cells expressing the C<sub>2</sub>B-/C<sub>2</sub>C-domains of E-Syt2 revealed that the C<sub>2</sub>B-/C<sub>2</sub>C-domain fragment was insoluble even after extraction of the cells with 1% Triton X-100 (Fig. 3.9.A). This result suggested a possible relation of E-Syt2 to the cytoskeleton which is also Triton X-100 insoluble, prompting us to test the effects of disrupting the actin cytoskeleton with Latrunculin, or the microtubule cytoskeleton with Nocodazole, on the solubility of the E-Syt2 C<sub>2</sub>B-/C<sub>2</sub>C-domain fragment. Cells were treated for 24 hours with high doses of Latrunculin-A or Nocodazole, harvested, and extracted with 1% Triton X-100. However, neither treatment altered the insolubility of the E-Syt2 C<sub>2</sub>B-/C<sub>2</sub>C-domain fragment (Fig. 3.9.A), in spite of the fact that at least in the case of Latrunculin-A, the actin cytoskeleton was disrupted as shown by phalloidin staining (Fig. 3.9.B). Thus the E-Syt2 C<sub>2</sub>B-/C<sub>2</sub>C-domain fragment is not simply anchored to the plasma membrane via the cortical cytoskeleton.

The results described above suggest that the E-Syt2 C<sub>2</sub>B-/C<sub>2</sub>C-domain fragment is not simply attached to the plasma membrane via a lipid interaction or a mechanism dependent on the cytoskeleton. To confirm that under these same conditions used for the biochemical analysis, the C<sub>2</sub>B-/C<sub>2</sub>C-domain fragment is in fact localized to the plasma membrane, I performed immunolocalization experiments under exactly the same conditions



as those used for the biochemical studies (Fig. 3.9.B). The results unequivocally demonstrate that under all treatment conditions, the C<sub>2</sub>B-/C<sub>2</sub>C-domain fragment was quantitatively associated with the plasma membrane. Thus, both the biochemical fractionation and the immunolocalization experiments suggest that the plasma membrane localization of the C<sub>2</sub>B-/C<sub>2</sub>C-domain fragment of E-Syt2 is dependent on neither lipids nor the cytoskeleton, but must be mediated by a novel mechanism.

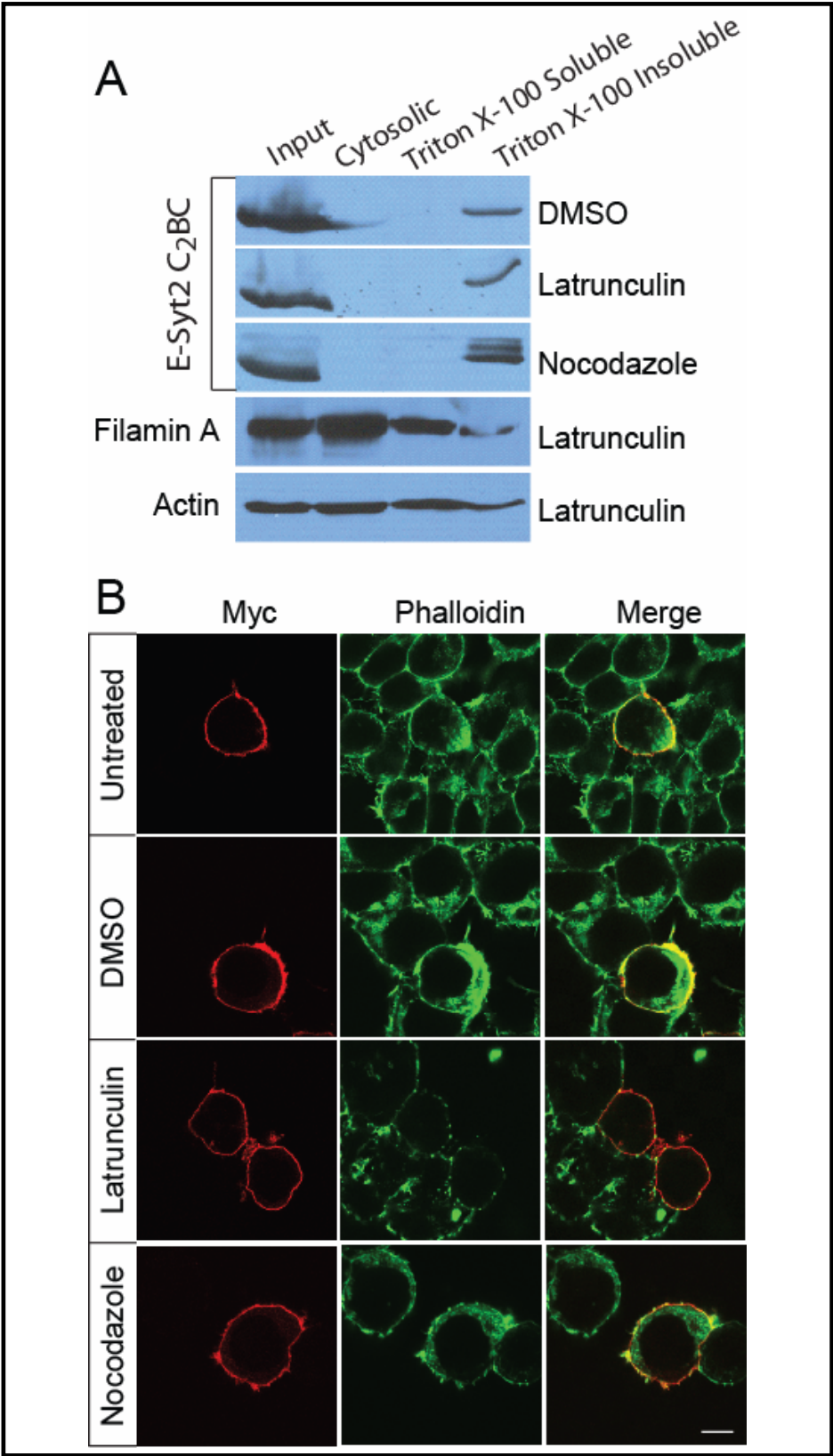


**Figure 3.9. Disruption of the actin or microtubule cytoskeleton does not alter plasma membrane localization of an E-Syt2 C<sub>2</sub>B-/C<sub>2</sub>C-domain fragment.** (A) Subcellular fractionation of E-Syt2 C<sub>2</sub>B-/C<sub>2</sub>C-domain fragment (see Fig. 7). Transfected HEK293 cells expressing the C<sub>2</sub>B-/C<sub>2</sub>C-domain fragment were treated with DMSO alone or with latrunculin or nocodazole for 24 hrs, lysed, and separated by centrifugation into a cytosolic fraction, a Triton X-100 solubilized fraction, and a Triton X-100 insoluble fraction. Samples were analysed by immunoblotting for the E-Syt2 fragment (top) and for actin and the actin-binding protein filamin A as a control. (B) Transfected HEK293 cells expressing E-Syt2 C<sub>2</sub>B-/C<sub>2</sub>C-domain fragment were either left untreated, or treated for 24 hrs with DMSO, latrunculin, and nocodazole. Cells were then fixed, permeabilized, and analyzed by staining for E-Syt2 and phalloidin. Note that the latrunculin treatment almost completely abolishes phalloidin staining, demonstrating that actin filaments are severed in these cells. Scale bar at the bottom of the right column (5  $\mu$ m) applies to all sections.

## Discussion

I here describe a family of membrane proteins with multiple C<sub>2</sub>-domains, referred to as E-Syts because like synaptotagmins, these proteins contain an N-terminal TMR and C-terminal cytoplasmic C<sub>2</sub>-domains. With the E-Syts, four families of evolutionarily conserved membrane proteins containing C<sub>2</sub>-domains that bind Ca<sup>2+</sup> have now been defined: synaptotagmins, ferlins, MCTPs, and E-Syts (22, 31, 33). All of these proteins contain a single TMR and of multiple C<sub>2</sub>-domains, from two C<sub>2</sub>-domains for synaptotagmins to at least six C<sub>2</sub>-domains for ferlins. E-Syts share other properties with synaptotagmins, ferlins, and MCTPs: two of the three E-Syt isoforms are localized to the plasma membrane, as are some of the synaptotagmin and ferlin isoforms, and E-Syts are ubiquitously expressed, although enriched in brain, as again shown for some synaptotagmin and ferlin isoforms. However, two of these protein families – synaptotagmins and E-Syts – contain an N-terminal TMR, whereas the other two – ferlins and MCTPs – contain a C-terminal TMR. Moreover, as described here, E-Syts differ from the other proteins with multiple C<sub>2</sub>-domains and a single TMR in three key properties:

1. The cytoplasmic sequences of E-Syts include an additional, highly conserved domain that is not found in other proteins with multiple C<sub>2</sub>-domains, here referred to as the ‘X-domain’ for want of a better name (Fig. 3.1).
2. E-Syts are the only proteins with a single TMR and multiple C<sub>2</sub>-domains that are conserved in yeast where they are closely related to ‘tricalbins’. However, although the overall domain structures of E-Syts and tricalbins are similar and they both share a conserved ‘X-domain’, their C<sub>2</sub>-domains exhibit significant differences. Most

- importantly, in all E-Syts the C<sub>2</sub>A-domain contains a signature Ca<sup>2+</sup>-binding motif that is characteristic of Ca<sup>2+</sup>-binding C<sub>2</sub>-domains and that mediates Ca<sup>2+</sup>-binding (Figs. 3.4 and 3.5), whereas in tricalbins, in spite of their name, none of the C<sub>2</sub>-domains contains a Ca<sup>2+</sup>-binding motif, making it highly unlikely that they bind Ca<sup>2+</sup>.
3. Although the C<sub>2</sub>A-domain of E-Syt2 appears to mediate Ca<sup>2+</sup>-dependent phospholipid binding, the defining properties of C<sub>2</sub>-domains as first described for the C<sub>2</sub>A-domain of synaptotagmin-1 (2, 3), its Ca<sup>2+</sup>-dependent phospholipid binding properties are unusual compared to those of other proteins containing a single TMR and multiple C<sub>2</sub>-domains. The E-Syt2 phospholipid-binding specificity is such that it does not require negatively charged phospholipids but also works with neutral phospholipids (Fig. 3.5.B). Moreover, the isolated C<sub>2</sub>A-domain does not appear to work efficiently but only exhibits a significant amount of Ca<sup>2+</sup>-dependent phospholipid binding when expressed in conjunction with either the 'X-domain' or the C<sub>2</sub>B-domain (Fig. 3.4), a property that I do not currently understand.

Overall, the characteristics of E-Syts suggest that E-Syts are Ca<sup>2+</sup>-regulatory proteins that function in conjunction with membranes. At present, the functions of E-Syts are unclear, but both synaptotagmins and ferlins are involved in the Ca<sup>2+</sup>-dependent regulation of exocytosis (reviewed in Refs. 22 and 34), suggesting that MCTPs and E-Syts may also have a role in membrane traffic. It is likely that E-Syts perform an important role because they are evolutionarily conserved, and because yeast tricalbins appear to be essential for survival (24). Moreover, the distinct localizations of E-Syt1 vs. E-Syt2 and E-Syt3 point to distinct functions, consistent with their different domain structures, but detailed genetic and cell-

biological studies will be required to determine the functions of E-Syts, and compare them to those of synaptotagmins, ferlins, and MCTPs.

In addition to characterizing the structures and biochemical properties of E-Syts, I studied their subcellular localizations. As assayed with myc-tagged proteins, E-Syt1 is localized to intracellular membranes whereas E-Syt2 and E-Syt3 are quantitatively deposited into the plasma membrane (Fig. 3.6). Unexpectedly, the intracellular vesicular localization of E-Syt1 and the plasma membrane localization of E-Syt2 and E-Syt3 were independent of their TMRs. Experiments with various fragments of E-Syt2 showed that its C<sub>2</sub>C-domain is both necessary and sufficient for its plasma membrane localization (Fig. 3.7). Although all of these results were obtained with exogenously expressed myc-tagged E-Syts because the low levels of endogenous protein and the low sensitivity of my antibodies which did not allow localization of endogenous proteins, the results are internally consistent as the isolated C<sub>2</sub>C-domain of E-Syt3 was also localized to the plasma membrane, whereas the C<sub>2</sub>E-domain of E-Syt1 was localized to intracellular membranes (Fig. 3.8). Thus the localization of E-Syts is mediated by their C-terminal C<sub>2</sub>-domains.

The role of C-terminal C<sub>2</sub>-domains of E-Syts in directing their localization is surprising, as I am not aware of a previous example in the literature where a C<sub>2</sub>-domain directs the localization of a protein, suggesting that the mechanism described here is novel. This mechanism presumably involves interaction of the E-Syt2 C<sub>2</sub>C-domain with another plasma membrane protein, similar to the interaction of the Munc13 C<sub>2</sub>A-domain with RIM (13), as suggested by two observations. First, the E-Syt2 C<sub>2</sub>B-/C<sub>2</sub>C-domain, localized to the plasma membrane, is detergent-insoluble, and thus not phospholipid-bound (Fig. 3.9.A).

Second, although the detergent-insolubility of the E-Syt2 C<sub>2</sub>B-/C<sub>2</sub>C-domain suggests a possible role for the cytoskeleton in its localization, drugs that disrupt either the actin or the microtubule cytoskeleton did not alter the plasma membrane localization or insolubility of the E-Syt2 C<sub>2</sub>B-/C<sub>2</sub>C-domain fragment (Figs. 3.9.A and 3.9.B). Together, these results suggest that although the E-Syt2 and E-Syt3 TMR is anchored in the plasma membrane (as evidenced by the extracellularly exposed N-terminal sequence), E-Syt2 and E-Syt3 are involved in an independent interaction with the plasma membrane via their C-terminal C<sub>2</sub>C-domain that presumably binds to a detergent insoluble, as yet unidentified plasma membrane component. This binding likely not only mediates the targeting of E-Syt2 and E-Syt3 to the plasma membrane, but is also probably involved in their unknown functions at the plasma membrane.

## References

1. Coussens, L., Parker, P. J., Rhee, L., Yang-Feng, T. L., Chen, E., Waterfield, M. D., Francke, U., and Ullrich, A. (1986) *Science* **233**, 859-866.
2. Davletov, B. A., and Südhof, T. C. (1993) *J. Biol. Chem.* **268**, 26386-26390.
3. Chapman, E. R., and Jahn, R. (1994) *J. Biol. Chem.* **269**, 5735-5741.
4. Persechini, A., Moncrief, N. D., and Kretsinger, R. H. (1989) *Trends Neurosci.* **12**, 462-467.
5. Sutton, R. B., Davletov, B. A., Berghuis, A. M., Südhof, T. C. and Sprang, S. R. (1995) *Cell* **80**, 929-938.
6. Rizo, J., and Südhof, T. C. (1998) *J. Biol. Chem.* **273**, 15879-15882.
7. Essen, L. O., Perisic, O., Cheung, R., Katan, M., and Williams, R. L. (1996) *Nature* **380**, 595-602.
8. Ubach, J., Zhang, X., Shao, X., Sudhof, T. C., and Rizo, J. (1998) *EMBO J.* **17**, 3921-3930.
9. Ubach, J., Garcia, J., Nittler, M. P., Sudhof, T. C., and Rizo, J. (1999) *Nat Cell Biol.* **1**, 106-112.
10. Lee, J. O., Yang, H., Georgescu, M. M., Di Cristofano, A., Maehama, T., Shi, Y., Dixon, J. E., Pandolfi, P., and Pavletich, N. P. (1999) *Cell* **99**, 323-334.
11. Dai, H., Tomchick, D. R., Garcia, J., Südhof, T. C., Machius, M., and Rizo, J. (2005) *Biochemistry* **44**, 13533-13542.
12. Dai, H., Shin, O. -H., Machius, M., Tomchick, D. R., Südhof, T. C., and Rizo, J. (2004) *Nat. Struct. Mol. Biol.* **11**, 844-849.
13. Lu, J., Machius, M., Dulubova, I., Dai, H., Südhof, T. C., Tomchick, D., and Rizo, J. (2006) *PLOS Biology* **4**, e192.
14. Tang, J., Maximov, A., Shin, O. -H., Dai, H., Rizo, J., and Südhof, T. C. (2006) *Cell* **126**, 1175-1187.
15. Pang *et al.*, *J. Neurosci.* In press.



16. Stahl, B., Chou, J. H., Li, C., Südhof, T. C., and Jahn, R. (1996) *EMBO J.* **15**, 1799-1809.
17. Giorgione, J. R., Lin, J. H., McCammon, J. A., and Newton, A. C. (2006) *J. Biol. Chem.* **281**, 1660-1669.
18. Choi, J. Y., Riekhof, W. R., Wu, W. I., and Voelker, D. R. (2006) *Biochem Soc Trans.* **34**, 404-8.
19. Denis, V., and Cyert, M. S. (2005) *Eukaryot Cell* **4**, 36-45.
20. Morvan, J., Froissard, M., Haguenaue-Tsapis, R., and Urban-Grimal, D. (2004) *Traffic* **5**, 383-392.
21. Südhof, T. C. (2002) *J. Biol. Chem.* **277**, 7629-7632.
22. Bansal D., and Campbell, K. P. (2004) *Trends Cell Biol.* **14**, 206-213.
23. Shin, O. -H., Han, W., Wang, Y., and Südhof, T. C. (2005) *J. Biol. Chem.* **280**, 1641-1651.
24. Creutz, C. E., Snyder, S. L., and Schulz, T. A. (2004) *Cell Mol Life Sci.* **61**, 1208-1220.
25. Morris, N. J., Ross, S. A., Neveu, J. M., Lane, W. S., and Lienhard, G. E. (1999) *Biochim Biophys Acta* **1431**, 525-530.
26. Guan, K. L., and Dixon, J. E. (1991) *Anal. Biochem.* **192**, 262-267.
27. Fernandez, I., Arac, D., Ubach, J., Gerber, S. H., Shin, O. -H., Gao, Y., Anderson, R. G. W., Südhof, T. C., and Rizo, J. (2001) *Neuron* **32**, 1057-1069.
28. Shin, O. -H., Rizo, J., and Südhof, T. C. (2002) *Nat. Neurosci.* **5**, 649-656.
29. Laemmli, U. K. (1970) *Nature* **227**, 680-685.
30. Johnston, P. A., Jahn, R., and Südhof, T. C. (1989) *J. Biol. Chem.* **264**, 1268-1273.
31. Shin, O.-H., Han, W., Wang, Y., and Südhof, T. C. (2005) *J. Biol. Chem.* **280**, 1641-1651.
32. Han, W., Rhee, J. S., Maximov, A., Lin, W., Hammer, R. E., Rosenmund, C., and Südhof, T. C. (2005) *J. Biol. Chem.* **280**, 5089-5100.

33. Perin, M. S., Fried, V. A., Mignery, G. A., Jahn, R., and Südhof, T. C. (1990) *Nature* **345**, 260-263.
34. Südhof, T. C. (2004) *Annu Rev Neurosci.* **27**, 509-547.

## **VITAE**

Sang-Won Min was born in Seoul, Korea on May 17th, 1974, the son of Byung-Mok Min and Sook-Hee Baik. After completing his work at Seoul Science High School, Seoul in 1993, he entered Department of Molecular Biology, College of Natural Sciences, Seoul National University in Seoul, Korea. He received the degree of Bachelor of Science with a major in Molecular Biology from Seoul National University in February 1997. In March 1997, he entered the Graduate School of Molecular Biology at Seoul National University and did his master course in the laboratory of Dr. Chin Ha Chung. He received the degree of Master of Science in February, 1999. In August 2000, he entered the Graduate School of Biomedical Sciences at the University of Texas Southwestern Medical Center at Dallas. He joined the laboratory of Dr. Thomas Südhof in May 2001. He graduated with a Ph.D. degree in December, 2006. He married Jiyeon Oh in July 2000.

Permanent Address: Seocho4-dong, Seocho-gu  
Jin-Heung Apt. 7-1005  
Seoul, Korea 137-074